Sapienza Università di Roma
Dottorato di Ricerca in Fisica
Scuola di dottorato "Vito Volterr"

SHEAR VISCOSITY OF NEUTRON MATTER FROM REALISTIC NUCLEON-NUCLEON INTERACTIONS

Thesis submitted to obtain the degree of
"Dottore di Ricerca" - *Doctor Philosophiæ*
PhD in Physics - XX cycle - October 2007

by

Marco Valli

Program Coordinator
Prof. Enzo Marinari

Thesis Advisor
Dott. Omar Benhar

Contents

Introduction

When a neutron star is perturbed by some external or internal event, it can be set into non-radial oscillations, emitting gravitational waves at the charateristic frequencies of its quasi-normal (i.e. damped) modes. This may happen, for instance, as a consequence of a glitch (a sudden increase in the rotation rate of a pulsar), of a close interaction with an orbital companion, of a phase transition occurring in the neutron star inner core or in the aftermath of a gravitational collapse. The frequencies and the damping times of the quasi-normal modes carry information on the structure of the star and on the properties of matter in its interior.

As Chandrasekhar first pointed out [1], emission of gravitational radiation (GR) following the excitation of non-radial oscillation modes may lead to the instability of rotating stars. Chandrasekhar's result was subsequently put on a more rigorous footing by Friedman and Schutz [2], who also proved that the instability, known as CFS instability, is such that *all rotating perfect fluid stars are unstable*.

The mechanism is easy to understand: consider a neutron star, rotating with angular velocity Ω, and a perturbation of this star with angular dependence $e^{im\phi}$; the perturbation creates time-dependent mass-multipoles, which cause the star to emit GR. If the perturbation propagates in the direction opposite the star rotation, the GR reduces the perturbation amplitude in such a way as to conserve angular momentum. In sufficiently rapidly rotating stars, however, these perturbations are forced to move in the same direction of the star rotation, as the waves are dragged along by the fluid in the star; in this case, conservation of angular momentum requires that the perturbation amplitude grow. Thus, any counter-rotating perturbation will become unstable when the star rotates rapidly enough to force it to corotate with the star. Of particular relevance is the instability driven by so called r-modes, oscillations of rotating stars whose restoring force is the Coriolis force [3].

The observation of stable rotating stars shows that some other mechanism must be active to prevent GR from driving these perturbations unstable. One such mechanism is internal dissipation in stellar matter: viscosity (and thermal conduction) quickly damps out any large gradient in velocity (or thermal) perturbations. These mechanisms, however, are poorly understood and therefore difficult to model in a realistic fashion.

At relatively low temperatures (below a few times 10^9 K) the main viscous dissipation mechanism arises from momentum transport due to particle scattering. In the standard approach these scattering events are modelled in terms of a macroscopic shear viscosity. In a normal fluid star, neutron-neutron scattering provides the most important contribution to shear viscosity, while in a superfluid electron-electron scattering dominates. In order to determine which stars are stable, a detailed analysis of their perturbations must be carried out including the influence of both GR *and* viscosity [4].

Early estimates of the shear viscosity coefficients of neutron star matter were obtained in the 70s by Flowers and Itoh, who used the measured scattering phase shifts to estimate the neutron-neutron scattering probability [5, 6]. Based on these results, Cutler and Lindblom carried out a systematic study of the effect of the viscosity on neutron-star oscillations, using a variety of different equations of state of neutron star matter [4].

The procedure followed by Cutler and Lindblom [4], while allowing for the first quantitative analysis of the damping of neutron-star oscillations, cannot be regarded as fully consistent. Ideally, the calculation of transport properties of neutron star matter and the determination of its equation of state should be carried out using the *same* dynamical model. The work discussed in this Thesis is aimed at making a first step towards this goal.

Realistic models of the neutron star matter equation of state are obtained from either nonrelativistic nuclear many-body theory [7, 8] or relativistic approaches based on the mean-field approximation [9]. The extension of these microscopic approaches to the description of transport properties, needed to calculate the viscosity coefficients, involves serious difficulties that cannot be handled with the available computational techniques. Transport properties are most effectively described within the more phenomenological approach proposed by Landau in 1956 [10].

In this Thesis we combine the results of Landau theory and nuclear many-body theory to obtain the shear viscosity coefficient of pure neutron matter, η, using the same model of the microscopic dynamics employed to model the equation of state.

The main difficulty associated with our approach is the calculation of the neutron-neutron scattering cross section in the nuclear medium. This calculation has been carried out using an *effective interaction* derived from a highly realistic nucleon-nucleon potential, and including the effect of many-nucleon forces. This is to be regarded as the most important feature of our work, as most previous studies of the viscosity were based on the assumption that the scattering probability in not affected by medium effects [11].

In Chapter 1 we review the main feautures of Landau theory of normal Fermi liquids, as well as its extensions, mainly due to Abrikosov and Khalatnikov [12], needed to express transport coefficients in terms of the scattering probability.

In Chapter 2, after recalling the available empirical information on nuclear matter

and nuclear forces, we analyze the structure of the nuclear hamiltonian used in nonrelativistic many-body theories.

Chapter 3 is devoted to a description of the formalism based on correlated many-body wave functions and cluster expansion techniques, known as Correlated Basis Function (CBF) perturbation theory. The effective interaction obtained from this approach has been tested by computing different nuclear matter properties, and comparing to the results of highly advanced calculations available in the literature.

In Chapter 4 we discuss the results of our calculations of the shear viscosity of pure neutron matter, showing that the inclusion of medium modifications of the scattering cross section leads to large differences, with respect to previously available estimates.

Finally, we summarize the main features of our work and point out the potential of our approach for further studies of different nuclear matter properties, as well as its limits of applicability.

Unless otherwise specified, throughout this Thesis we always use a system of units in which $\hbar = h/2\pi = c = K_B = 1$, where h is Plank's constant, c is the speed of light and K_B denotes Boltzmann's constant.

Chapter 1

Transport properties of normal Fermi liquids

In this Chapter we introduce the concept of viscosity at both macroscopic and microscopic level. After a short discussion based on classical fluid mechanics, in Sections 1.3 and 1.4 we outline the main ideas underlying Landau theory of normal Fermi liquids, and its application to the study of their transport properties. Finally we discuss the derivation of the shear viscosity coefficient, whose calculation is the main aim of this Thesis.

1.1 Macroscopic theory

It is an every-day-life observation that "thicker" liquids (like honey) move less easily than others (like water): viscosity measures the ease with which a fluid yields to an external stress [13].

In hydrostatic equilibrium, and in all cases for a non-viscous fluid, stresses are always normal to any surface inside the fluid: the normal force per unit area is just the pressure. When a velocity gradient exists in a fluid, a shearing stress is developed between two layers of fluid with differential velocities. The shear viscosity is given by the ratio of the shearing stress to the transverse velocity gradient. Perfect fluids cannot sustain a shear stress, while, in general, in real liquids the sort of internal friction we call viscosity cannot be neglected [13, 14].

First of all, we recall an important experimental fact: in all circumstances, the velocity of a fluid is exactly zero at the surface of a solid, even if we take into account the possibility that there might be a shear force between the liquid and the solid.

As we said, there are no shear stresses in static conditions. However, if we exert a force on a fluid, as long as we push on it, and before equilibrium is reached, there can be shear forces. To get an estimate, consider the classical experiment of viscous

drag between two parallel planes, schematically illustrated in Fig. 1.1. Suppose we have two solid surfaces with a fluid between them; we keep one stationary while moving the other, parallel to it, at the low speed v_0.

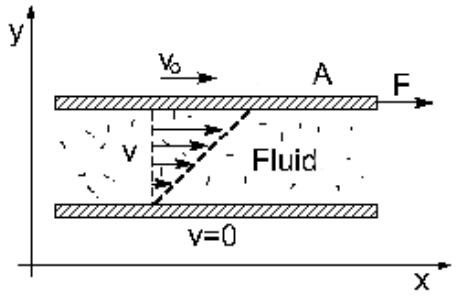

Figure 1.1. Schematic representation of viscous drag.

We observe that, as we go from the upper plate to the lower one, the fluid velocity decreases from the value v_0 to zero on the surface of the stationary plate. Measuring the force F required to keep the upper plate moving, we find that it is proportional to the area A of the plate and to the velocity v_0, while being inversely proportional to the distance d between the plates. Hence, the shear stress F/A is proportional to v_0/d,

$$\frac{F}{A} = \eta \frac{v_0}{d} \ . \tag{1.1}$$

The above equation defines the coefficient of shear viscosity η.

In common language, the word "dense" is often used in place of "viscous". However, although denser fluids are usually more viscous, it is sometimes more convenient, for macroscopic considerations, to use the specific viscosity, defined as η divided by the mass density. Moreover, and as it will become clear after the next section, viscosity usually depends strongly on temperature.

1.2 Microscopic description

As we saw, shear viscosity is related to the variation (spatial gradient) of the velocity flow of a fluid in the transverse direction.

The microscopic description of the state of a moving fluid [14] requires the knowledge of the velocity field

$$\mathbf{v} = \mathbf{v}(\mathbf{r}, t) \ , \tag{1.2}$$

and any two termodynamic parameters, e.g. density and pressure, respectively given by

$$\rho = \rho(\mathbf{r}, t) \quad , \quad p = p(\mathbf{r}, t) \ . \tag{1.3}$$

Note that the coordinate $\mathbf{r}$ specifies a fixed point in space and not the position of a moving particle of the fluid.

Mass conservation is expressed through the *continuity equation*

$$\frac{\partial \rho}{\partial t} + \boldsymbol{\nabla} \cdot (\rho \mathbf{v}) = 0 \ . \tag{1.4}$$

For an ideal fluid, the equation of motion is obtained by taking into account that the force exerted by the surrounding fluid on a fluid element of unit volume is just minus the pressure gradient, i.e. $\mathbf{F} = -\boldsymbol{\nabla} p$. This leads to the *Euler equation*

$$\frac{\partial \mathbf{v}}{\partial t} + (\mathbf{v} \cdot \boldsymbol{\nabla}) = -\frac{1}{\rho} \boldsymbol{\nabla} p \ . \tag{1.5}$$

Euler equation describes the motion of a fluid in the absence of processes leading to energy dissipation, occuring due to viscosity (i.e. internal friction) and heat exchange between different fluid elements.

For an *incompressible* fluid, i.e. a fluid whose density does not depends on either $\mathbf{r}$ or t, Euler equation (1.5) does not change, while the continuity equation (1.4) simplifies to

$$\boldsymbol{\nabla} \cdot \mathbf{v} = 0 \ . \tag{1.6}$$

Let us consider the rate of change of momentum (per unit volume) during the fluid motion, given by $\partial (\rho \mathbf{v}) / \partial t$. Making use of the continuity equation (1.4) and Euler equation (1.5), we obtain

$$\begin{aligned} \frac{\partial}{\partial t} (\rho v_i) &= \rho v_k \frac{\partial v_i}{\partial x_k} - \frac{\partial p}{\partial x_i} - \frac{\partial}{\partial x_k} (\rho v_k) v_i \\ &= -\frac{\partial p}{\partial x_i} - \frac{\partial}{\partial x_k} (\rho v_i v_k) \\ &\equiv -\frac{\partial \Pi_{ik}}{\partial x_k} \ , \end{aligned} \tag{1.7}$$

where we introduced the *momentum-flux tensor*

$$\Pi_{ik} = p \delta_{ik} + \rho v_i v_k \ . \tag{1.8}$$

The component Π_{ik} of the momentum flux tensor is the i-th component of the momentum flowing through a surface of unit area, perpendicular to the x_k axis, per unit time.

Consider now the effect of energy dissipation on the fluid motion; this requires the inclusion of an additional term to the equation of motion describing an ideal fluid.

The continuity equation (1.4), expressing conservation of matter, is not affected by energy dissipation. On the other hand, the Euler equation needs to be modified. The momentum flux tensor (1.8) describes a *reversible* transfer of momentum, resulting from motion of fluid particles and the pressure force acting in the fluid. In the presence of viscosity there is an additional, *irreversible* transfer of momentum from points of higher velocity to points of lower velocity [14].

The equation of motion of a viscous fluid can be obtained by adding to the ideal momentum flux tensor (1.8) a term $-\sigma'_{ik}$ describing the irreversible flux. We write

$$\begin{aligned} \Pi_{ik} &= p\delta_{ik} + \rho v_i v_k - \sigma'_{ik} \\ &= -\sigma_{ik} + \rho v_i v_k \ , \end{aligned} \tag{1.9}$$

where

$$\sigma_{ik} = -p\delta_{ik} + \sigma'_{ik} \tag{1.10}$$

is called the *stress tensor*, while σ'_{ik} is the *viscous stress tensor*.

Conservation laws and symmetry considerations require σ'_{ik} to be of the form [14]

$$\sigma'_{ik} = \eta\left(\frac{\partial v_i}{\partial x_k} + \frac{\partial v_k}{\partial x_i} - \frac{2}{3}\delta_{ik}\frac{\partial v_\ell}{\partial x_\ell}\right) + \xi\delta_{ik}\frac{\partial v_\ell}{\partial x_\ell} \ , \tag{1.11}$$

where the coefficients η and ξ are called *first* (or *shear*) and *second* (or *bulk*) *viscosity*, respectively. They are both positive [14] and independent of velocity, while they may, in general, depend on pressure and temperature, thus being not costant throughout the fluid. In most cases, however, η and ξ depend weakly on $\mathbf{r}$ and can be treated as constants.

The equation of motion in the presence of viscosity can be simply obtained by adding $\partial\sigma'_{ik}/\partial x_k$ to the rhs of Eq. (1.5) [14].

Note that for an incompressible fluid $\boldsymbol{\nabla}\cdot\mathbf{v} = 0$ and the stress tensor of Eq. (1.10) reduces to

$$\sigma_{ik} = -p\delta_{ik} + \eta\left(\frac{\partial v_i}{\partial x_k} + \frac{\partial v_k}{\partial x_i}\right) \ , \tag{1.12}$$

i.e. it only depends on the shear viscosity coefficient η.

The shear viscosity is the transport coefficient that characterizes the diffusion of momentum transverse to the direction of propagation, due to the collisions of fluid particles in the medium. It is proportional to the mean free path of the excitations in the medium, and inversely proportional to the scattering cross section between particles constituing the fluid. These two quantities are strongly temperature dependent, and so is the viscosity.

1.3 Landau theory of normal Fermi liquids

Landau theory of normal Fermi liquids (FL), developed by its author in 1956 [10], is a phenomenological theory, allowing for a description of static and trasport properties of (strongly) interacting systems of Fermi (i.e. spin one-half) particles in the normal (i.e. non superconducting) state [15, 16]. The analysis of transport properties of FL was further developed by Abrikosov and Khalatnikov, who gave an approximate solution of the equation for the transport coefficients back in 1959 [12]; the exact solution was finally obtained by Brooker and Sykes in 1970 [17, 18].

Landau theory (LT) provides a way of parametrizing low temperature properties of FL - thus enablying one to relate experimentally measurable quantities to each other - in terms of a rather small number of parameters; the results of LT mainly follow from general arguments, conservation laws and symmetry principles, and do not depend on the microscopic details of the interparticle forces. Finally, LT has been shown to be correct from microscopic first-principles calculations, based on the Green function formalism and diagrammatic techniques, confirming Landau's intuitions [19].

1.3.1 Basic assumptions

Landau theory deals with systems of interacting $s = 1/2$ particles in the normal state. Examples of normal FL are liquid ^{3}He and ^{3}He-^{4}He mixtures, nuclear matter - relevant to the description of heavy nuclei and the neutron star core - and the electron liquid, that can be found in metals and white dwarfs.

Experimental analyses of liquid ^{3}He, that became feasible in the early 50s, provided the first strong evidence that the ideal gas model fails to reproduce the observed low temperature properties.

The calculation of thermodynamic properties of an ideal (non interacting) Fermi system is a standard textbook exercise in statistical mechanics. Consider a system of N particles enclosed in a volume V, with N,$V \to \infty$ and the number density $\rho = N/V$ kept fixed at a finite value (termodynamic limit); the key ingredient to calculate all quantities of interest is the partition function

$$\mathcal{Z} = \sum_s \mathrm{e}^{-\beta(\epsilon_s - \mu)} \ , \tag{1.13}$$

where $\beta = 1/T$, T being the temperature. In the above equation, μ is the chemical potential, s specifies the set of relevant quantum numbers (momentum $\mathbf{p}$, spin projection σ, ...) and ϵ_s denotes the energy of the single-particle states.

Once the partition function is known, termodynamic properties (like pressure, internal energy, ...) can be simply calculated as derivatives of $\mathcal{Z}$.

The fermionic nature of the particles is embedded in the properties of the distribution function $n(\epsilon_s)$, yielding the mean occupation number of the state with energy ϵ_s. At zero temperature, the system is in its ground state; due to the Pauli principle, every single-particle state is filled with two particles (one for each spin projection), up to the maximum energy ϵ_F, called Fermi energy, while the states with energies larger than ϵ_F are all empty. A particle added to the system will have at least an energy ϵ_F, so that, at $T = 0$, the Fermi energy is the chemical potential. The distribution function at zero temperature is then given by the step function

$$n(\epsilon_s,T = 0) = \theta(\epsilon_F - \epsilon_s) \ . \tag{1.14}$$

From now on, we will only consider the case $s \equiv \mathbf{p}$, thus suppressing spin and other indices. The single-particle energy is then written as $\epsilon(\mathbf{p})$ or $\epsilon_\mathbf{p}$ and the distribution function of the system is indicated as $n(\epsilon)$ or $n_\mathbf{p}$.

According to the dispersion relation $\epsilon = \epsilon(\mathbf{p})$, the Fermi energy ϵ_F defines a surface in momentum space, known as the Fermi surface; for an isotropic system, the Fermi surface is a sphere, with radius given by the Fermi momentum $\mathbf{p}_F$, whose magnitude is simply related to the density ρ through $|\mathbf{p}_F| = (6\pi^2\rho/\nu)^{1/3}$, where ν specifies the degeneracy of the momentum eigenstates. For a system of non relativistic free particles, the dispersion relation is given by

$$\epsilon_\mathbf{p} = \frac{\mathbf{p}^2}{2m} \ . \tag{1.15}$$

An excited state of the system is obtained by moving some particles to empty states above the Fermi surface, giving rise to the so-called particle-type excitations, while leaving some empty energy levels, or hole-type excitations, below the Fermi surface. Due to particle number conservation, particle and hole excitations always appear in equal numbers.

At finite temperature, equilibrium is characterized by the Fermi-Dirac distribution

$$n_\mathbf{p} = \frac{1}{\mathrm{e}^{\beta(\epsilon_\mathbf{p}-\mu)} + 1} \ . \tag{1.16}$$

Comparison with Eq.(1.14) shows that, due to thermal effects, the jump of $n_\mathbf{p}$ from unity to zero takes place over an energy range $\sim T$ around μ.

For an interacting system, this picture is no longer consistent. Even if we knew exactly the details of the interparticle interactions (and this is not our case, as we shall discuss later in detail), we would not be able to determine the exact eigenstates of the system and, as a consequence, to calculate the partition function. Due to interactions, the very concept of single-particle level is no longer correct: the state of a given particle depends on those of all the others and the excited states of the system cannot be built up by simply moving particles to excited single-particle levels.

However, at very low temperatures, we can resort to some reasonable assumptions that greatly simplifies the problem, and led Landau to the formulatation of his theory.

Landau's reasoning went as follows: consider an interacting system and imagine to turn off interactions; the equilibrium state is characterized by a step distribution function $n^0_{\mathbf{p}}$. If we now turn on the interaction adiabatically, as a consequence of Pauli principle particles have no empty states to scatter to (they are said to be Pauli blocked), and every non-interacting state will eventually give rise to a specific state of the interacting system. Hence, we can assume that there is a one-to-one correspondence between the states of the ideal gas and those of the real liquid. Under these circumstances, the energy spectrum of the liquid is constructed according to the very same principles as that of the perfect gas: levels are occupied from below, taking into account spin degeneracy, up to the energy ϵ_F which, in general, is different from that of the non interacting system.

In the low temperature limit, only the first energy levels really affect the partition function; if we were able to develop a consistent description of these states, the termodynamic properties of the system could be easily calculated. As shown by Landau, the characteristics of the energy spectrum can be inferred by using very general considerations and regardless of the strength and specific features of the interaction.

1.3.2 Quasiparticles

Landau theory is based on the concept of *elementary excitations* of a many-particle system.

Consider the system in its ground state, plus a particle with $|\mathbf{p}| > p_F$: such a state has momentum $\mathbf{p}$ and energy $\epsilon_{\mathbf{p}}$ (with $\epsilon_{\mathbf{p}} \neq \epsilon^0_{\mathbf{p}}$). Every excited state of the whole system can be written as a rather complicated superposition of single-particle excited states (the set of eigenstates of the non interacting system still being a basis in Hilbert space), corresponding to a rather discontinuos distribution function $n_{\mathbf{p}}$, which can be made smooth by averaging over a set of neighbouring states, with narrow energy spread. Landau calls this state a *quasiparticle* state.

Quasiparticles (QP) are the elementary excitations of the FL; being the result of interactions between all particles, QP pertain to the system as a whole and not to its separate constituents.

As they are not exact eigenstates of the system, quasiparticle states are unstable: transitions via decay or scattering have nonzero probability, leading to a damping of the excitations. Decay occurs for high energy excitations, while scattering is the dominant damping mechanism when the number of excitations grows.

A description of the system in terms of a gas of weakly interacting QP is meaningful only if their attenuation is small, i.e. when the packet width is much smaller

than its energy.

By simple phase-space considerations [19], it can be shown that the lifetime of the QP excitations, of energy ϵ and at temperature T, can be expressed as

$$\frac{1}{\tau} \propto a(\epsilon - \mu)^2 + bT^2 \ . \tag{1.17}$$

In the neighborhood of the Fermi surface and at sufficiently low T, quasiparticle states are long-lived and behave pretty much like stable single-particle states. These are the limits of validity of Landau theory. Under these conditions we can simply describe the properties of the system through a distribution function $n_{\mathbf{p}}$, which is now to be interpreted as a quasiparticle distribution function.

As already mentioned, due to interactions the energy of a QP depends on the state of all the others; therefore, Landau assumes $\epsilon_{\mathbf{p}}$ to be a *functional* of the QP distribution function, writing

$$\epsilon_{\mathbf{p}} = \epsilon_{\mathbf{p}}\left[n_{\mathbf{p}}\right] \ . \tag{1.18}$$

The total energy of the system is also a functional of the distribution function

$$E = E\left[n_{\mathbf{p}}\right] = E^0 + \sum_{\mathbf{p}} \epsilon_{\mathbf{p}}\, \delta n_{\mathbf{p}} \ , \tag{1.19}$$

where E^0 is the ground state energy (which can't be determined within the framework of LT), implying that the QP energy is the *functional derivative* of the energy of the system

$$\epsilon_{\mathbf{p}} = \frac{\delta E}{\delta n_{\mathbf{p}}} \ . \tag{1.20}$$

A noticeable feature of interacting systems is that the phase-space volume is not changed by interactions: for an isotropic system p_F remains unchanged too[1].

A Fermi surface is still associated with the discontinuity of the momentum distribution. However, there are unoccupied states below p_F and occupied states above.

The QP distribution function $n_{\mathbf{p}}$ can be determined, just as for the perfect gas, by minimizing the total energy of the N particles system

$$E = T\,S + \mu\,N \ , \tag{1.21}$$

where S is the entropy, with respect to $n_{\mathbf{p}}$, under the constraints of particle number and energy conservation.

The expression of the entropy S remains the same as for the non interacting system, being determined by combinatorics and by the assumption of the one-to-one correspondence between states of the interacting and non interacting systems.

[1]This result is sometimes referred to as Landau theorem; the analog result for systems with a periodic structure is known as Luttinger theorem.

It is given by

$$S = -\sum_{\mathbf{p}} \left\{ n_{\mathbf{p}} \log n_{\mathbf{p}} + (1 - n_{\mathbf{p}}) \log(1 - n_{\mathbf{p}}) \right\} . \tag{1.22}$$

The resulting $n_{\mathbf{p}}$ has the appearence of a Fermi-Dirac distribution (compare to Eq.(1.16))

$$n_{\mathbf{p}} = \left\{ 1 + \exp\Big(\beta \left(\epsilon_{\mathbf{p}} \left[\mathrm{n}_{\mathbf{p}} \right] - \mu \right) \Big) \right\}^{-1} . \tag{1.23}$$

It has to be emphasized, however, that, due to the functional dependence of $\epsilon_{\mathbf{p}}$ on $n_{\mathbf{p}}$, the above equation provides a rather complicated implicit definition of $n_{\mathbf{p}}$.

1.3.3 Quasiparticle interaction and Landau parameters

Interactions between QP are taken into account by the second term of the functional expansion of the energy

$$E = E^0 + \sum_{\mathbf{p}} \epsilon^0_{\mathbf{p}} \, \delta n_{\mathbf{p}} + \frac{1}{2} \sum_{\mathbf{p},\mathbf{p}'} f_{\mathbf{p}\mathbf{p}'} \, \delta n_{\mathbf{p}} \, \delta n_{\mathbf{p}'} \ , \tag{1.24}$$

where $\epsilon^0_{\mathbf{p}}$ is the *isolation energy*, i.e. the energy of an isolated QP, and $f_{\mathbf{p}\mathbf{p}'}$ is the *interaction energy* of a QP in the state of momentum $\mathbf{p}$ interacting with one carrying momentum $\mathbf{p}'$.

In order to better understand the meaning of the quantity $f_{\mathbf{p}\mathbf{p}'}$ and its relation to the *physical* interaction between particles, it is useful to introduce the Landau parameters.

First of all, we specify the additional quantum numbers relevant to the description of different physical systems. In the low temperature regime, spin interactions may be relevant. Including the spin in the formalism of Landau theory is straightforward:

$$\epsilon_{\sigma\mathbf{p}} = \epsilon^0_{\sigma\mathbf{p}} + \sum_{\sigma'} \int \frac{d^3\mathbf{p}'}{(2\pi)^3} \, f_{\sigma\mathbf{p},\sigma'\mathbf{p}'} \, \delta n_{\sigma'\mathbf{p}'} \ . \tag{1.25}$$

If invariance under spin-rotations holds, then

$$f_{\sigma\mathbf{p},\sigma'\mathbf{p}'} = f^s_{\mathbf{p},\mathbf{p}'} + f^a_{\mathbf{p},\mathbf{p}'} \left(\boldsymbol{\sigma} \cdot \boldsymbol{\sigma}' \right) , \tag{1.26}$$

with

$$f^{s,a}_{\mathbf{p},\mathbf{p}'} = \frac{f^{\uparrow\uparrow}_{\mathbf{p},\mathbf{p}'} \pm f^{\uparrow\downarrow}_{\mathbf{p},\mathbf{p}'}}{2} \ . \tag{1.27}$$

For nuclear and neutron matter (to be discussed in detail in the following Chapters), isospin should also be considered.

For very low T, only states in the close vicinity of the Fermi surface are relevant (due, once again, to Pauli blocking); this implies that the magnitude of the momenta

appearing in the quantities $f_{\mathbf{pp}'}$ is fixed to be approximately equal to the Fermi momentum, i.e. $|\mathbf{p}| \simeq |\mathbf{p}'| \simeq p_F$, as $T \to 0$, and only the relative orientation matters.

The interaction parameters have dimension of an energy density; by multiplying them by the density of states (i.e. the number of states for a given density and unit volume), we obtain the dimensionless quantities

$$N(0) f^{s,a}_{\mathbf{p},\mathbf{p}'} \equiv F^{s,a}_{\mathbf{p},\mathbf{p}'} = \sum_{\ell=0}^{\infty} F^{s,a}_{\ell} \, \mathcal{P}_{\ell} \left(\cos\theta \right) \ , \tag{1.28}$$

where $F^{s,a}$ has been expanded in Legendre polynomials, θ being the angle between $\mathbf{p}$ and $\mathbf{p}'$.

The numbers $F^{s,a}_{\ell}$ are known as *Landau F-parameters*; they totally embed the effects of interactions and cannot be determined by the theory, but have to be extracted from measurements. Intuitively, they are connected to the scattering amplitudes: this relation can be made precise within the Green function formalism [19]. As we shall see, the Fermi liquids corrections, which enter through the F's, do not affect the low temperature behaviour of the transport coefficients we will be focusing on. Hence, we will not discuss Landau parameters any further (a detailed account can be found in Refs.[15, 16]).

For an isotropic system, and in the absence of magnetic fields, the QP energy only depends on $p = |\mathbf{p}|$; in the vicinity of the Fermi surface, where Landau theory is expected to be applicable, it can be written as

$$\epsilon_{\mathbf{p}} - \epsilon_F \equiv \frac{\mathbf{p}^2}{2m^{\star}} \approx v_F \left(p - p_F \right) \ , \tag{1.29}$$

where we introduced the *effective mass* $m^{\star}$ and the *Fermi velocity* v_F, defined by

$$v_F \equiv \left(\frac{\partial \epsilon_{\mathbf{p}}}{\partial p} \right) \Bigg|_{p=p_F} = \frac{p_F}{m^{\star}} \ . \tag{1.30}$$

The effective mass $m^{\star}$ embodies the effect of interactions at the quasiparticle level, and it is related to the bare mass m by the Landau F-parameters [15, 16].

1.4 Transport properties

Transport properties are relevant to the description of a system in a state which differ slightly from the equilibrium state. Under these nonequilibrium and/or nonhomogeneous conditions, the macroscopic parameters which characterize equilibrium (T, μ, ...) depend on position, $\mathbf{r}$, and time, t.

The system can be described through a distribution function $n_{\mathbf{p}} = n_{\mathbf{p}}(\mathbf{r}, t)$, itself depending on space and time coordinates, as well as on momentum.

The description of many-particle systems at very low temperature requires that quantum effects be properly taken into account; for this reason, defining a distribution function which simultaneously depends on the particle positions and momenta may look questionable. In fact, we know that, according to Heisenberg uncertainty principle, the position of a (quasi)particle of definite momentum $\mathbf{p}$ cannot be determined with arbitrary accuracy. However, if the spatial inhomogeneity of the system occurs over a typical lenght Δr, particles are localized in space only within the same distance; on the other side, if the system is at temperature T, the distribution function in momentum space varies only over a characteristic width of $\Delta p \sim T/v_F$. As long as $\Delta r \Delta p \gg \hbar$, or

$$\Delta r \gg \frac{\hbar v_F}{T} \ ,$$

the uncertainty principle causes no troubles, and the use of a "classical" distribution function is legitimate [15]. For example, in nuclear matter at equilibrium density and $T = 1$ MeV (corresponding to $\sim 10^{10}$ K)

$$\Delta r \Delta p \gtrsim \hbar \Longrightarrow \Delta r \gtrsim \frac{\hbar v_F}{T} \sim 80\,\mathrm{fm} \ . \tag{1.31}$$

1.4.1 Boltzmann-Landau equation

If the distribution $n_{\mathbf{p}}(\mathbf{r}, t)$ can be regarded as a classical distribution function, its space and time evolution is determined by a kinetic equation, known as the *Boltzmann-Landau equation* [15], in analogy with the Boltzmann equation of classical fluid mechanics (see, e.g., Ref.[14]). For simplicity, in the following we shall neglect forces acting on the spin degrees of freedom, and omit spin indices.

The kinetic equation for $n_{\mathbf{p}}$ takes the form of a nonhomogeneus continuity equation (compare to Eq.(1.4)):

$$\frac{\partial n_{\mathbf{p}}(\mathbf{r}, t)}{\partial t} + \frac{\partial n_{\mathbf{p}}(\mathbf{r}, t)}{\partial \mathbf{r}} \cdot \mathbf{v} + \frac{\partial n_{\mathbf{p}}(\mathbf{r}, t)}{\partial \mathbf{p}} \cdot \mathbf{F} = I[n_{\mathbf{p}}(\mathbf{r},t)] \ . \tag{1.32}$$

The rhs of the above equation is the *collision integral*. It takes care of collisions in which QP momenta undergo sudden changes. We will describe the collision integral in the next Section.

Continuous changes in the quasiparticle positions and momenta are taken into account by the lhs of Eq.(1.32). Following Landau's interpretation of the QP energy as the single-particle hamiltonian, and making use of the Hamilton equation of motion, we can write

$$\frac{\partial \epsilon}{\partial \mathbf{p}} = \mathbf{v}_{\mathbf{p}} \quad , \quad \frac{\partial \epsilon}{\partial \mathbf{r}} = -\mathbf{F} \ . \tag{1.33}$$

The first equation simply states that $\mathbf{v_p}$ is the QP group velocity, while the second expresses the fact that, for a system out of equilibrium, the (spatial) gradient of the chemical potential acts as a generalized force.

Plugging Eq.(1.33) into Eq.(1.32), we obtain the Boltmann-Landau equation (BLE)

$$\frac{\partial n_{\mathbf{p}}}{\partial t} + \frac{\partial \epsilon_{\mathbf{p}}}{\partial \mathbf{p}} \cdot \frac{\partial n_{\mathbf{p}}}{\partial \mathbf{r}} - \frac{\partial \epsilon_{\mathbf{p}}}{\partial \mathbf{r}} \cdot \frac{\partial n_{\mathbf{p}}}{\partial \mathbf{p}} = I[n_{\mathbf{p}}] \ . \tag{1.34}$$

In spite of its being similar to the equation used to decribe weakly interacting gases, the BLE includes important additional physical features. First of all, the QP velocity, $\nabla_{\mathbf{p}}\epsilon_{\mathbf{p}}$, depends on position and time; moreover, the force term, $\nabla_{\mathbf{r}}\epsilon_{\mathbf{p}}$, includes the Fermi liquid corrections. In fact, even in the absence of external potentials, $\epsilon_{\mathbf{p}}$ depends on position because it depends, through the QP distribution function, on the position of all other QP. This contribution is represented by the term

$$\nabla_{\mathbf{r}}\epsilon_{\mathbf{p}} = \int \frac{d^3\mathbf{p}'}{(2\pi)^3} f_{\mathbf{p},\mathbf{p}'} \nabla_{\mathbf{r}} n'_{\mathbf{p}}(\mathbf{r}, t) \ . \tag{1.35}$$

As we are interested in slightly off-equilibrium conditions, we can linearize the lhs of the BLE in $\delta n_{\mathbf{p}} = n_{\mathbf{p}} - n^0_{\mathbf{p}}$, the deviation of the distribution function from the equilibrium (at $T = 0$) one. Note that this also implies that the QP energies are changed, according to

$$\epsilon_{\mathbf{p}} = \epsilon^0_{\mathbf{p}} + \delta\epsilon_{\mathbf{p}} \ . \tag{1.36}$$

The linearized BLE reads [15]:

$$\frac{\partial\, \delta n_{\mathbf{p}}}{\partial t} + \mathbf{v_p} \cdot \boldsymbol{\nabla}_{\mathbf{r}} \left(\delta n_{\mathbf{p}} - \frac{\partial n^0}{\partial \epsilon_{\mathbf{p}}} \delta\epsilon_{\mathbf{p}} \right) = I[\delta n_{\mathbf{p}}] \ , \tag{1.37}$$

where $\mathbf{v_p} = \nabla_{\mathbf{p}}\epsilon_{\mathbf{p}}$ and $\partial n^0_{\mathbf{p}}/\partial\epsilon_{\mathbf{p}}$ are evaluated at equilibrium; the collision integral also has to be linearized: we defer this calculation to the next Section.

A technical note In most application of kinetic theory, the system is in a state of *local* equilibrium at each point, characterized by a local temperature $T(\mathbf{r}, t)$, a local chemical potential $\mu(\mathbf{r}, t)$ and a local fluid velocity $\mathbf{u}(\mathbf{r}, t)$. Hence, we can define a local equilibrium distribution function

$$n(\epsilon_{\mathbf{p}}, \mathbf{r}, t) = \left[\exp\left(\frac{\epsilon_{\mathbf{p}} - \mathbf{p} \cdot \mathbf{u}(\mathbf{r}, t) - \mu(\mathbf{r}, t)}{T(\mathbf{r}, t)} \right) + 1 \right]^{-1} \ . \tag{1.38}$$

The parameters $T, \mu, \mathbf{u}$ in the local equilibrium distribution function are chosen in such a way as to give the same local density, energy and velocity as the true (global equilibrium) function [15].

For this reason, we should distinguish between

$$\delta n_{\mathbf{p}}(\mathbf{r}) = n_{\mathbf{p}}(\mathbf{r}) - n^0(\epsilon^0) \ , \tag{1.39}$$

the deviation of the distribution function from *global* equilibrium, where n^0 is evaluated at the true QP energy, and

$$\delta \tilde{n}_{\mathbf{p}}(\mathbf{r}) = n_{\mathbf{p}}(\mathbf{r}) - n^0(\epsilon) \quad , \tag{1.40}$$

the deviation from *local* equilibrium.

We can write

$$n^0(\epsilon^0) = n^0(\epsilon) - \frac{\partial n^0}{\partial \epsilon} \delta\epsilon \ , \tag{1.41}$$

so that

$$\delta \tilde{n}_{\mathbf{p}} = \delta n_{\mathbf{p}} - \frac{\partial n^0}{\partial \epsilon} \int \frac{d^3\mathbf{p}'}{(2\pi)^3} \ f_{\mathbf{p},\mathbf{p}'} \ \delta n_{\mathbf{p}'} \ . \tag{1.42}$$

From the above discussion it follows that $\delta\tilde{n}$ contains the Fermi liquid corrections; it satisfies the stationary equation

$$\mathbf{v}_{\mathbf{p}} \cdot \boldsymbol{\nabla}_{\mathbf{r}} \delta \tilde{n}_{\mathbf{p}} = I[\delta \tilde{n}_{\mathbf{p}}] \ , \tag{1.43}$$

which is the same as the one satisfied by δn with $f_{\mathbf{p},\mathbf{p}'} \equiv 0$.

It can be shown [15, 20] that, in the calculation of the transport coefficients in the zero temperature limit, the effects of Fermi liquid corrections are indeed very small; at lowest order, the equation to be solved is then given by

$$\mathbf{v}_{\mathbf{p}} \cdot \boldsymbol{\nabla}_{\mathbf{r}} \delta n_{\mathbf{p}} = I[\delta n_{\mathbf{p}}] \ . \tag{1.44}$$

This approximation has been proved to be completely satisfactory for the calculation of the *shear viscosity* and *thermal conductivity* coefficients, while a more accurate treatment is required for the analysis of the *zero sound* and the *magnetoresistance* [20].

1.4.2 The collision integral

In order to carry out the explicit calculation of the viscosity, we must specify the details of the collision integral.

First of all we note that, at low temperature, the density of thermally excited QP is also low, and we can safely neglect all the processes in which more than two QP at a time are involved; therefore, we only have to consider binary collisions.

Denoting with "1,2 ..." the states $|\mathbf{p}_1,\sigma_1\rangle$, $|\mathbf{p}_2,\sigma_2\rangle$ ..., the collision process can be indicated as $1,2 \rightarrow 3,4$. We also have to consider the inverse process $3,4 \rightarrow 1,2$; moreover, as we deal with identical particles, the final states 3 and 4 are

indistinguishable. Due to the exclusion principle, the process $1,2 \to 3,4$ is possible only if states 1 and 2 are initially occupied and states 3 and 4 are initially free. The opposite holds true for the inverse process.

We now define the transition probability; writing the transition amplitude for the process $1,2 \to 3,4$ as $\langle 3,4|\mathcal{T}|1,2\rangle$, and assuming that QP states are normalized in a box of volume V, the transition probability is given by Fermi's golden rule

$$\frac{2\pi}{\hbar}\,|\langle 3,4|\mathcal{T}|1,2\rangle|^2 \equiv \frac{1}{V^2}\,\mathcal{W}(12;34)\,\delta^{(3)}(\mathbf{p}_1+\mathbf{p}_2-\mathbf{p}_3-\mathbf{p}_4)\delta(\sigma_1+\sigma_2-\sigma_3-\sigma_4)\ , \quad (1.45)$$

where the δ-functions express conservation of momentum and spin projection (assuming a common quantization axis).

The collision integral $I[n_1]$ represents the net rate at which occupation of the state 1 is increased. Hence, it is given by difference between the rate for the process $3,4 \to 1,2$ and the rate for $1,2 \to 3,4$, summed over *all* states 2 and over *distinguishable* states 3 and 4. Its final expression is then given by

$$\begin{aligned} I[n_1] \;&=\; \frac{1}{V^2}\sum_{2}\sum_{34}{}' \,\mathcal{W}(12;34)\,\delta(\epsilon_1+\epsilon_2-\epsilon_3-\epsilon_4) && (1.46)\\ &\quad\times \delta^{(3)}(\mathbf{p}_1+\mathbf{p}_2-\mathbf{p}_3-\mathbf{p}_4)\delta(\sigma_1+\sigma_2-\sigma_3-\sigma_4)\\ &\quad\times \Big[n_3n_4(1-n_1)(1-n_2)-n_1n_2(1-n_3)(1-n_4)\Big]\ , && (1.47)\end{aligned}$$

where the prime on the sum symbol denotes summation over dinstinguishable final states only.

We now turn to the linearization of $I[n]$, at each point, around the deviation of the distribution function from the local equilibrium one. Note that the collision integral vanishes only if we put into it the distribution functions evaluated at the true QP energies. In fact, in global equilibrium all currents and fluxes are identically zero and there is no transport of particle density, energy or momentum. Introducing the linear deviation from local equilibrium by writing

$$\delta n_i \equiv -\frac{\partial n_i^0}{\partial \epsilon_i}\,\Phi_i\ , \quad i=1,\ldots,4 \quad , \quad (1.48)$$

and using momentum conservation, we obtain the final expression for the linearized collision integral [15]:

$$\begin{aligned} I[n_1] \;&=\; -\frac{1}{TV^2}\sum_{2}\sum_{34}{}' \,n_1n_2(1-n_3)(1-n_4)\,\mathcal{W}(12;34)\\ &\quad\times \delta(\sigma_1+\sigma_2-\sigma_3-\sigma_4)\,\delta(\epsilon_1+\epsilon_2-\epsilon_3-\epsilon_4)\\ &\quad\times \Big[\Phi_1+\Phi_2-\Phi_3-\Phi_4)\Big]\ , \quad (1.49)\end{aligned}$$

where the quantities n_i, ϵ_i and $\mathcal{W}$ are evaluated at local equilibrium. The deviation from local equilibrium that occurs in the approximate form of the collision integral automatically ensures consistency with the conservation laws of particle number, energy and momentum [15].

Now we have to solve the linearized BLE (1.44), with the linearized collision integral given by Eq.(1.49). The key element is obviously the transition probability $\mathcal{W}$: its explicit determination will be the main subject of this Thesis. For the moment, we just note that it is dictated by the dynamical model employed to describe particle interactions, and that it cannot be determined within the framework of LT. In LT the effects of interactions are taken into account at the mean field level; even if Landau parameters are connected to the forward scattering amplitudes, they cannot capture the complete energy and momentum transfer dependence of the scattering cross section (see, e.g. Ref.[21])

For the moment, we solve the equation that determines the coefficient of shear viscosity leaving $\mathcal{W}$ undetermined. Its explicit form will be specified at a later stage.

1.4.3 Calculation of the transport coefficients

The general procedure to obtain the expression of the transport coefficients is rather simple [20]. In non-equilibrium conditions, (small) gradients of the quantities that characterize equilibrium $(T, \mu, \mathbf{u})$ act like *generalized forces*; the response of the system shows in a *current*, which is proportional to the gradient of the relevant thermodynamic quantity that is varying: the factor of proportionality is the transport coefficient. A temperature gradient, for example, produces a heat current $\mathbf{j}_T$, which turns out to be proportional to $\boldsymbol{\nabla} T$ via the *thermal conductivity*,

$$\mathbf{j}_T = -\kappa_T \, \boldsymbol{\nabla} T \ . \tag{1.50}$$

We have to write down a microscopic expression for the current, in terms of an integral over the phase-space of the velocity times the quantity that is transported by the fluid motion: in the case of the heat flow, this is simply

$$\mathbf{j}_T = \sum_\sigma \int \frac{d^3\mathbf{p}}{(2\pi)^3} \, \mathbf{v}_p \, (\epsilon_\mathbf{p} - \mu) \delta n_\mathbf{p} \ . \tag{1.51}$$

We then have to express the driving term, in the lhs of Eq. (1.44), as a function of the relevant gradient. If we consider slight displacements from local equilibrium, the responses of the system are linear in the generalized forces, and we can safely treat each effect separately. In the calculation of thermal conductivity, this is achieved by writing

$$\mathbf{v}_\mathbf{p} \cdot \boldsymbol{\nabla}_\mathbf{r} \delta n_\mathbf{p} = -\frac{\partial n^0}{\partial \epsilon_\mathbf{p}} \Big(\frac{\epsilon_\mathbf{p} - \mu}{T} \Big) \, \mathbf{v}_\mathbf{p} \cdot \boldsymbol{\nabla}_\mathbf{r} T \ . \tag{1.52}$$

As we have seen, it is customary rewriting the deviation from local equilibrium in the form (1.48); in this way, we actually separate δn into a singular part, given by minus the derivative of the equilibrium distribution (for $T \to 0$ this factor tends to a δ function, as the distribution function rapidly varies only around the Fermi surface) and a regular part Φ. As now both sides of the kinetic equation contain the factors $\mathbf{v_p}$ and $\partial n^0/\partial\epsilon$, it reduces to an integral equation for Φ, containing the scattering amplitude $\mathcal{W}$ as the only external input. The form of the solution, which can be obtained using a variational approach [20], is specified by the particular transport phenomenon we are dealing with.

1.4.4 The Abrikosov-Khalatnikov solution

The first attempt to solve the integral equation for the transport coefficients of a Fermi liquid was carried out by Abrikosov and Khalatnikov (AK) in 1959 [12], shortly after the appearance of the seminal papers by Landau. Their approximate solution turned to be in good agreement with the experimental measurements of η in very low temperature dilute solutions of ^{3}He in superfluid ^{4}He, while the thermal conductivity κ_T turned out to be a factor 2 larger than the experimental value.

After further work (for a detailed account, see [15]), an exact analytical solution for the transport coefficients was finally given by Brooker and Sykes (BS) in 1970 [17, 18].

It has to be emphasized that the work of AK had the merit of showing the possibility of a separation between the energy integral and the angular ones; they also set the basic notation. For these reasons, we first discuss their results and then rapidly quote the exact solution of BS.

Phase-space separation Consider the collision between QP 1 and 2, scattering to the states 3 and 4. We are interested in the low-T regime: only QP states in the vicinity of the Fermi surface are involved in collisions. For this reason, the energies of the states 1,...,4 are very close to ϵ_F, while the corresponding momenta, $\mathbf{p}_1, \ldots, \mathbf{p}_4$ have magnitude fixed to be approximately equal to Fermi momentum p_F.

We now define a reference frame to describe the collision process. Let θ be the angle between the incoming momenta, $\mathbf{p}_1$ and $\mathbf{p}_2$, and ϕ the angle between the plane containing the initial momenta and that containing the final ones, $\mathbf{p}_3$ and $\mathbf{p}_4$: this is generally referred to as the AK reference frame.

Recalling that momentum conservation implies $\mathbf{p}_1 + \mathbf{p}_2 = \mathbf{p}_3 + \mathbf{p}_4$, and that all these momenta have equal magnitudes, we can rewrite [15]

$$d^3\mathbf{p}_2\, d^3\mathbf{p}_3 = \frac{m^{\star 3}}{2\cos(\theta/2)}\, d\epsilon_2\, d\epsilon_3\, d\epsilon_4\, \sin\theta\, d\theta\, d\phi\, d\phi_2 \;, \tag{1.53}$$

where ϕ_2 is the azimuthal angle of $\mathbf{p}_2$.

Because of the presence of the Fermi distributions and of the δ-function expressing energy conservation in the collision integral (1.47), the integration limits over QP energies may be extended to $\pm\infty$.

The scattering probability $\mathcal{W}(12;34)$ only depends on spin and the angular variables θ and ϕ. In the absence of magnetic field, we can sum over spin variables, obtaining

$$\sum_{\sigma_2} \sum_{\sigma_3,\sigma_4}{}' \mathcal{W}(12;34) \equiv 2\mathcal{W}(\theta,\phi) \ , \tag{1.54}$$

which represents the average scattering probability for σ_2 unpolarized with respect to σ_1. Note that, given σ_1, for each value of σ_2 the sum $\sigma_3+\sigma_4$ is fixed by conservation of spin projection, and we must sum only over distinguishable final states.

Let us introduce

$$\tau \equiv \frac{8\pi^4}{m^{\star 3}\langle\mathcal{W}\rangle\, T^2} \ , \tag{1.55}$$

$$\langle\mathcal{W}\rangle \equiv \int \frac{d\Omega}{2\pi}\, \frac{\mathcal{W}(\theta,\phi)}{\cos(\theta/2)} \ , \tag{1.56}$$

the QP relaxation time and the angle-averaged scattering probability, respectively. Note that the angular integral is performed over 2π and not over the whole solid angle 4π, due to indistinguishability of the final states.

Calculation of the shear viscosity Now we specialize our discussion to the case of the coefficient of shear viscosity, η.

In order to calculate η, we assume that the system be in local equilibrium, and in motion with a small local fluid velocity $\mathbf{u}(\mathbf{r})$ varying in space. Without any loss of generality, we refer to the case in which the fluid motion is in the x direction, and we observe a variation of the velocity in the y direction; the value of η is clearly not affected by such a choice. The local equilibrium distribution function is then given by (compare to Eq.(1.38))

$$n(\epsilon_{\mathbf{p}},\mathbf{r},t) = \left[\exp\left(\frac{\epsilon_{\mathbf{p}} - p_x\, u_x - \mu(\mathbf{r},t)}{T(\mathbf{r},t)}\right) + 1\right]^{-1} \ . \tag{1.57}$$

For an incompressible fluid, the xy component of the viscous stress tensor (1.11) is given by

$$\sigma'_{xy} = \eta\, \frac{\partial u_x}{\partial y} \ . \tag{1.58}$$

Note that, even if the fluid is compressibile, the term proportional to $\boldsymbol{\nabla}\cdot\mathbf{v}$ appears in the diagonal component of the stress tensor only; moreover, in the low temperature limit $\zeta/\eta \sim T^2$ [15], so that the bulk viscosity is never relevant to our discussion.

A small deviation from equilibrium produces a change in the dissipative stress tensor; at lowest order in δn, this is given by

$$\sigma'_{xy} = -\sum_{\sigma} \int \frac{d^3\mathbf{p}}{(2\pi)^3}\, p_x (v_{\mathbf{p}})_y \delta n_{\mathbf{p}} \ . \tag{1.59}$$

Furthermore, at lowest order in the low temperature expansion the driving term can be written as

$$\mathbf{v_p} \cdot \boldsymbol{\nabla}_{\mathbf{r}} \delta n_{\mathbf{p}} = -\frac{\partial n^0}{\partial \epsilon}\, p_x (v_{\mathbf{p}})_y \, \frac{\partial u_x}{\partial y} \ . \tag{1.60}$$

Collecting all the above results togheter, we finally obtain the AK expression for the coefficient of shear viscosity [12]:

$$\eta_{AK} = \frac{1}{5} \rho m^\star v_F^2 \tau \, \frac{2}{\pi^2 (1 - \lambda_\eta)} \ , \tag{1.61}$$

where τ is given by Eq.(1.55), while the quantity λ_η is defined as

$$\lambda_\eta = \frac{\langle \mathcal{W}(\theta,\phi)[1 - 3\sin^4(\theta/2)\sin^2\phi] \rangle}{\langle \mathcal{W}(\theta,\phi) \rangle} \ . \tag{1.62}$$

Note that, for any $\mathcal{W}$, the value of λ_η is restricted to the range [17, 18]

$$-2 \leq \lambda_\eta < 1 \ . \tag{1.63}$$

It has to be pointed out that the value $\lambda_\eta = 1$ is not allowed, as it corresponds to scattering taking place only between particles with parallel momenta. These processes do not alter the momentum flux, thus giving rise to a singularity in η [15].

1.4.5 Exact solution for η

As we have seen, the general equation for the transport coefficients is an integral equation for the regular part of the deviation of the distribution function from local equilibrium, Φ, due to a small gradient of the equilibrium parameters. The AK solution to this equation relied on an approximation which turned out to be uncontrolled; in fact, the resulting η was in good agreement with experimental data, while the thermal condutivity failed to reproduce the results of measurements by a factor ~ 2.

The exact analytical solution was finally given by Brooker and Sykes in 1970 [17, 18]; it turned out to be the expression of AK multiplied by a correction factor, written in the form of a power series.

The method of BS is a standard eigenfunction expansion for the integral kernel; its explicit derivation can be used for solving only this particular problem, and does

not teach us to solve a wider class of equations. For this reason, we only quote the final result, referring to the orginal papers [17, 18] and to [15] for the details of the calculation.

The BS result for η is

$$\eta = \eta_{AK} \left\{ \frac{1-\lambda_\eta}{4} \sum_{k=0}^{\infty} \frac{4k+3}{(k+1)(2k+1)[(k+1)(2k+1)-\lambda_\eta]} \right\} . \tag{1.64}$$

It is interesting to note that the explicit calculation of the correction factor for all the allowed values of λ_η, given by Eq.(1.63), yields results in the range [17, 18, 15]

$$0.750 < (\eta/\eta_{AK}) < 0.925 , \tag{1.65}$$

thus showing that the AK approximation was indeed rather good.

Chapter 2

Nuclear matter and nuclear forces

Nuclear matter can be thought of as a giant nucleus, with given numbers of protons and neutrons interacting through nuclear forces only. As the typical thermal energies are negligible compared to the nucleon Fermi energies, such a system can be safely considered to be at zero temperature.

A quantitative understanding of the properties of nuclear matter, whose calculation is greatly simplified by translational invariance, is needed both as an intermediate step towards the description of real nuclei and for the development of realistic models of matter in the neutron star core.

The large body of data on nuclear masses can be used to extract empirical information on the equilibrium properties of symmetric nuclear matter (SNM), consisting of equal numbers of protons and neutrons.

The A-dependence of the binding energy of nuclei of mass number A and electric charge Z is well described by the semiempirical mass formula

$$\frac{B}{A} = \frac{1}{A}\left[\, a_{\rm V}A - a_{\rm s}A^{2/3} - a_{\rm c}\frac{Z^2}{A^{1/3}} - a_A\frac{(A-2Z)^2}{4A} + \lambda\; a_{\rm p}\frac{1}{A^{1/2}}\,\right] \ . \qquad (2.1)$$

In the $A \to \infty$ limit, and neglecting the effect of Coulomb repulsion between protons, the only contribution surviving in the case $Z = A/2$ is the term linear in A. Hence, the coefficient a_V can be identified with the binding energy per particle of SNM.

The equilibrium density of SNM, ρ_0, can be inferred exploiting the saturation of nuclear densities, i.e. the experimental observation that the central charge density of atomic nuclei, measured by elastic electron-nucleus scattering, does not depend upon A for large A. This property is illustrated in Fig. 2.1.

The empirical values of the binding energy and equilibrium density of SNM are

$$\rho_0 = 0.16\,{\rm fm}^{-3} \ \ , \ \ E = -15.7\,{\rm MeV} \ . \qquad (2.2)$$

In principle, additional information can be obtained from measurements of the excitation energies of nuclear vibrational states, yielding the (in)-compressibility module

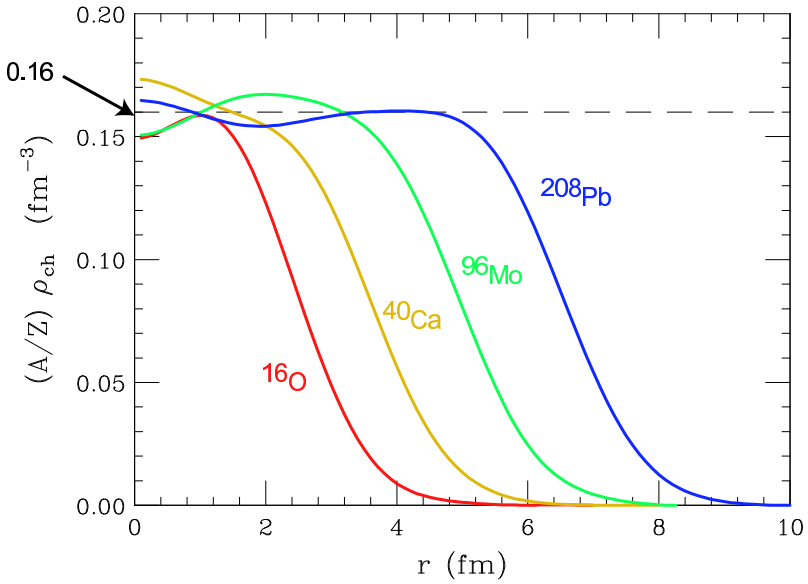

Figure 2.1. Saturation of central nuclear densities measured by elastic electron-nucleus scattering.

K. However, the data analyis of these experiments is non trivial, and the resulting values of K range from $K \sim 200$ MeV (corresponding to more compressible nuclear matter, i.e. to a *soft* equation of state (EOS)) to $K \sim 300$ MeV (corresponding to a *stiff* EOS) [22].

The main goal of nuclear matter theory is deriving a EOS at zero temperature (i.e. the density dependence of the binding energy per particle $E = E(\rho)$) capable to explain the above data starting from the elementary nucleon-nucleon (NN) interaction. However, many important applications of nuclear matter theory require that its formalism be also flexible enough to describe the properties of matter at finite temperature, including the transport coefficients introduced in Chapter 1.

Unfortunately, due to the coplexity of the fundamental theory of strong interactions, the quantum chromo-dynamics (QCD), an *ab initio* description of nuclear matter at finite density and zero temperature is out of reach of the present computational techniques. As a consequence, one has to rely on dynamical models in which nucleons and mesons play the role of effective degrees of freedom.

In this work we adopt the approach based on nonrelativistic quantum mechanics and phenomenological nuclear hamiltonians, that allows for a quantitative description of both the two-nucleon bound state and the nucleon-nucleon scattering data.

After a short introduction on the astrophysical relevance of nuclear matter, in this Chapter we outline the main features of nuclear interactions and briefly describe the structure of the NN potential models employed in many-body calculations.

2.1 Neutron star matter

As stated in the Introduction, this work is mainly aimed at applying nuclear matter theory to the study of properties relevant to the structure and stability of neutron stars. Therefore, we start with a brief review on these astrophysical objects [23].

The existence of compact stars made of neutrons is said to have been conjectured by Bohr, Landau and Rosenfeld right after the discovery of the neutron, by Chadwick, in 1932. In 1934, it was suggested by Baade and Zwicky that a neutron star may be formed in the aftermath of a supernova explosion. Neutron stars were finally observed in 1968 as pulsars, radio souces blinking on and off at a constant frequency.

Neutron stars are believed to be one of the possible endpoints of stellar evolution. The first quantitative study of neutron star structure was carried out by Oppenheimer and Volkov in 1939, within the framework of general relativity. Combining Einstein's equations and hydrostatic equilibrium, they found that the mass of a star consisting of noninteracting neutrons cannot exceed the value $\sim 0.8\,M_\odot$, where $M_\odot$ is the mass of the Sun. The idea of a critical mass had been already introduced by Chandrasekar in the theory of white dwarfs, stellar objects mainly made of degenerate electrons, in which the gravitational contraction is balanced by the pressure due to the fermionic nature of its consituents. However, the critical mass found by Oppenheimer and Volkov turns out to be much smaller than the observed neutron star masses (typically $\sim 1.4\,M_\odot$): this fact clearly shows that, at the density typical of neutron stars (of the order of ρ_0, corresponding to matter density $\sim 2\ 10^{14}$ g/cm^3), strong interactions between nucleons cannot be disregarded, as they provide an additional contribution to the pressure of dynamical origin.

The internal structure of neutron stars, schematically represented in Fig. 2.2, features a sequence of layers of different composition. While the properties of matter in the outer crust, corresponding to densities ranging from $\sim 10^7$ g/cm^3 to the neutron drip density $\sim 4\ 10^{11}$ g/cm^3, can be obtained directly from nuclear data, models of the EOS at $4\ 10^{11} < \rho < 2\ 10^{14}$ g/cm^3 are somewhat based on extrapolations of the available empirical information, as the extremely neutron rich nuclei appearing in this density regime are not observed on earth.

The density of the neutron star core ranges between $\sim \rho_0$, at the boundary with the inner crust, and a central value that can be as large as $1 \div 4\ 10^{15}$ g/cm^3. All models of EOS based on hadronic degrees of freedom predict that in the density range $\rho_0 \lesssim \rho \lesssim 2\rho_0$ neutron star matter consists mainly of neutrons, with the admixture of a small number of protons, electrons and muons. At any given density the fraction of protons and leptons is determined by the requirements of weak equilibrium and charge neutrality. Most calculations suggest that this fraction is rather small, of the order of $\sim 10\%$. Hence, for many applications, modelling neutron star matter with pure neutron matter can be regarded as a reasonable approximation.

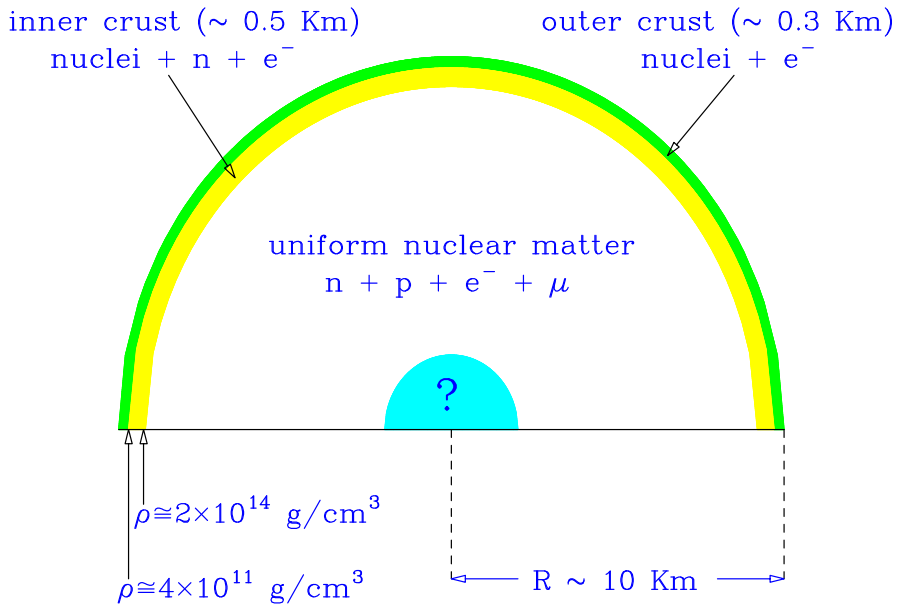

Figure 2.2. Schematic representation of the cross section of a nuetron star.

This picture may change significantly at larger density with the appearance of heavy strange baryons produced in weak interaction processes. For example, although the mass of the Σ^- exceeds the neutron mass by more than 250 MeV, the reaction $n + e^- \rightarrow \Sigma^- + \nu_e$ is energetically allowed as soon as the sum of the neutron and electron chemical potentials becomes equal to the Σ^- chemical potential.

Finally, as nucleons are known to be composite objects of size $\sim 0.5 - 1.0$ fm, corresponding to a density $\sim 10^{15}$ g/cm^3, it is expected that, if the density in the neutron star core reaches this value, matter undergoes a transition to a new phase, in which quarks are no longer clustered into nucleons or hadrons.

Ideally, one may be able to infer the composition and the EOS of neutron star matter from observations. For example, the knowledge of mass and radius of a neutron star would allow one to severely constrain the EOS. However, while many neutron star masses have been measured with remarkable accuracy (a compilation of the data is shown in Fig. 2.3), the experimental determination of the radii involves seriuos difficulties, and the available estimates are still controversial.

The large interferometric gravitational wave detectors are also expected to provide relevant information on neutron star. The results of theoretical calculations suggest that, as the gravitational wave signal contains information on the frequency and damping times of the star quasi-normal oscillation modes, its detection may shed light on the structure and dynamics of the emitting stars [25, 26, 27]. As

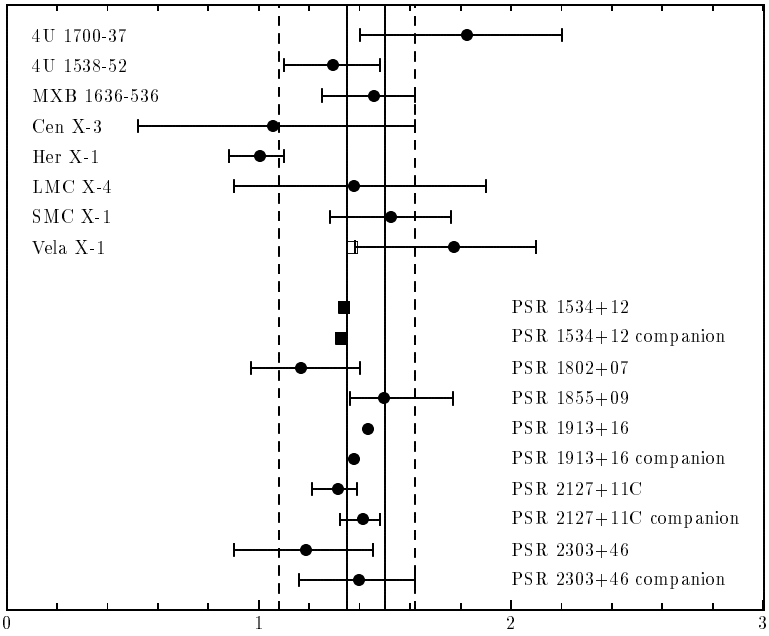

Figure 2.3. Compilation of measured neutron star masses, given in units of solar mass [24].

pointed out in the Introduction, understanding neutron star oscillation modes and the role played by viscosity in their damping is in fact one of the main motivations of our work.

2.2 Nuclear forces

The main features of the NN interaction, inferred from the analysis of nuclear systematics, may be summarized as follows.

- The *saturation* of nuclear density (see Fig. 2.1), i.e. the fact that density in the interior of atomic nuclei is nearly constant and independent of the mass number A, tells us that nucleons cannot be packed together too tightly. Hence, at short distance the NN force must be repulsive. Assuming that the interaction can be described by a nonrelativistic potential v depending on the interparticle distance, $\mathbf{r}$, we can then write:

$$v(\mathbf{r}) > 0 \quad , \quad |\mathbf{r}| < r_c \ , \tag{2.3}$$

  r_c being the radius of the repulsive core.

- The fact that the nuclear binding energy per nucleon is roughly the same for all nuclei with $A \geq 20$, its value being

$$\frac{B}{A} \sim 8.5 \text{ MeV} , \tag{2.4}$$

suggests that the NN interaction has a finite range r_0, i.e. that

$$v(\mathbf{r}) = 0 \quad , \quad |\mathbf{r}| > r_0 . \tag{2.5}$$

- The spectra of the so called *mirror nuclei*, i.e. pairs of nuclei having the same A and charges differing by one unit (implying that the number of protons in a nucleus is the same as the number of neutrons in its mirror companion), e.g. $^{15}_{7}$N ($A = 15$, $Z = 7$) and $^{15}_{8}$O ($A = 15$, $Z = 8$), exhibit striking similarities. The energies of the levels with the same parity and angular momentum are the same up to small electromagnetic corrections, showing that protons and neutrons have similar nuclear interactions, i.e. that nuclear forces are *charge symmetric*.

Charge symmetry is a manifestation of a more general property of the NN interaction, called *isotopic invariance*. Neglecting the small mass difference, proton and neutron can be viewed as two states of the same particle, the nucleon (N), described by the Dirac equation obtained from the lagrangiam density

$$\mathcal{L} = \bar{\psi}_N \left(i\gamma^\mu \partial_\mu - m \right) \psi_N \tag{2.6}$$

where

$$\psi_N = \begin{pmatrix} p \\ n \end{pmatrix} , \tag{2.7}$$

p and n being the four-spinors associated with the proton and the neutron, respectively. The lagrangian density (2.6) is invariant under the $SU(2)$ global phase transformation

$$U = \mathrm{e}^{i\alpha_j \tau_j} , \tag{2.8}$$

where $\boldsymbol{\alpha}$ is a constant (i.e. independent of x) vector and the τ_j (j = 1,2,3) are Pauli matrices (whose properties are briefly collected in Appendix A). The above equations show that the nucleon can be described as a doublet in isospin space. Proton and neutron correspond to isospin projections $+1/2$ and $-1/2$, respectively. Proton-proton and neutron-neutron pairs always have total isospin T=1 whereas a proton-neutron pair may have either $T = 0$ or $T = 1$. The two-nucleon isospin states $|T,M_T\rangle$ can be summarized as follows (see also Appendix A)

$$|1,1\rangle \;\; = \;\; |pp\rangle$$

$$
\begin{aligned}
|1,0\rangle &= \frac{1}{\sqrt{2}}\left(|pn\rangle + |np\rangle\right) \\
|1,-1\rangle &= |nn\rangle \\
|0,0\rangle &= \frac{1}{\sqrt{2}}\left(|pn\rangle - |np\rangle\right) \ .
\end{aligned}
$$

Isospin invariance implies that the interaction between two nucleons separated by a distance $r = |\mathbf{r}_1 - \mathbf{r}_2|$ and having total spin S depends on their total isospin T but not on its projection M_T. For example, the potential $v(\mathbf{r})$ acting between two protons with spins coupled to $S = 0$ is the same as the potential acting between a proton and a neutron with spins and isospins coupled to $S = 0$ and $T = 1$.

2.2.1 The two-nucleon system

The details of the NN interaction can be best understood in the two-nucleon system. There is *only one* NN bound state, the nucleus of deuterium, or deuteron (^{2}H), consisting of a proton and a neutron coupled to total spin and isospin $S = 1$ and $T = 0$, respectively. This is a clear manifestation of the *spin dependence* of nuclear forces.

Another important piece of information can be inferred from the observation that the deuteron exhibits a nonvanishing electric quadrupole moment, implying that its charge distribution is not spherically symmetric. Hence, the NN interaction is *noncentral*.

Besides the properties of the two-nucleon bound state, the large data base of phase shifts measured in NN scattering experiments (the Nijmegen data base [28] includes $\sim$ 4000 data points, corresponding to energies up to 350 MeV in the lab frame) provides valuable additional information on the nature of NN forces.

The theoretical description of the NN interaction was first attempted by Yukawa in 1935. He made the hypotesis that nucleons interact through the exchange of a particle, whose mass μ can be related to the interaction range r_0 according to

$$
r_0 \sim \frac{1}{\mu} \ . \tag{2.9}
$$

Using $r_0 \sim 1$ fm, the above relation yields $\mu \sim 200$ MeV (1 fm$^{-1} = 197.3$ MeV).

Yukawa's idea has been successfully implemented identifying the exchanged particle with the π meson (or *pion*), discovered in 1947, whose mass is $m_\pi \sim 140$ MeV. Experiments show that the pion is a spin zero pseudoscalar particle[1] (i.e. it has spin-parity 0^-) that comes in three charge states, denoted π^+, π^- and π^0. Hence, it

[1]The pion spin has been deduced from the balance of the reaction $\pi^+ + {}^2\mathrm{H} \leftrightarrow p + p$, while its intrinsic parity was determined observing the π^- capture from the K shell of the deuterium atom, leading to the appearance of two neutrons: $\pi^- + d \rightarrow n + n$.

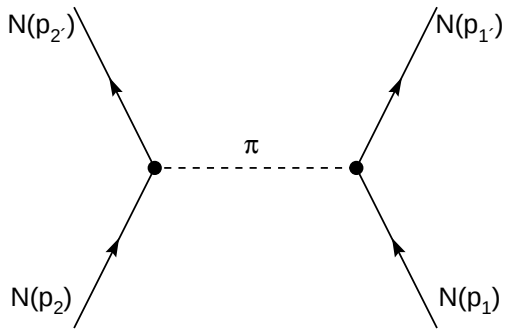

Figure 2.4. Feynman diagram describing the one-pion-exchange process between two nucleons. The corresponding amplitude is given by Eq. (2.10).

can be regarded as an isospin T=1 triplet, the charge states being associated with isospin projections M_T=+ 1, 0 and −1, respectively.

The simplest π-nucleon coupling compatible with the observation that nuclear interactions conserve parity has the pseudoscalar form $ig\gamma^5\boldsymbol{\tau}$, where g is a coupling constant and $\boldsymbol{\tau}$ describes the isospin of the nucleon. With this choice for the interaction vertex, the amplitude of the process depicted in Fig. 2.4 can readily be written, using standard Feynman's diagram techniques, as

$$\langle f|M|i\rangle = -ig^2\ \frac{\bar{u}(p_2',s_2')\gamma_5 u(p_2,s_2)\bar{u}(p_1',s_1')\gamma_5 u(p_1,s_1)}{k^2-m_\pi^2}\ \langle\boldsymbol{\tau}_1\cdot\boldsymbol{\tau}_2\rangle\ , \tag{2.10}$$

where $k = p_1' - p_1 = p_2 - p_2'$, $k^2 = k_\mu k^\mu = k_0^2 - |\mathbf{k}|^2$, $u(p,s)$ is the Dirac spinor associated with a nucleon of four momentum $p \equiv (\mathbf{p},E)$ (E=$\sqrt{\mathbf{p}^2+m^2}$) and spin projection s and

$$\langle\boldsymbol{\tau}_1\cdot\boldsymbol{\tau}_2\rangle = \eta_{2'}^\dagger\boldsymbol{\tau}\eta_2\ \eta_{1'}^\dagger\boldsymbol{\tau}\eta_1\ , \tag{2.11}$$

η_i being the two-component Pauli spinor describing the isospin state of particle i.

In the nonrelativistic limit, Yukawa's theory leads to define a NN interaction potential that can be written in coordinate space as

$$\begin{aligned} v_\pi &= \frac{g^2}{4m^2}\ (\boldsymbol{\tau}_1\cdot\boldsymbol{\tau}_2)(\boldsymbol{\sigma}_1\cdot\boldsymbol{\nabla})(\boldsymbol{\sigma}_2\cdot\boldsymbol{\nabla})\ \frac{e^{-m_\pi r}}{r} \\ &= \frac{g^2}{(4\pi)^2}\ \frac{m_\pi^3}{4m^2}\ \frac{1}{3}(\boldsymbol{\tau}_1\cdot\boldsymbol{\tau}_2)\left\{\left[(\boldsymbol{\sigma}_1\cdot\boldsymbol{\sigma}_2)+S_{12}\left(1+\frac{3}{x}+\frac{3}{x^2}\right)\right]\frac{e^{-x}}{x}\right. \\ &\qquad \left. -\frac{4\pi}{m_\pi^3}(\boldsymbol{\sigma}_1\cdot\boldsymbol{\sigma}_2)\delta^{(3)}(\mathbf{r})\right\}\ , \end{aligned} \tag{2.12}$$

where $x = m_\pi |\mathbf{r}|$ and

$$S_{12} = \frac{3}{r^2}(\boldsymbol{\sigma}_1 \cdot \mathbf{r})(\boldsymbol{\sigma}_2 \cdot \mathbf{r}) - (\boldsymbol{\sigma}_1 \cdot \boldsymbol{\sigma}_2) \ , \tag{2.13}$$

reminiscent of the operator describing the noncentral interaction between two magnetic dipoles, is called the tensor operator. The properties of S_{12} are described in Appendix A

For $g^2/(4\pi) \sim 14$, the above potential provides an accurate description of the long range part ($|\mathbf{r}| > 1.5$ fm) of the NN interaction, as shown by the very good fit of the NN scattering phase shifts in states of high angular momentum. In these states, due to the strong centrifugal barrier, the probability of finding the two nucleons at small relative distances becomes in fact negligibly small.

At medium- and short-range other more complicated processes, involving the exchange of two or more pions (possibly interacting among themselves) or heavier particles (like the ρ and the ω mesons, whose masses are $m_\rho = 770$ MeV and $m_\omega = 782$ MeV, respectively), have to be taken into account. Moreover, when their relative distance becomes very small ($|\mathbf{r}| \lesssim 0.5$ fm) nucleons, being composite and finite in size, are expected to overlap. In this regime, NN interactions should in principle be described in terms of interactions between nucleon constituents, i.e. quarks and gluons, as dictated by QCD.

Phenomenological potentials describing the *full* NN interaction are generally written as

$$v = \widetilde{v}_\pi + v_R \tag{2.14}$$

where $\widetilde{v}_\pi$ is the one-pion-exchange potential, defined by Eqs. (2.12) and (2.13), stripped of the δ-function contribution, whereas v_R describes the interaction at medium and short range. The spin-isospin dependence and the noncentral nature of the NN interactions can be properly described rewriting Eq. (2.14) in the form

$$v(ij) = \sum_{ST} \left[v_{TS}(r_{ij}) + \delta_{S1} v_{tT}(r_{ij}) S_{12} \right] P_{2S+1} \Pi_{2T+1} \ , \tag{2.15}$$

S and T being the total spin and isospin of the interacting pair, respectively. In the above equation P_{2S+1} ($S = 0,1$) and Π_{2T+1} ($T = 0,1$) are the spin and isospin projection operators, whose definition and properties are given in Appendix A.

The functions $v_{TS}(r_{ij})$ and $v_{tT}(r_{ij})$ describe the radial dependence of the interaction in the different spin-isospin channels and reduce to the corresponding components of the one-pion-exchange potential at large r_{ij}. Their shapes are chosen in such a way as to reproduce the available NN data (deuteron binding energy, charge radius and quadrupole moment and the NN scattering data).

An alternative representation of the NN potential, based on the set of six operators (see Appendix A)

$$O_{ij}^{n \leq 6} = [1, (\boldsymbol{\sigma}_i \cdot \boldsymbol{\sigma}_j), S_{ij}] \otimes [1, (\boldsymbol{\tau}_i \cdot \boldsymbol{\tau}_j)] \ , \tag{2.16}$$

is given by

$$v(ij) = \sum_{n=1}^{6} v^{(n)}(r_{ij}) O_{ij}^{(n)} \ . \tag{2.17}$$

While the static potential of Eq.(2.17) provides a reasonable account of deuteron properties, in order to describe NN scattering in S and P wave, one has to include the two additional momentum dependent operators

$$O_{ij}^{n=7,8} = \mathbf{L} \cdot \mathbf{S} \otimes [1, (\boldsymbol{\tau}_i \cdot \boldsymbol{\tau}_j)] \ , \tag{2.18}$$

L being the orbital angular momentum.

The potentials yielding the best available fits of NN scattering data, with a χ^2/datum ~ 1, are written in terms of eighteen operators, with

$$O_{ij}^{n=9,\ldots,14} = [\mathbf{L}^2, \mathbf{L}^2(\boldsymbol{\sigma}_i \cdot \boldsymbol{\sigma}_j), (\mathbf{L} \cdot \mathbf{S})^2] \otimes [1, \boldsymbol{\tau}_i \cdot \boldsymbol{\tau}_j] \ , \tag{2.19}$$

$$O_{ij}^{n=15,\ldots,18} = [1, \boldsymbol{\sigma}_i \cdot \boldsymbol{\sigma}_j, S_{ij}] \otimes T_{ij} \ , \ (\tau_{zi} + \tau_{zj}) \tag{2.20}$$

where

$$T_{ij} = \frac{3}{r^2} (\boldsymbol{\tau}_i \cdot \mathbf{r})(\boldsymbol{\tau}_j \cdot \mathbf{r}) - (\boldsymbol{\tau}_i \cdot \boldsymbol{\tau}_j) \ . \tag{2.21}$$

The $O_{ij}^{n=15,\ldots,18}$ take care of small charge symmetry breaking effects, due to the different masses and coupling constants of the charged and neutral pions.

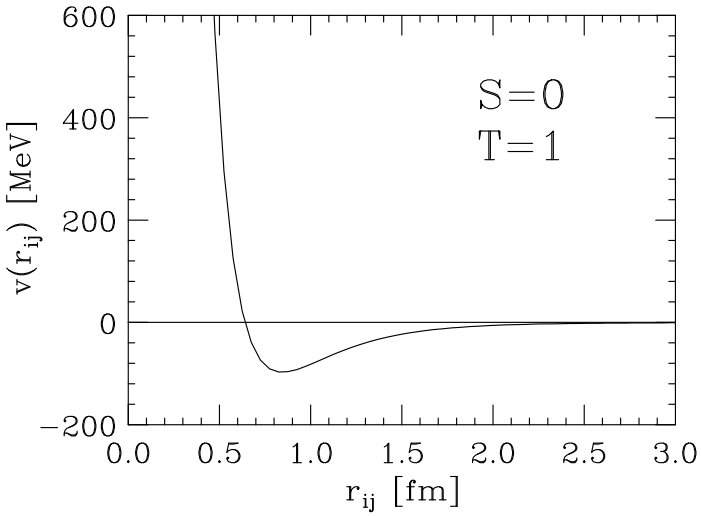

Figure 2.5. Radial dependence of the NN potential describing the interaction between two nucleons in the state of relative angular momentum $\ell = 0$, and total spin and isospin $S = 0$ and $T = 1$.

The calculations discussed in this Thesis are based on a widely employed potential model, obtained within the phenomenological approach outlined in this Section, generally referred to as Argonne v_{18} potential [29]. It is written in the form

$$v(ij) = \sum_{n=1}^{18} v^n(r_{ij}) O_{ij}^n \ . \tag{2.22}$$

As an example of the quality of the phase shifts obtained from the Argonne v_{18} potential, in Fig. 2.6 we show the results for the $^1S_0$ and $^1D_2$ partial waves (see Appendix D), compared with the predictions of the one-pion-exchange model (OPEP).

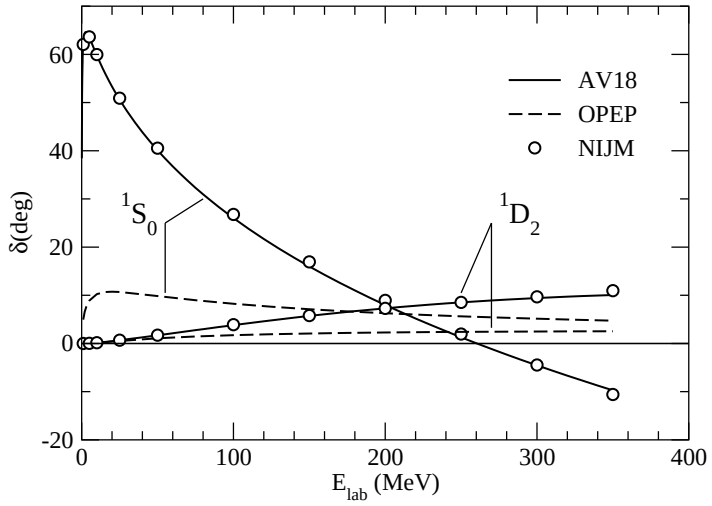

Figure 2.6. Comparison between the $^1S_0$ and $^1D_2$ phase shifts resulting from the Nijmegen analysis [28] (open circles) and the predictions of the Argonne v_{18} (AV18) and one-pion-exchange (OPEP) potentials.

We have also used a simplified version of the above potential, obtained including the operators $O_{ij}^{n\leq 8}$, originally proposed in Ref.[30]. It reproduces the scalar part of the full interaction in all S and P waves, as well as in the $^3D_1$ wave and its coupling to the $^3S_1$.

The typical shape of the NN potential in the state of relative angular momentum $\ell = 0$ and total spin and isospin $S = 0$ and $T = 1$ is shown in Fig. 2.5. The short-range repulsive core, to be ascribed to heavy-meson exchange or to more complicated mechanisms involving nucleon constituents, is followed by an intermediate-range attractive region, largely due to two-pion-exchange processes. Finally, at large interparticle distance the one-pion-exchange mechanism dominates.

2.2.2 Three-nucleon interactions

The NN potential determined from the properties of the two-nucleon system can be used to solve the many-body nonrelativistic Schrödinger equation for $A > 2$. In the case $A = 3$ the problem can be still solved exactly, but the resulting ground state energy, E_0, turns out to be slightly different from the experimental value. For example, for ^{3}He one typically finds $E_0 = 7.6$ MeV, to be compared to $E_{exp} = 8.48$ MeV. In order to exactly reproduce E_{exp} one has to add to the nuclear hamiltonian a term containing three-nucleon interactions described by a potential V_{ijk}. The most important process leading to three-nucleon interactions is two-pion exchange associated with the excitation of a nucleon resonance in the intermediate state, depicted in Fig. 2.7.

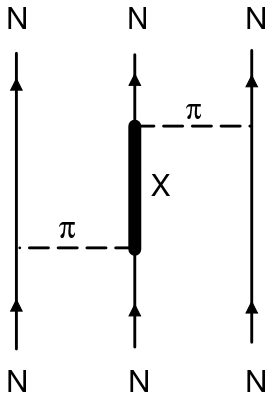

Figure 2.7. Diagrammatic representation of the process providing the main contribution to the three-nucleon interaction. The thick solid line corresponds to an excited state of the nucleon.

The three-nucleon potential is usually written in the form

$$V_{ijk} = V_{ijk}^{2\pi} + V_{ijk}^{N} \ , \tag{2.23}$$

where the first contribution takes into account the process of Fig. 2.7 while V_{ijk}^N is purely phenomenological. The two parameters entering the definition of the three-body potential are adjusted in such a way as to reproduce the properties of ^{3}H and ^{3}He [31]. Note that the inclusion of V_{ijk} leads to a very small change of the total potential energy, the ratio $\langle v_{ij} \rangle / \langle V_{ijk} \rangle$ being ~ 2 %.

For $A > 3$ the Scrödinger equation is no longer exactly solvable. However, very accurate solutions can be obtained using stochastic techniques, such as variational Monte Carlo (VMC) and the Green function Monte Carlo (GFMC) methods [32].

The GFMC approach has been succesfully employed to describe the ground state and the low lying excited states of nuclei having A up to 8. The results of VMC and

GFMC calculations, summarized in Fig. 2.8, show that the nonrelativistic approach, based on a dynamics modeled to reproduce the properties of two- and three-nucleon systems, has a remarkable predictive power.

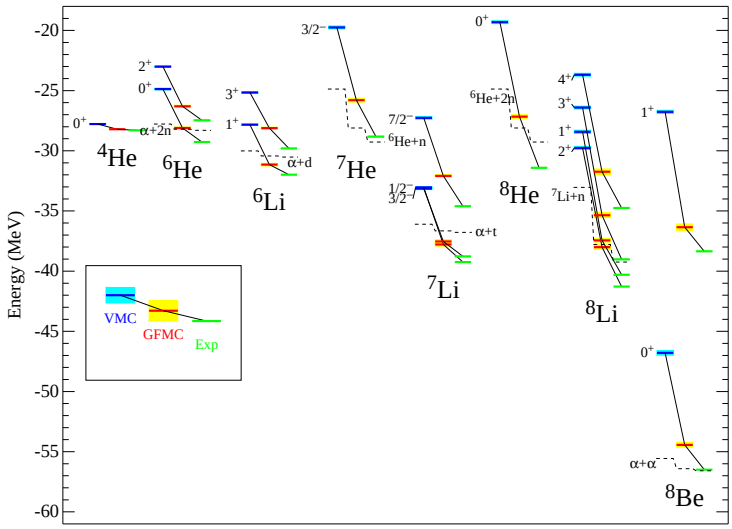

Figure 2.8. VMC and GFMC energies of nuclei with $A \leq 8$ compared to experiment (from Ref.[32]).

Chapter 3

Nuclear matter theory

Understanding the properties of matter at densities comparable to the central density of atomic nuclei is made difficult by *both* the complexity of the interactions *and* the approximations implied in any theoretical description of quantum mechanical many-particle systems.

The main problem associated with the use of the nuclear potential models described in Chapter 2 in a many-body calculation lies in the strong repulsive core of the NN force, which cannot be handled within standard perturbation theory.

Within nonrelativistic many-body theory (NMBT), a nuclear system is seen as a collection of pointlike protons and neutrons whose dynamics are described by the hamiltonian

$$H = \sum_i t(i) + \sum_{j>i} v(ij) + \dots \ , \tag{3.1}$$

where $t(i)$ and $v(ij)$ denote the kinetic energy operator and the *bare* NN potential, respectively, while the ellipses refer to the presence of additional many-body interactions (see Chapter 2).

Carrying out perturbation theory in the basis provided by the eigenstates of the noninteracting system requires a renormalization of the NN potential. This is the foundation of the widely employed approach developed by Brückner, Bethe and Goldstone, in which $v(ij)$ is replaced by the well-behaved G-matrix, describing NN scattering in the nuclear medium (see, e.g. Ref.[33]). Alternatively, the many-body Schrödinger equation, with the hamiltonian of Eq.(3.1), can be solved using either the variational method or stochastic techniques. These approaches have been succesfully applied to the sudy of both light nuclei [32] and uniform neutron and nuclear matter [7, 34, 35, 36].

Our work has been carried out using a scheme, formally similar to standard perturbation theory, in which nonperturbative effects due to the short-range repulsion are embodied in the basis functions. The details of this approach will be discussed in the following Sections.

It has to be emphasized that within NMBT the interaction is completely determined by the analysis of the exactly solvable two- and few-nucleon systems. As a consequence, the uncertainties associated with the dynamical model and the many-body calculations are decoupled, and the properties of nuclear systems ranging from deuteron to neutron stars can be obtained in a fully consistent fashion, without including any adjustable parameters.

3.1 Correlated basis function theory

The *correlated* states of nuclear matter are obtained from the Fermi gas (FG) states $|n_{FG}\rangle$ through the transformation [37, 38]

$$|n) = \frac{F|n_{\rm FG}\rangle}{\langle n_{\rm FG}|F^\dagger F|n_{\rm FG}\rangle^{1/2}} \ . \tag{3.2}$$

The operator F, embodying the correlation structure induced by the NN interaction, is written in the form

$$F(1,\ldots,N) = \mathcal{S} \prod_{j>i=1}^{N} f_{ij} \ , \tag{3.3}$$

where $\mathcal{S}$ is the symmetrization operator which takes care of the fact that, in general,

$$[f_{ij},f_{ik}] \neq 0 \ . \tag{3.4}$$

The structure of the two-body *correlation functions* f_{ij} must reflect the complexity of the NN potential. Hence, it is generally cast in the form (compare to Eq.(2.17))

$$f_{ij} = \sum_{n=1}^{6} f^n(r_{ij}) O_{ij}^n \ , \tag{3.5}$$

with the O_{ij}^n defined by Eq.(2.16). Note that the operators included in the above definition provide a fairly accurate description of the correlation structure of the two-nucleon bound state. The shape of the radial functions $f^n(r_{ij})$ is determined through functional minimization of the expectation value of the nuclear hamiltonian in the correlated ground state

$$E_0^V = (0|H|0) \ . \tag{3.6}$$

The correlated states defined in Eq.(3.2) are not orthogonal to one another. However, they can be orthogonalized using an approach, based on standard techniques of many-body theory, that preserves diagonal matrix elements of the hamiltonian [39].

Denoting the orthogonalized states by $|n\rangle$, the procedure of Ref. [39] amounts to defining a transformation $\widehat{T}$ such that

$$|n) \rightarrow |n\rangle = \widehat{T}|n) \ , \tag{3.7}$$

with

$$(n|H|n) = \langle n|H|n\rangle \ . \tag{3.8}$$

Correlated basis function (CBF) perturbation theory is based on the decomposition of the nuclear hamiltonian

$$H = H_0 + H_I \ , \tag{3.9}$$

where H_0 and H_I denote the diagonal and off-diagonal components of H, respectively, defined by the equations

$$\langle m|H_0|n\rangle = \delta_{mn}\langle m|H|n\rangle \ , \tag{3.10}$$

$$\langle m|H_I|n\rangle = (1-\delta_{mn})\langle m|H|n\rangle \ . \tag{3.11}$$

The above definitions obviously imply that, if the correlated states have large overlaps with the eigenstates of H, the matrix elements of H_I are small, and the perturbative expansions in powers of H_I is rapidly convergent.

Let us consider, for example, the Green function describing the propagation of a nucleon in a hole state [40]

$$G(\mathbf{k},E) = \langle\widetilde{0}|a^\dagger_{\mathbf{k}} \ \frac{1}{H-E_0-E-i\eta} \ a_{\mathbf{k}}|\widetilde{0}\rangle / \langle\widetilde{0}|\widetilde{0}\rangle \ . \tag{3.12}$$

In the above equation, $\eta = 0^+$, $a^\dagger_{\mathbf{k}}$ and $a_{\mathbf{k}}$ are creation and annihilation operators and the *exact* ground state $|\widetilde{0}\rangle$, satisfying the Schrödinger equation $H|\widetilde{0}\rangle = E_0|\widetilde{0}\rangle$ can be obtained from the expansion [41, 42]

$$|\widetilde{0}\rangle = \sum_n (-)^n \left(\frac{H_I - \Delta E_0}{H_0 - E_0^V}\right)^n |0\rangle \ , \tag{3.13}$$

where $\Delta E_0 = E_0 - E_0^V$, with E_0^V defined by Eq.(3.6).

In principle, using Eq.(3.13) and the similar expansion [41, 42]

$$\frac{1}{H-E_0-E-i\eta} = \frac{1}{H_0-E_0^V-E-i\eta} \ \sum_n (-)^n \left(\frac{H_I-\Delta E_0}{H_0-E_0^V-E-i\eta}\right)^n \ , \tag{3.14}$$

the Green function can be consistently computed at any order in H_I. However, the calculation of the matrix elements of the hamiltonian appearing in Eqs.(3.12)-(3.14) involves prohibitive difficulties and requires the development of a suitable approximation scheme, to be discussed in the following Section.

3.2 Cluster expansion formalism

The correlation operator of Eq.(3.3) is defined in such a way that, if any subset of the particles, say $i_1, \ldots i_p$, is removed far from the remaining $i_{p+1}, \ldots i_N$, it factorizes according to

$$F(1,\ldots,N) \to F_p(i_1,\ldots i_p)F_{N-p}(i_{p+1},\ldots i_N) \ . \tag{3.15}$$

The above property is the basis of the cluster expansion formalism, that allows one to write the matrix element of a many-body operator between correlated states as a sum, whose terms correspond to contributions arising from isolated subsystems (clusters) involving an increasing number of particles.

Let us consider the expectation value of the hamiltonian in the correlated state $|0\rangle$, defined as in Eq.(3.2). We will closely follow the derivation of the corresponding cluster expansion given in Ref. [38] and neglect, for the sake of simplicity, the three body potential V_{ijk}.

The starting point is the definition of the generalized normalization integral

$$I(\beta) = \langle 0|\exp[\beta(H - T_0)]|0\rangle \ , \tag{3.16}$$

where T_0 is the FG ground state energy. Using Eq.(3.16) we can rewrite the expectation value of the hamiltonian in the form

$$\langle H\rangle = \frac{\langle 0|H|0\rangle}{\langle 0|0\rangle} = T_0 + \frac{\partial}{\partial\beta}\ln I(\beta)\bigg|_{\beta=0} \ . \tag{3.17}$$

Exploiting the cluster property of F we can also define a set of $N!/(N-p)!p!$ subnormalization integrals for each p-particle subsystem ($p = 1,\ldots,N$)

$$\begin{aligned} I_i(\beta) &= \langle i|\exp[\beta(t(1) - \epsilon_i^0)]|i\rangle \ , \\ I_{ij}(\beta) &= \langle ij|F_2^\dagger(12)\exp[\beta(t(1) + t(2) + v(12) - \epsilon_i^0 - \epsilon_j^0)]F_2(12)|ij\rangle_a \ , \\ &\vdots \\ I_{1\ldots N}(\beta) &= I(\beta) \ , \end{aligned} \tag{3.18}$$

where the indices i,j,... label states belonging to the Fermi sea, ϵ_i^0 is the kinetic energy eigenvalue associated with the state $|i\rangle$ and the subscript a refers to the fact that the corresponding two-particle state is antisymmetrized, i.e.

$$|ij\rangle_a = \frac{1}{\sqrt{2}}\ (|ij\rangle - |ji\rangle) \ . \tag{3.19}$$

To express $\ln I(\beta)$ in terms of the $\ln I_{i_1\ldots i_p}(\beta)$, we start noting that I_{ij} is close to the product of I_i and I_j. It would be equal if we could neglect the interaction,

described by the potential $v(12)$, and the correlations induced by *both* $F_2(12)$ and Pauli exclusion principle. This observation suggests that I_{ij} can be written as

$$I_{ij} = I_i I_j Y_{ij} \ . \tag{3.20}$$

Extending the same argument to the I's with more than two indices, we find

$$\begin{aligned} I_i &= Y_i \\ I_{ij} &= Y_i Y_j Y_{ij} \\ &\vdots \\ I_{1\ldots N} &= I = \prod_i Y_i \ \prod_{j>i} Y_{ij} \ldots Y_{1\ldots N} \ , \end{aligned} \tag{3.21}$$

implying

$$\ln I(\beta) = \sum_i \ln Y_i + \sum_{j>i} \ln Y_{ij} + \ldots + \ln Y_{1\ldots N} \ . \tag{3.22}$$

It can be shown [38] that each term in the rhs of Eq.(3.22) goes like N in the thermodynamic limit. In addition, the p-th term collects all individual contributions to the cluster development of $\ln I(\beta)$ involving, in a connected manner, exactly p Fermi sea orbitals. Therefore, the p-th term can be referred to as the p-body cluster contribution to $\ln I(\beta)$.

The decomposition (3.21) allows one to rewrite the expectation value of the hamiltonian in the form

$$\langle H \rangle = T_0 + (\Delta E)_2 + (\Delta E)_3 + \ldots + (\Delta E)_N \tag{3.23}$$

with

$$(\Delta E)_p = \sum_{i_1<i_2<\ldots<i_p} \frac{\partial}{\partial \beta} \ln Y_{i_1 i_2 \ldots i_p} \bigg|_{\beta=0} \ . \tag{3.24}$$

To make the last step we have to use Eq.(3.21) to express $(\Delta E)_p$ in terms of the $I_{i_1\ldots i_p}$. Substitution of the resulting expressions

$$\begin{aligned} Y_i &= I_i \\ Y_{ij} &= I_{ij}(I_i I_j)^{-1} \ , \qquad (3.25) \\ &\vdots \qquad (3.26) \end{aligned}$$

into Eq.(3.24) with $p = 2$ yields

$$(\Delta E)_2 = \sum_{i<j} \left[\frac{1}{I_{ij}} \frac{\partial I_{ij}}{\partial \beta} - \left(\frac{\partial I_i}{\partial \beta} + \frac{\partial I_j}{\partial \beta} \right) \right]_{\beta=0} = \sum_{i<j} \ w_{ij} \ , \tag{3.27}$$

with

$$w_{ij} = \langle ij| \ \frac{1}{2} F_2^\dagger(12) \left[t(1) + t(2),\ F_2(12) \right] + \text{adj} + F_2^\dagger(12) v(12) F_2(12) \ |ij\rangle_a \ , \quad (3.28)$$

where, assuming that the correlation operator be hermitean, $F_2(12) = F_2^\dagger(12) = f_{12}$ (see Eq.(3.3)).

Each term of the expansion (3.23) can be represented by a diagram featuring p vertices, representing the nucleons in the cluster, connected by lines corresponding to dynamical and statistical correlations. The terms in the resulting diagrammatic expansion can be classified according to their topological structure and selected classes of diagrams can be summed up to all orders solving a set of coupled integral equations, called Fermi hyper-netted chain (FHNC) equations [43, 44].

3.3 Effective interaction

At lowest order of CBF, the effective interaction V_{eff} is defined by the equation

$$\langle H \rangle = \langle 0_{FG} | T_0 + V_{\text{eff}} | 0_{FG} \rangle \ . \quad (3.29)$$

As the above equation suggests, the approach based on the effective interaction allows one to obtain any nuclear matter observables using perturbation theory in the FG basis. However, as discussed in the previous Section, the calculation of the hamiltonian expectation value in the correlated ground state, needed to extract V_{eff} from Eq.(3.29), involves severe difficulties.

In this Thesis we follow the procedure developed in Refs. [45, 46], whose authors derived the effective interaction by carrying out a cluster expansion of the rhs of Eq.(3.29), and keeping only the two-body cluster contribution. The resulting expression reads

$$V_{\text{eff}} = \sum_{i<j} v_{\text{eff}}(ij) = \sum_{i<j} f_{ij} \left[-\frac{1}{m} (\nabla^2 f_{ij}) - \frac{2}{m} (\boldsymbol{\nabla} f_{ij}) \cdot \boldsymbol{\nabla} + v(ij) f_{ij} \right] \ , \quad (3.30)$$

where the laplacian and the gradient operate on the relative coordinate. Note that v_{eff} defined by the above equation exhibits a momentum dependence due to the operator $(\boldsymbol{\nabla} f_{ij}) \cdot \boldsymbol{\nabla}$, yielding contributions to nuclear matter energy through the exchange terms. However, the results of numerical calculations show that these contributions are small, compared to the ones associated with the momentum independent terms. As a consequence, the results discussed in this Thesis have been obtained using only the static part of the effective interaction (3.30), i.e. setting

$$v_{\text{eff}}(ij) = f_{ij} \left(-\frac{1}{m} \nabla^2 + v(ij) \right) f_{ij} = \sum_n v_{\text{eff}}^n(r_{ij}) O_{ij}^n \ , \quad (3.31)$$

The properties of the operators O^n with $n = 1,\ldots,6$, leading to the above result, are given in Appendix A.

The definition of $v_{\rm eff}$ given by Eqs.(3.30) and (3.31) obviously neglects the effect of three-nucleon interactions, whose inclusion in the hamiltonian is known to be needed in order to explain the binding energies of the few-nucleon systems, as well as the saturation properties of nuclear matter. To circumvent this problem, we have used the approach originally proposed by Lagaris and Pandharipande [47], in which the main effect of the three-body force is simulated through a density dependent modification of the two-nucleon potential at intermediate range, where two-pion exchange is believed to be the dominant interaction mechanism. Neglecting, for simplicity, the charge-symmetry breaking components of the interaction, the resulting potential can be written in the form

$$\widetilde{v}(ij) = \sum_{n=1,14} \left[v_\pi^n(r_{ij}) + v_I^n(r_{ij}) \mathrm{e}^{-\gamma_1 \rho} + v_S^n(r_{ij}) \right] O_{ij}^n \ , \tag{3.32}$$

where v_π^n, v_I^n and v_S^n denote the long- (one-pion-exchange), intermediate- and short-range part of the potential, respectively. The above modification results in a repulsive contribution to the binding energy of nuclear matter. The authors of Ref.[47] also include the small additional attractive contribution

$$\Delta E_{TNA} = \gamma_2 \rho^2 (3 - 2\beta) \mathrm{e}^{-\gamma_3 \rho} \ , \tag{3.33}$$

with $\beta = (\rho_p - \rho_n)/(\rho_p + \rho_n)$, where ρ_p and ρ_n denote the proton and neutron density, respectively. The values of the parameters γ_1, γ_2 and γ_3 appearing in Eqs.(3.32) and (3.33) have been determined in such a way as to reproduce the binding energy and equilibrium density of nuclear matter [47].

Besides the bare two body-potential $v(ij)$, the effective interaction is determined by the correlation operators f_{ij} defined by Eq.(3.5). The shapes of the radial functions $f^n(r_{ij})$ are obtained from the functional minimization of the energy at the two-body cluster level, yielding a set of coupled differential equations to be solved with the boundary conditions

$$f^n(r_{ij} \geq d) = \left\{ \begin{array}{ll} 1 \ , & n = 1 \\ 0 \ , & n = 2,3,4 \end{array} \right. \ , \tag{3.34}$$

$$f^n(r_{ij} \geq d_t) = 0 \ , \ n = 5,6 \tag{3.35}$$

and

$$\begin{aligned} \left. \frac{df^n}{dr_{ij}} \right|_{r_{ij}=d} &= 0 \ , \ n = 1,2,3,4 \\ \left. \frac{df^n}{dr_{ij}} \right|_{r_{ij}=d_t} &= 0 \ , \ n = 5,6 \ , \end{aligned} \tag{3.36}$$

d and $d_t > d$ being variational parameters. The above conditions simply express the requirements that i) for relative distances larger than the interaction range the two-nucleon wave function reduces to the one describing non interacting particles and ii) tensor interactions have longer range.

For any given value of nuclear matter density, we have solved the Euler-Lagrange equations, whose form is given in Appendix C, using the values of d and d_t obtained by the authors of Ref.[7] through a highly accurate minimization, carried out within the FHNC-SOC scheme [48].

The results corresponding to nuclear matter at equilibrium density are illustrated in Fig.3.1, showing the central component of the correlation functions acting between a pair of nucleon carriyng total spin and isospin S and T, respectively. The relations between the f_{TS} of Fig.3.1 and the f^n of Eq.(3.5) are given in Appendix A. The shapes of the f_{TS} clearly reflect the nature of the interaction. In the $T = 0$ $S = 0$ channel, in which the potential exhibits a strong repulsive core, the correlation function is very small at $r \lesssim 0.5$ fm. On the other hand, in the $T = 0$ $S = 1$ channel, the spin-isospin state corresponding to the deuteron, the repulsive core is much weaker and the potential becomes attractive at $r \gtrsim 0.7$ fm. As a consequence, the correlation function does not approach zero as $r \to 0$ and exceeds unity at intermediate range.

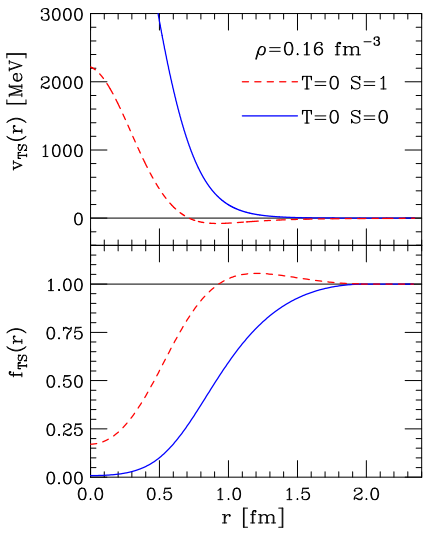

Figure 3.1. Interaction potentials (upper panel) and correlation functions (lower panel) acting in the spin-isospin channels $S = 0$ and $T = 0$ (solid lines) and $S = 0$ and $T = 1$ (dashed lines). The potential is the Argonne v_8' and the correlation functions correspond to nuclear matter at equilibrium density.

In Fig.3.2 the components of the effective interaction at equilibrium density are compared to the corresponding components of the truncated v_8' potential. It clearly appears that screeening effects due to NN correlations lead to a significant quenching of the interaction.

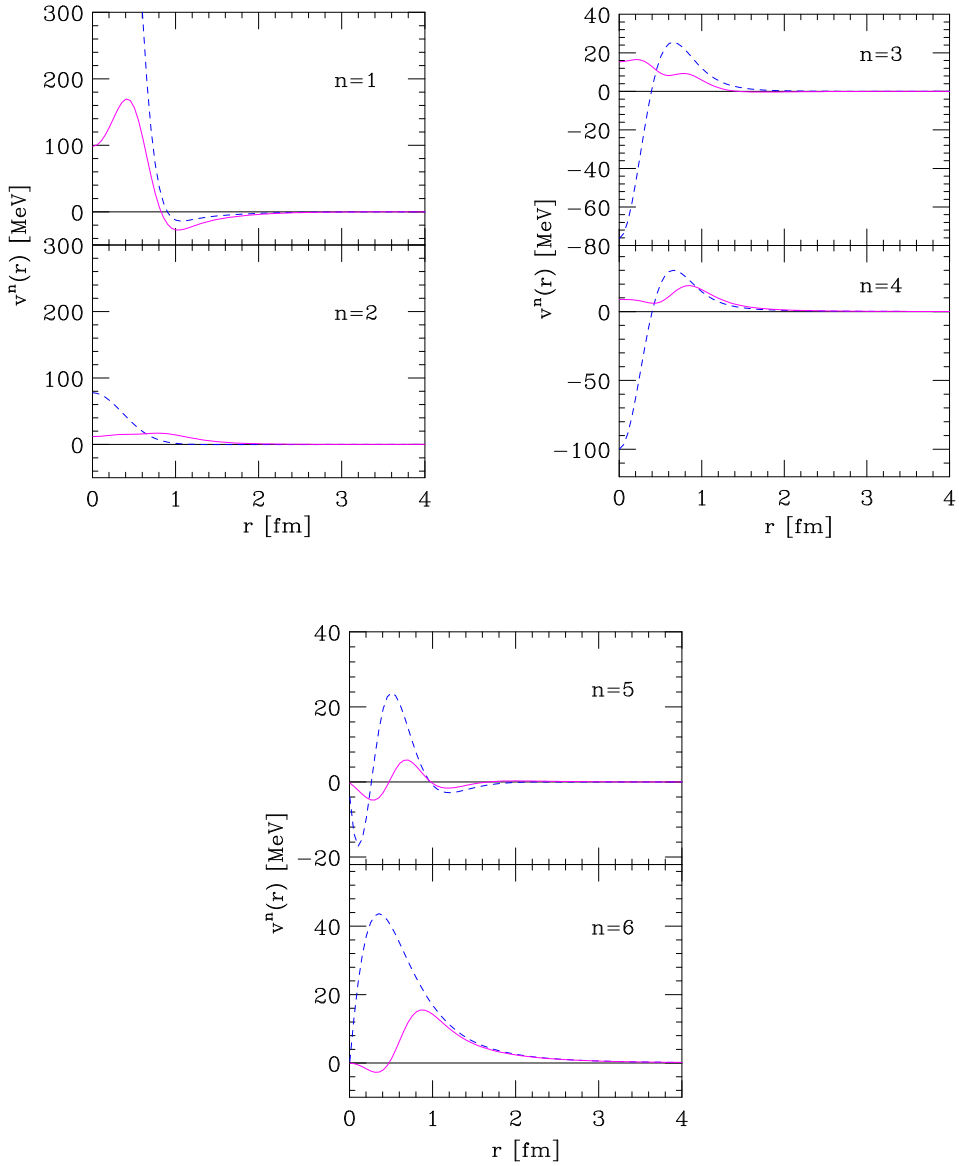

Figure 3.2. Comparison between the components of the bare Argonne v_8' potential (dashed lines) and the effective potential defined by Eq.(3.31) (solid lines), calculated at nuclear matter equilibrium density.

Figure 3.3 shows a comparison between the central ($n = 1$, left panel) and spin-isospin ($n = 4$, right panel) components of the effective interaction of Eq.(3.31), calculated at different densities using the Argonne v_8' potential. The density dependence associated with the correlation functions, that depend on ρ through the correlation ranges, d and d_t, and the Fermi distributions (see Appendix C) turns out to be rather weak in the range $0.04 \leq \rho \leq 0.32$.

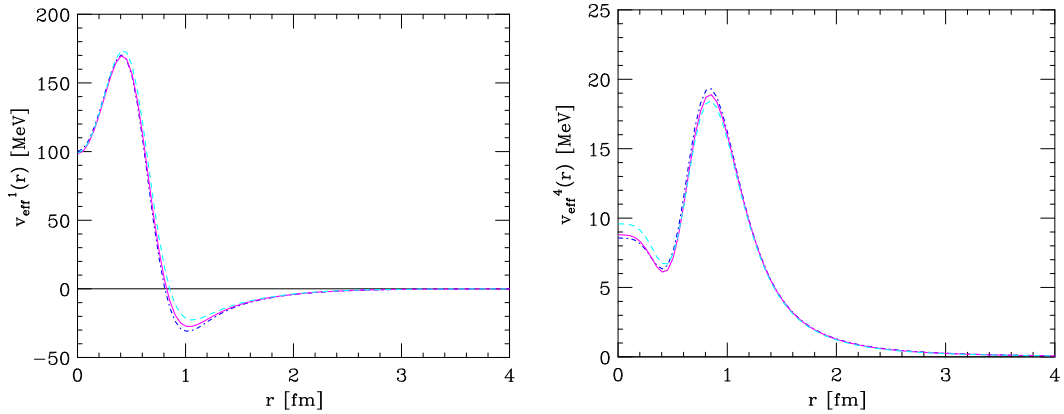

Figure 3.3. Density dependence of the central ($n = 1$, left panel) and spin-isospin ($n = 4$, right panel) components of the effective interaction of Eq.(3.31), calculated using the Argonne v_8' potential. The dot-dash, dashed and solid lines correspond to $\rho = 0.04$, 0.16 and 0.32 fm^{-3}, respectively.

3.3.1 Energy per particle of neutron and nuclear matter

The effective interaction described in the previous Section was tested by computing the energy per particle of symmetric nuclear matter and pure neutron matter in first order perturbation theory using the FG basis.

Let us consider nuclear matter at density

$$\rho = \sum_{\lambda=1}^{4} \rho_\lambda \ , \tag{3.37}$$

where $\lambda = 1,2,3,4$ labels spin-up protons, spin-down protons, spin-up neutrons and spin-down neutrons, respectively, the corresponding densities being $\rho_\lambda = x_\lambda \rho$, implying $\sum_\lambda x_\lambda = 1$. Within our approach, the energy of such a system can be obtained

from

$$\frac{E}{N} = \frac{3}{5} \sum_{\lambda} \frac{{p_F^\lambda}^2}{2m} + \frac{\rho}{2} \sum_{\lambda\mu} \sum_{n} x_\lambda x_\mu \int d^3r \; v_{\rm eff}^n \left[A_{\lambda\mu}^n - B_{\lambda\mu}^n \ell(p_F^\lambda r) \ell(p_F^\mu r) \right] \; . \quad (3.38)$$

In the above equation, $p_F^\lambda = (6\pi^2\rho_\lambda)^{1/3}$ and the Slater function ℓ is defined as

$$\ell(p_F^\lambda r) = \sum_{\mathbf{k}} \; {\rm e}^{i\mathbf{k}\cdot\mathbf{r}} \; \theta(p_F^\lambda - |\mathbf{k}|) \; . \quad (3.39)$$

The explicit expression of the matrices

$$A_{\lambda\mu}^n = \langle \lambda\mu | O^n | \lambda\mu \rangle \quad , \quad B_{\lambda\mu}^n = \langle \lambda\mu | O^n | \mu\lambda \rangle \; , \quad (3.40)$$

where $|\lambda\mu\rangle$ denotes the two-nucleon spin-isospin state, is given in Appendix A.

In Fig. 3.4 our results are compared to those of Refs. [8] and [35]. The calculations of Ref. [8] (solid lines) have been carried out using a variational approach based on the FHNC-SOC formalism, with a hamiltonian including the Argonne v_{18} NN potential and the Urbana IX three-body potential [31]. The results of Ref. [35] (dashed line of the lower panel) have been obtained using the v_8' and the same three-body potential, within the framework of the Auxiliary field diffusion Monte Carlo (AFDMC) approach.

The results of Fig. 3.4 show that the effective interaction provides a fairly reasonable description of the EOS over a broad density range. The empirical equilibrium properties of symmetric nuclear matter are accounted for without including the somewhat *ad hoc* density dependent correction of Ref. [8]. This is probably to be ascribed to the fact that, unlike the Urbana IX potential, the three-nucleon interaction (TNI) model of Ref. [47] also takes into account the contribution of many-body forces. It should also be emphasized that, using $v_{\rm eff}$ of Eq.(3.31) and the TNI model, one effectively includes the contribution of clusters involving more than two nucleons. Note that, in addition to the correct binding energy per nucleon and equilibrium density ($E/N = 15.96$ MeV at $\rho = 0.16$ fm^{-3}), our calculation also yields a very reasonable value of the compressibility module, which turns out to be $K = 230$ MeV.

It is worth reminding that our approach does not involve adjustable parameters. The correlation ranges d and d_t have been taken from Ref. [7], while the parameters entering the definition of the three-nucleon interaction (TNI) have been determined by the authors of Ref. [47] through a fit of nuclear matter equilibrium properties.

3.3.2 Effective mass

Within the approach based on $v_{\rm eff}$, the effective mass can be obtained from the single-particle energies $e_\lambda(\mathbf{p})$, that can be easily computed in Hartree-Fock approximation.

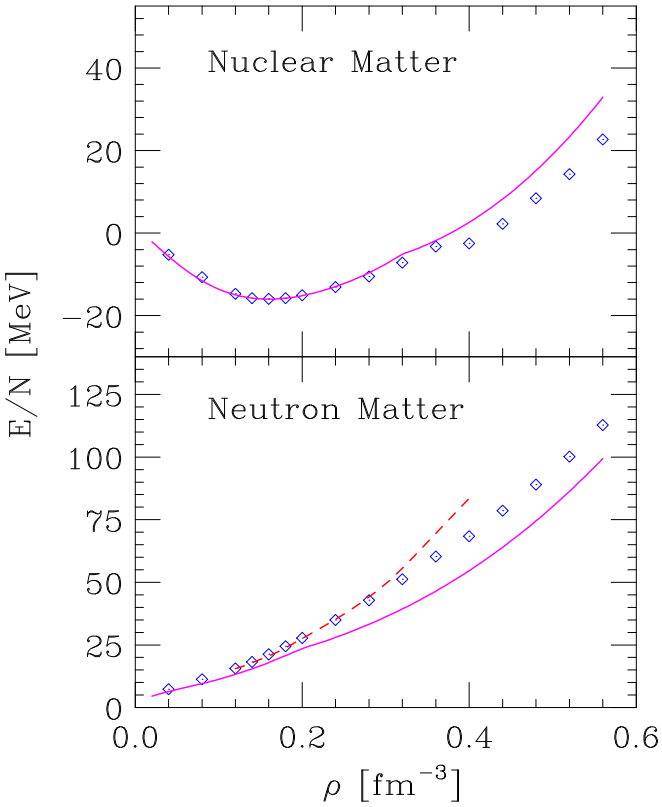

Figure 3.4. Energy per particle of symmetric nuclear matter (upper panel) and pure neutron matter (lower panel). The diamonds represent the results obtained using Eq.(3.38), whereas the solid lines correspond to the results of Akmal, Pandharipande and Ravenhall [8]. The dashed line of the lower panel represents the results of the AFDMC approach or Ref. [35].

The resulting expression is (compare to Eq.(3.38):

$$e_\lambda(p) = \frac{p^2}{2m} + \frac{\rho}{2}\sum_\mu \sum_n x_\mu \int d^3r v^n_{\rm eff}(r)\left[A^n_{\lambda\mu} - B^n_{\lambda\mu} j_0(pr)\ell(p_F r)\right] \ , \qquad (3.41)$$

where $p = |\mathbf{p}|$ and j_0 is the spherical Bessel function: $j_0(x) = \sin(x)/x$.

The relation between the effective mass, $m^\star$, and the single-particle energies is given by

$$\frac{1}{m^\star} = \frac{1}{p}\,\frac{de}{dp} \ . \qquad (3.42)$$

The density dependence of the effective masses of PNM, obtained from the $v_{\rm eff}$ discussed in this Chapter, is shown in Fig. 3.5. It is worth mentioning that for SNM

at equilibrium, we find $m^\star(p_F)/m = 0.65$, in close agreement with the lowest order CBF result of Ref. [49]. Comparing to the zero-th order CBF result is consistent with the Hartree-Fock approximation employed to calculate the single-particle energies. The 20% enhancement of the effective mass at the Fermi surface resulting from the second order CBF calculation [49] is in fact due to effects not included in the present implementation of our approach.

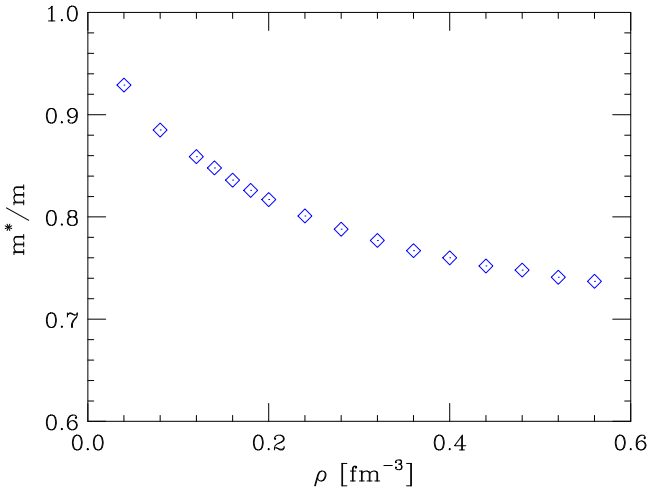

Figure 3.5. Density dependence of the ratio $m^\star/m$ obtained from Eqs.(3.41) and (3.42) using the effective interaction described in the text.

3.3.3 Spin susceptibility of neutron matter

The results of numerical calculations show that the energy per particle of nuclear matter can be accurately approximated using the expression

$$\frac{1}{N}\, E(\alpha,\beta,\gamma) = E_0 + E_\sigma \alpha^2 + E_\tau \beta^2 + E_{\sigma\tau}\gamma^2 \ , \tag{3.43}$$

with

$$\begin{aligned} \alpha &= (x_3 - x_4) + (x_1 - x_2) \\ \beta &= (x_3 + x_4) - (x_1 + x_2) \\ \gamma &= (x_3 - x_4) - (x_1 - x_2) \ . \end{aligned} \tag{3.44}$$

In symmetric nuclear matter $x_\lambda = 1/4$ for all values of λ, yielding $E/N = E_{\rm SNM} = E_0$, while in pure neutron matter, corresponding to $x_1 = x_2 = 0$ and $x_3 = x_4 = 1/2$,

$E/N = E_{\rm PNM} = E_0 + E_\tau$, implying that E_τ can be identified with the symmetry energy.

Let us consider fully spin-polarized neutron matter. The two degenerate states corresponding to $x_3 = 1$ and $x_4 = 0$ ($\alpha = 1$, spin-up) and $x_3 = 0$ and $x_4 = 1$ ($\alpha = -1$, spin-down) have energy,

$$E^{\uparrow} = E^{\downarrow} = E_{\rm PNM} + \widetilde{E}_\sigma \ , \tag{3.45}$$

with $\widetilde{E}_\sigma = E_\sigma + E_{\sigma\tau}$. For arbitrary polarization α, the energy can be obtained from the expansion

$$E(\alpha) = E(0) + \left.\frac{\partial E}{\partial \alpha}\right|_{\alpha=0} \alpha + \frac{1}{2}\left.\frac{\partial^2 E}{\partial \alpha^2}\right|_{\alpha=0} \alpha^2 + \dots \ . \tag{3.46}$$

As E must be an even function of α (see Eq.(3.45)), the linear term in the above series must be vanishing and, neglecting terms of order α^3, we can write

$$\Delta E = E(\alpha) - E(0) = \frac{1}{2}\left.\frac{\partial^2 E}{\partial \alpha^2}\right|_{\alpha=0} \alpha^2 \ . \tag{3.47}$$

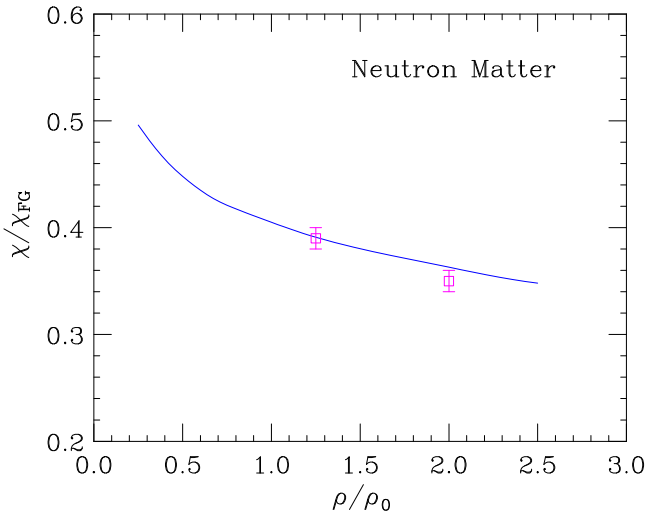

Figure 3.6. Ratio between the spin susceptibility obtained from Eqs.(3.53) and (3.38) and the FG model result. The points with error bars show the AFDMC results of Ref.[50].

In the presence of a uniform magnetic field $\mathbf{B}$ the energy of the system becomes

$$E_B(\alpha) = E(\alpha) - \alpha\mu B, \tag{3.48}$$

where B denotes the magnitude of the external field, whose direction is chosen as spin quantization axis, and μ is the neutron magnetic moment.

Assuming that equilibrium is achieved at $\alpha = \alpha_0$, i.e. that

$$\left.\frac{\partial E}{\partial \alpha}\right|_{\alpha=\alpha_0} - \mu B = 0 \ , \tag{3.49}$$

we obtain

$$\alpha_0 = \mu B \left(\frac{\partial^2 E}{\partial \alpha^2}\right)^{-1}_{\alpha=0} \ . \tag{3.50}$$

From the definitions of the total magnetization

$$M = \mu(\rho_3 - \rho_4) = \mu\alpha_0\rho = \mu^2 \left(\frac{\partial^2 E}{\partial \alpha^2}\right)^{-1}_{\alpha=0} B\rho \ , \tag{3.51}$$

and the spin susceptibility χ

$$M = \chi B \ , \tag{3.52}$$

we finally obtain

$$\chi = \mu^2 \left(\frac{\partial^2 E}{\partial \alpha^2}\right)^{-1}_{\alpha=0} \rho = \mu^2 \frac{1}{2(E^{\uparrow} - E_{\rm PNM})} \ \rho \ . \tag{3.53}$$

The above equation shows that, within our approach, the spin susceptibility of neutron matter can be easily calculated from Eq.(3.38)

Figure 3.6 shows the density dependence of the ratio between the susceptibility of neutron matter obtained from the effective interaction and that corresponding to the FG model. For comparison, the results of Ref.[50], obtained within the AFDMC approach using the Argonne v_8' NN potential and the Urbana IX three-body force, are also displayed. It appears that the inclusion of interactions leads to a substancial decrease of the susceptibility over the whole density range, and that the agreement between the two theoretical calculations is remarkably good.

3.4 Thermal effects

The CBF formalism described in the previous Sections assumes that nuclear matter can be described as a *cold*, zero-temperature, system. As pointed out in Chapter 2, this approximation is justified as long as the thermal energy, $\sim T$, is negligible compared to the typical nucleon energy.

In principle, to apply the CBF formalism to the calculation of the shear viscosity, which is the ultimate goal of our work, this assumption should be released. However, the thermal regime relevant to the astrophysical aplications of our results

corresponds to temperatures of few MeV at most. Since these energies are much lower than the mass of the lightest strongly interacting particle - the π meson, whose mass is $m_\pi \sim 140$ MeV - it is reasonable to assume that the dynamics, described by the NN potential, is not affected by the finite temperature.

Thermal effects also enter the calculation of the correlation functions through the Fermi distribution, yielding the occupation probability of the single-particle states. The Euler-Lagrange equations to be solved to obtain the f_{ij} at $T \neq 0$ can be easily obtained from those corresponding to $T = 0$ (see Appendix C), replacing the Slater functions of Eq.(3.39) with

$$L(p_F^\lambda r,T) = \sum_{\mathbf{k}} \mathrm{e}^{i\mathbf{k}\cdot\mathbf{r}} n_\lambda(\mathbf{k},T) \ , \tag{3.54}$$

where $n_\lambda(\mathbf{k},T)$ is the Fermi distribution defined in Chapter 1, which reduces to the step function of Eq.(3.39) in the limit $T \to 0$. The temperature dependence of $L(p_F^\lambda r,T)$ for the case of symmetric nuclear matter at equilibrium density (corresponding to $p_F^\lambda = 1.33$ fm^{-1} for all values of λ) is illustrated in Fig. 3.7.

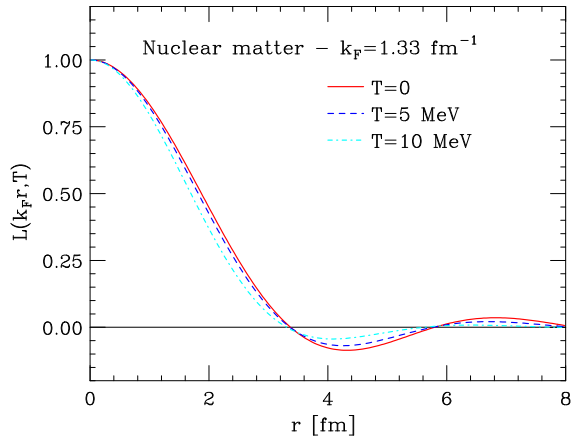

Figure 3.7. Radial dependence of the generalized Slater functions at finite temperature, defined by Eq.(3.54), calculated in symmetric nuclear matter at equilibrium density. The solid, dashed and dot-dash lines correspond to $T =$ 0, 5 and 10 MeV, respectively.

Figure 3.8 shows the temperature dependence of the correlation function in the two-nucleon channel corresponding to $S = 1$ and $T = 0$. The quantity diplayed in the figure is the relative deviation with respect to the zero temperature result

$$\Delta f_{TS}(r,T) = \frac{f_{TS}(r,T) - f_{TS}(r,T=0)}{f_{TS}(r,T=0)} \ . \tag{3.55}$$

It clearly appears that even for rather large temperatures, of the orders of tens of MeV, the thermal modifications of the Fermi distributions have a negligible effect, leading to a few percent deviation.

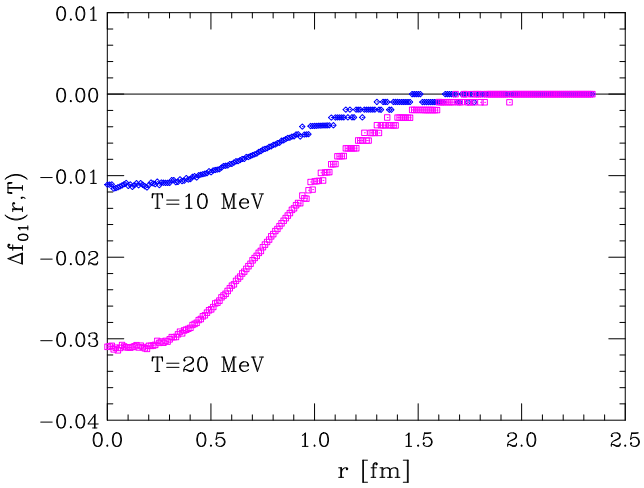

Figure 3.8. Radial and temperature dependence of the quantity $\Delta f_{TS}(r,T)$, defined in Eq.(3.55), corresponding to the $S = 1$, $T = 0$ channel and nuclear matter equilibrium density.

Chapter 4

Shear viscosity of neutron matter

In this Chapter we discuss the calculation of the shear viscosity coefficient of pure neutron matter. As a first step, we compare with the results of existing calculations, in which the scattering probability entering the definition of η is obtained from the NN scattering cross section in vacuum. The modifications due to the presence of the nuclear medium, whose consistent inclusion has to be regarded as the main aim of our work, have been taken into account replacing the bare NN potential with the CBF effective interaction decribed in Chapter 3. Most of the original results presented in this Chapter are taken from Ref. [51].

4.1 Comparison with existing results

Early estimates of the shear viscosity coefficient of neutron star matter were obtained in the 70s by Flowers and Itoh [5, 6], who used the measured scattering phase shifts to estimate the neutron-neutron scattering probability entering the definition of η (see Eqs.(1.55) and (1.61)). However, in principle, the effect of the nuclear medium on NN scattering should also be taken into account, using the same dynamical model employed to obtain the neutron star matter EOS.

In Ref. [52], the relation between NN scattering in vacuum and in nuclear matter has been analyzed under the assumption that the nuclear medium mainly affects the flux of incoming particles and the phase-space available to the final state particles, while leaving the transition probability unchanged. Within this picture $\mathcal{W}(\theta,\phi)$ can be extracted from the NN scattering cross section measured in free space, $(d\sigma/d\Omega)_{\rm vac}$, according to

$$\mathcal{W}(\theta,\phi) = \frac{16\pi^2}{m^{\star 2}} \left(\frac{d\sigma}{d\Omega}\right)_{\rm vac} \tag{4.1}$$

where $m^\star$ is the nucleon effective mass and θ and ϕ are related to the kinematical

variables in the center of mass frame through [6]

$$E_{cm} = \frac{p_F^2(1-\cos\theta)}{2m} \quad , \quad \theta_{cm} = \phi \ . \tag{4.2}$$

The above procedure has been followed in Ref. [11], whose authors have used the available tables of vacuum cross sections obtained from partial wave analysis [53]. In order to compare with the results of Ref. [11], we have first carried out a calculation of the viscosity using Eqs.(1.55), (1.56), (1.61), (1.62) and (1.64), and the free-space neutron-neutron cross section obtained from the Argonne v_{18} potential, discussed in Chapter 2.

The calculation of the cross section has been carried out using a partial wave expansion of the scattering wave-function, solution of the Lipmann-Schwinger equation

$$|\mathbf{p},SM,T\rangle^{(\pm)} = |\mathbf{p},SM,T\rangle_0 + \frac{1}{E - H_0 \pm i\eta} v |\mathbf{p},SM,T\rangle^{(\pm)} \ , \tag{4.3}$$

H_0 and $|\mathbf{p},SM,T\rangle_0$ being the free hamiltonian and the corresponding eigenstate. In the above equation $\mathbf{p}$ is the relative momentum, while S, M and T specify the pair spin, spin projection and isospin. Note that labeling the state with the isospin projection in not necesssary, due to charge invariance of the nuclear potential v. Hence, we can set $M_T = 0$. The structure of the Schrödinger equations for the different partial waves is discussed in Appendix D.

From the scattering wave function one can readily obtain the elements of the $\mathcal{T}$-matrix

$$\mathcal{T}(S,M,M',T;\mathbf{p}) = \ {}_0\langle \mathbf{p}',S'M',T'|v|\mathbf{p},SM,T\rangle^+ \ , \tag{4.4}$$

entering the calculation of the cross section. For example, in the case of proton-proton or neutron-neutron scattering, i.e. of pure $T = 1$ states, we find

$$\frac{d\sigma_{pp}}{d\Omega} = \frac{d\sigma_{nn}}{d\Omega} = |a_{10}|^2 + \sum_{MM'} |a_{11}^{MM'}|^2 \ , \tag{4.5}$$

where the scattering amplitudes a_{T0} and $a_{T1}^{MM'}$ are trivially related to the $\mathcal{T}$-matrix elements through

$$a_{T0} = \frac{\mu}{2\pi}\mathcal{T}(0,0,0,T;\mathbf{p}) \quad , \quad a_{T1}^{MM'} = \frac{\mu}{2\pi}\mathcal{T}(1,M,M',T;\mathbf{p}) \ , \tag{4.6}$$

μ being the reduced mass of the two-nucleon system.

Being fit to the full Nijmegen phase shifts data base [28], as well as to low energy scattering parameters and deuteron properties, the Argonne v_{18} potential provides an accurate description of the scattering data by construction. In order to show the accuracy of our calculation of the free-space cross section, in Fig.4.1 we compare

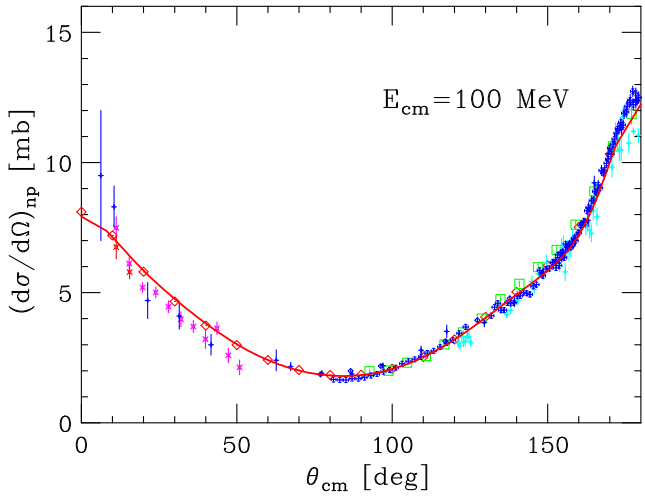

Figure 4.1. Differential proton-neutron scattering cross section at $E_{cm} = 100$ MeV, as a function of the scattering angle in the center of mass frame. The data are taken from Ref. [54].

our results to the experimental data, available online from Ref. [54], for the case of proton-neutron scattering at $E_{cm} = 100$ MeV.

In Fig. 4.2, we show the quantity ηT^2 a function of density. Our results are represented by the solid line, while the dot-dash line corresponds to the results obtained from Eqs.(43) and (46) of Ref. [11]. Both calculations have been carried out using the effective masses discussed in Chapter 3 and illustrated in Fig. 3.5. The differences between the two curves are likely to be ascribed to the correction factor of Eq.(1.64), not taken into acount by the authors of Ref. [11], and to the extrapolation needed to determine the cross sections at small angles within their approach.

To gauge the model dependence of our results, we have replaced the full Argonne v_{18} potential with its simplified form, referred to as v_8' [30]. The corresponding results, represented by the dashed line, show that using the v_8' potential leads to a few percent change of ηT^2 over the density range corresponding to $1/4 < (\rho/\rho_0) < 2$.

4.2 Inclusion of medium effetcs

To improve upon the approximation of Eq.(4.1) and include the effects of medium-modifications of the NN scattering amplitude, we have replaced the bare NN potential with the CBF effective interaction $v_{\rm eff}$ discussed in Chapter 3.

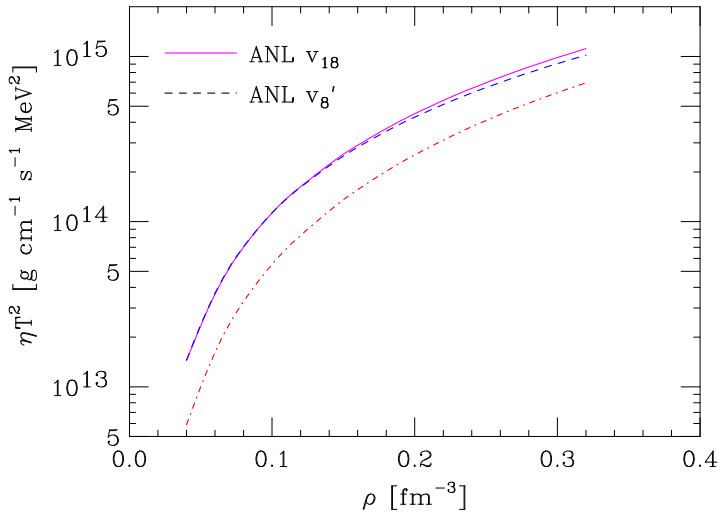

Figure 4.2. Neutron matter ηT^2 as a function of density. Solid line: results obtained using free-space cross section corresponding to the Argonne v_{18} potential and $m^\star$ computed from to the effective interaction described in Chapter 3. Dot-dash line: results obtained from Eqs.(43) and (46) of Ref. [11] using the same $m^\star$. Dashed line: same as the solid line, but with the Argonne v_{18} replaced by its reduced form v_8'.

Knowing $v_{\rm eff}$, the in-medium scattering probability can be readily obtained from Fermi's golden rule. The corresponding cross section at momentum transfer $\mathbf{q}$ reads

$$\frac{d\sigma}{d\Omega} = \frac{m^{\star 2}}{16\pi^2}\,|\hat{v}_{\rm eff}(\mathbf{q})|^2\ , \tag{4.7}$$

$\hat{v}_{\rm eff}$ being the Fourier transform of the effective potential. The details of the calculation of the scattering probability appearing in the above equation are given in Appendix E.

In Fig. 4.3 the in-medium neutron-neutron cross section at $E_{cm} = 100$ MeV obtained from the effective potential, with $\rho = \rho_0$ and $\rho_0/2$, is compared to the corresponding free-space result. As expected, screening of the bare interaction leads to an appreciable suppression of the scattering cross section.

Replacing the cross section in vacuum with the one defined in Eq.(4.7), the medium modified scattering probability can be obtained from Eq.(4.1). The resulting $\mathcal{W}(\theta,\phi)$ can then be used to calculate the quasiparticle lifetime τ, from Eq.(1.55) and ηT^2, from Eq.(1.64).

Figure 4.4 shows the Fermi momentum dependence of the product τT^2, with τ computed from Eq.(1.55) using both the free space and medium modified scattering probabilities. It clearly appears that the suppression of the cross section (see Fig.

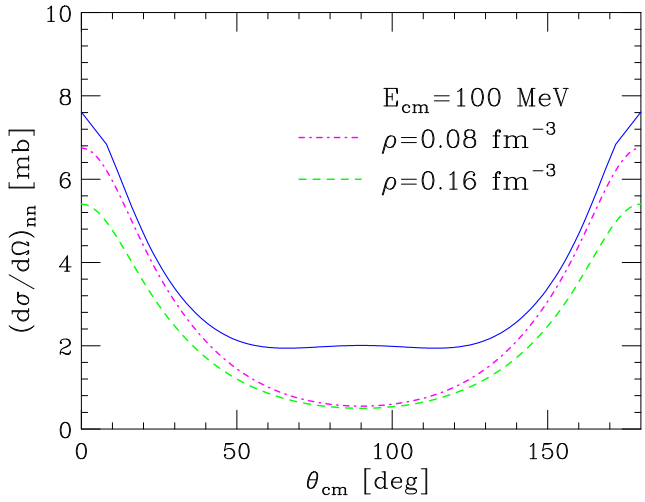

Figure 4.3. Differential neutron-neutron scattering cross section at $E_{cm} = 100$ MeV, as a function of the scattering angle in the center of mass frame. Solid line: cross section in vacuum, calculated with the v_8' potential. Dot-dash line: medium modified cross section obtained from the effective interaction described in the text at $\rho = 0.08$ fm^{-3}. Dashed line: same as the dot-dash line, but for $\rho = 0.16$ fm^{-3}.

4.3) results in a significant increase of the quasiparticle lifetime. For comparison, we also report the results of Ref.[55], whose authors derived an effective interaction using G-matrix perturbation theory and the Reid soft-core NN potential. The predictions of the two approaches based on effective interactions are close to one another for $p_F \lesssim 1.7$ fm^{-1}, corresponding to $\rho \lesssim \rho_0$. The differences observed at larger density are likely to be ascribed to the fact that the calculations of Ref.[55] does not include three-nucleon interactions, whose effects become more and more important as the density increases.

The effect of using the medium modified cross section in the calculation of η is illustrated in Fig. 4.5. Comparison between the solid and dashed lines shows that inclusion of medium modifications leads to a large increase of the viscosity, ranging between $\sim 75\%$ at half nuclear matter density to a factor of ~ 6 at $\rho = 2\rho_0$. Such an increase is likely to produce appreciable effects on the damping of neutron-star oscillations.

It has to be emphasized that our results are only applicable at temperatures $T > T_c$, $T_c \sim 10^9$ K being the superfluid transition temperature of neutron matter.

At temperature below T_c the main contribution to shear viscosity of neutron star matter arises from the electrons [5]. The viscosity in a neutron star containing neutrons in the superfluid state can be modelled according to [4]

$$\eta_s(T) = [1 - \theta(T)]\eta + \theta(T)\eta_e \ , \tag{4.8}$$

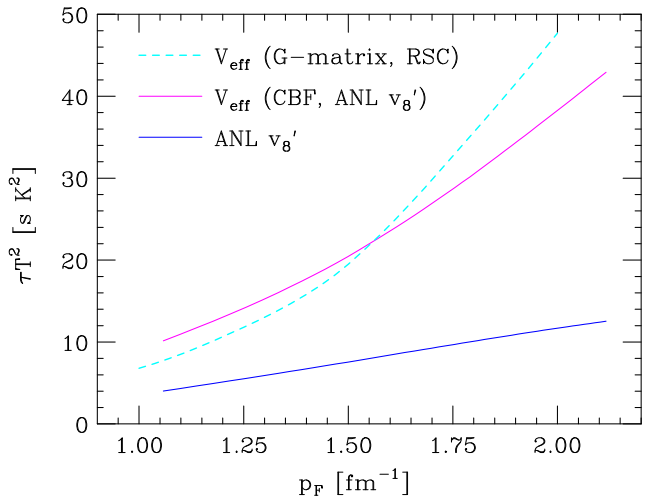

Figure 4.4. Fermi momentum dependence of τT^2, with the quasiparticle lifetime τ computed from Eq.(1.55) using the free-space (dashed line) and in-medium (solid line) scattering probabilities. The dot-dash line corresponds to the results of Ref.[55], obtained using G-matrix perturbation theory and the Reid soft-core potential.

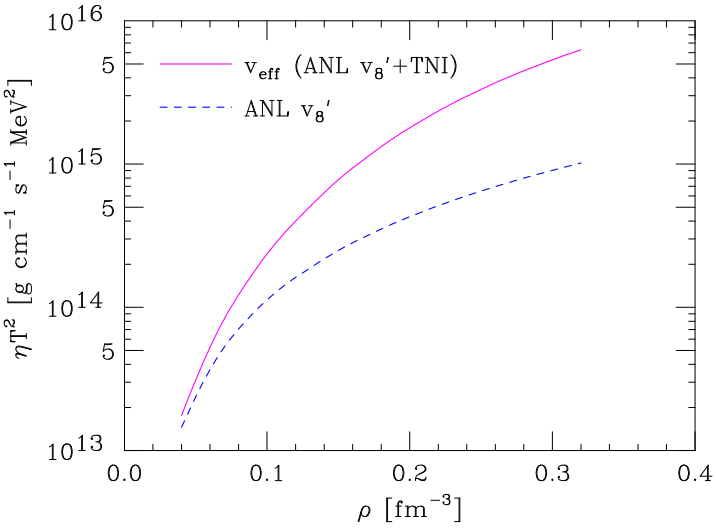

Figure 4.5. Neutron matter ηT^2 as a function of density. Solid line: results obtained using the effective interaction described in the Chapter 3. Dashed line: ηT^2 obtained from the free space cross section corresponding to the v_8' potential.

where η and η_e denote the shear viscosity coefficients associated with neutrons and

electrons, and

$$\theta(T) = \begin{cases} 0 & T > T_c \\ 1 & T < T_c \ . \end{cases} \tag{4.9}$$

In this context, it is worth mentioning that within the approach developed in this Thesis, the viscosity coefficients and the superfluid gap can be consistently obtained from the same dynamical model.

Conclusions & Outlook

We have carried out a calculation of the shear viscosity of pure neutron matter in which medium modifications of the scattering probability are consistently taken into account.

Viscosity plays a pivotal role in damping oscillations associated with gravitational waves emission, that may lead to the CFS instability of rotating neutron stars. Hence, its quantitative understanding is required to determine whether an oscillation mode is stable or not.

The calculation has been performed using a many-body approach based on an effective interaction, derived from a realistic NN potential within the framework of CBF theory. Our work improves upon existing effective interaction models [45, 46] in that it includes the effects of many-nucleon forces, which become sizable, indeed dominant, in the high density region relevant to the studies of neutron star properties.

The energy per nucleon of both symmetric nuclear matter and pure neutron matter, obtained from our effective interaction model, turns out to be in fairly good agreement with the results of highly refined many-body calculations, based on similar dynamical models. A comparable agreement with the results available in the literature has also been found for single-particle properties, e.g. the effective mass, and the spin susceptibility. The emerging picture suggests that our approach captures the relevant physics, allowing one to obtain reasonable estimates of a number of different quantities using standard perturbation theory in the Fermi gas basis.

Our results show that using a medium modified cross section leads to a large increase of the viscosity. While these results are interesting in their own right, as they can be employed in a quantitative analysis of the effect of viscosity on neutron-star oscillations, we emphasize that our work should be seen as a first step towards the development of a general computational scheme, allowing for a consistent evaluation of the properties of neutron star matter.

The most straightforward extension of our approach is the calculation of the equation of state of matter in weak equilibrium (see Eqs.(3.38) and (3.41)). The corresponding transport coefficients can also be easily obtained from the generalization of Landau theory to the case of a multicomponent liquid.

Other quantities relevant to the description of neutron star observables are the supefluid gap and the response of nuclear matter to interactions with low energy neutrino. Both quantities have been previously studied within the CBF formalism [46, 56] and can be obtained using our effective interaction model.

As a final remark, it has to be pointed out that, while our approach can and should be further developed, the possible improvements only pertain the structure of the effective interaction and the inclusion of perturbative corrections, and *do not* involve going to higher order in the cluster expansion.

Although the contribution of clusters involving more than two nucleons is known to be, in general, non negligible, effective theories are in fact *designed* to provide *lowest order* results reasonably accounting for the available data.

In this context, the most obvious improvement is the inclusion in v_{eff} of the non static components of the NN potential, which are known to be needed to reproduce scattering data.

On the other hand, inclusion of higher order terms in the perturbative expansion is necessary to take into account more complex mechanisms, that play a role in determining several properties of many-body systems. For example, second order CBF corrections produce a $\sim 20\%$ increase of the effective mass at the Fermi surface [49]. Although such an enhancement does not significantly affect the conclusions of the present work, a numerical study of these corrections using the effective interaction and the FG basis will be needed for future applications.

Higher order effects leading to the appearance of long-range correlations can be also taken into account, implementing the effective interaction in the Random Phase or Tamm-Dancoff approximation schemes [46]. Long-range correlations dominate the nuclear response in the region of low momentum transfer, where the space resolution of the probe is much larger than the average separation between nucleons. Using the effective interaction allows one to describe short- and long-range correlations in a fully consistent fashion.

Finally, it is worth mentioning that, for $T \ll m_\pi$, the effective interaction approach can be easily generalized to include thermal effects. Understanding this low temperature regime is relevant to the study of matter in both supernovæ and proto-neutron stars.

Appendix A

Properties of the operators O^n_{ij}

In this Appendix, we discuss the properties of the six operators defined in Eq.(2.16), as well as some useful properties of the Pauli matrices.

A.1 Pauli matrices

In the standard representation, in which σ^3 is chosen to be diagonal, the threee Pauli matrices are given by (we specialize here to the spin matrices σ^i: analog properties obviously hold for the isospin matrices τ^i)

$$\sigma^1 = \begin{pmatrix} 0 & 1 \\ 1 & 0 \end{pmatrix} \ , \ \sigma^2 = \begin{pmatrix} 0 & -i \\ i & 0 \end{pmatrix} \ , \ \sigma^3 = \begin{pmatrix} 1 & 0 \\ 0 & -1 \end{pmatrix} . \tag{A.1}$$

The Pauli matrices satisfy

$$\sigma^i\sigma^j = \delta_{ij} + i\epsilon_{ijk}\sigma^k \ , \tag{A.2}$$
$$\epsilon_{ijk}\sigma^j\sigma^k = 2i\sigma^i \ , \tag{A.3}$$

that can be put in the form

$$[\sigma^i, \sigma^j] = 2i\epsilon_{ijk}\sigma^k \ , \tag{A.4}$$
$$\{\sigma^i, \sigma^j\} = 2\delta_{ij} \ , \tag{A.5}$$

where ϵ_{ijk} is the totally antisymmetric tensor and i,j,k = 1,2,3. The first properties shows that the Pauli matrices are the generators of an $SU(2)$ algebra.

A.2 Projection operators

Let now $\boldsymbol{\sigma}_1$ and $\boldsymbol{\sigma}_2$ be the vectors of Pauli matrices for particle 1 and 2, respectively (i.e. $\boldsymbol{\sigma}_1 \equiv \{\sigma_1^1, \sigma_1^2, \sigma_1^3\}$). From the properties (A.2)-(A.3), it follows that

$$(\boldsymbol{\sigma}_1 \cdot \boldsymbol{\sigma}_2)^2 = 3 - 2(\boldsymbol{\sigma}_1 \cdot \boldsymbol{\sigma}_2) \ . \tag{A.6}$$

As $(\boldsymbol{\sigma}_1 \cdot \boldsymbol{\sigma}_2)$ is a scalar quantity, we can interpret the above equation as an algebraic one, with solutions $(\boldsymbol{\sigma}_1 \cdot \boldsymbol{\sigma}_2) = -3$ and $(\boldsymbol{\sigma}_1 \cdot \boldsymbol{\sigma}_2) = 1$. They correspond to the states of total spin $S = 0$ (spin singlet channel) and $S = 1$ (spin triplet channel), respectively. It is thus useful introducing the operators P_{2S+1} (and the analog Π_{2T+1} for the isospin states), defined as

$$P_{(S=0)} \equiv P_1 = \frac{1 - (\boldsymbol{\sigma}_1 \cdot \boldsymbol{\sigma}_2)}{4} \ , \tag{A.7}$$

$$P_{(S=1)} \equiv P_3 = \frac{3 + (\boldsymbol{\sigma}_1 \cdot \boldsymbol{\sigma}_2)}{4} \ , \tag{A.8}$$

which project onto states of definte total spin 0 or 1, respectively:

$$P_{2S+1}|S'\rangle = \delta_{SS'}|S'\rangle \ , \tag{A.9}$$

The projection operators satisfy to

$$P_{2S+1}^2 = P_{2S+1} \ , \tag{A.10}$$

$$P_1 + P_3 = \mathbb{1} \ , \tag{A.11}$$

$$P_1 P_3 = P_3 P_1 = 0 \ , \tag{A.12}$$

where $\mathbb{1}$ is the two-dimensional identity matrix.

A.3 Spin and isospin exchange operators

Consider the two-nucleon spin states (or the analog isospin states)

$$\begin{aligned} |0\,0\rangle &= \frac{1}{\sqrt{2}}\left(|\uparrow\downarrow\rangle - |\downarrow\uparrow\rangle\right) \ , \\ |1\,-1\rangle &= |\downarrow\downarrow\rangle \ , \\ |1\,0\rangle &= \frac{1}{\sqrt{2}}\left(|\uparrow\downarrow\rangle + |\downarrow\uparrow\rangle\right) \ , \\ |1\,1\rangle &= |\uparrow\uparrow\rangle \ , \end{aligned}$$

where $|0\,0\rangle \equiv |S=0\,M_S=0\rangle$ etc., and the inverse relations

$$\begin{aligned} |\uparrow\uparrow\rangle &= |1\,1\rangle \ , \\ |\uparrow\downarrow\rangle &= \frac{1}{\sqrt{2}}\left(|1\,0\rangle + |0\,0\rangle\right) \ , \\ |\downarrow\uparrow\rangle &= \frac{1}{\sqrt{2}}\left(|1\,0\rangle - |0\,0\rangle\right) \ , \\ |\downarrow\downarrow\rangle &= |1\,-1\rangle \ . \end{aligned}$$

From properties (A.9), and from

$$\begin{aligned} (P_3 - P_1)\,|\uparrow\uparrow\rangle = |\uparrow\uparrow\rangle \quad , \quad (P_3 - P_1)\,|\downarrow\downarrow\rangle = |\downarrow\downarrow\rangle \ , \\ (P_3 - P_1)\,|\uparrow\downarrow\rangle = |\downarrow\uparrow\rangle \quad , \quad (P_3 - P_1)\,|\downarrow\uparrow\rangle = |\uparrow\downarrow\rangle \ , \end{aligned}$$

it follows that $P_\sigma \equiv P_3 - P_1$ is the spin-exchange operator, satisfying

$$P_\sigma |S\,M_S\rangle = (-)^{S+1} |S\,M_S\rangle \ . \tag{A.13}$$

A similar exchange operator can be defined for isospin, $P_\tau \equiv \Pi_3 - \Pi_1$, with

$$P_\tau |T\,M_T\rangle = (-)^{T+1} |T\,M_T\rangle \ . \tag{A.14}$$

Combining the above results we find

$$P_{\sigma\tau} \equiv P_\sigma P_\tau = \frac{1}{4}\Big(1 + (\boldsymbol{\sigma}_1 \cdot \boldsymbol{\sigma}_2)\Big)\Big(1 + (\boldsymbol{\tau}_1 \cdot \boldsymbol{\tau}_2)\Big) \ , \tag{A.15}$$

with

$$P_{\sigma\tau} |S\,M_S, T\,M_T\rangle = (-)^{S+T} |S\,M_S, T\,M_T\rangle \ . \tag{A.16}$$

A.4 The tensor operator S_{12}

The tensor operator S_{12} is defined as

$$S_{12} \equiv \frac{3}{r^2}\ (\boldsymbol{\sigma}_1 \cdot \mathbf{r})\ (\boldsymbol{\sigma}_2 \cdot \mathbf{r}) - (\boldsymbol{\sigma}_1 \cdot \boldsymbol{\sigma}_2) \ , \tag{A.17}$$

where $\mathbf{r}$ is the relative coordinate of particels 1 and 2 while $r = |\mathbf{r}|$.

Making use of Eq.(A.2), it can be shown that

$$S_{12}(\boldsymbol{\sigma}_1 \cdot \boldsymbol{\sigma}_2) = (\boldsymbol{\sigma}_1 \cdot \boldsymbol{\sigma}_2) S_{12} = S_{12} \ . \tag{A.18}$$

As we saw, $(\boldsymbol{\sigma}_1 \cdot \boldsymbol{\sigma}_2) = 1$ on triplet states, while $(\boldsymbol{\sigma}_1 \cdot \boldsymbol{\sigma}_2) = -3$ on singlet states. The above equation thus implies that the tensor operator only acts on triplet states and

$$[S_{12},\, P_3] = 0 \ . \tag{A.19}$$

Moreover,

$$S_{12}^2 = 6 - 2S_{12} + 2(\boldsymbol{\sigma}_1 \cdot \boldsymbol{\sigma}_2) \ . \tag{A.20}$$

The tensor operator is a function of $\mathbf{r}$ satisfying

$$\boldsymbol{\nabla} S_{12} = \frac{3}{r^2}\left[\boldsymbol{\sigma}_1 (\boldsymbol{\sigma}_2 \cdot \mathbf{r}) + \boldsymbol{\sigma}_2 (\boldsymbol{\sigma}_1 \cdot \mathbf{r}) - 2\frac{\mathbf{r}}{r^2} (\boldsymbol{\sigma}_1 \cdot \mathbf{r}) \ (\boldsymbol{\sigma}_2 \cdot \mathbf{r})\right] \ , \tag{A.21}$$

$$\nabla^2 S_{12} = -\frac{6}{r^2} S_{12} \ . \tag{A.22}$$

For any function $u(r)$, Eq.(A.21) implies

$$(\boldsymbol{\nabla} u) \cdot (\boldsymbol{\nabla} S_{12}) = \frac{du}{dr} \ \frac{\mathbf{r}}{r} \cdot (\boldsymbol{\nabla} S_{12}) = 0 \ . \tag{A.23}$$

Moreover

$$(\boldsymbol{\nabla} S_{12})^2 = \frac{6}{r^2} (8 - S_{12}) \ , \tag{A.24}$$

$$[S_{12}, \ (\boldsymbol{\nabla} S_{12})] = \frac{36}{r^2} \ i \ (\mathbf{S} \times \mathbf{r}) \ , \tag{A.25}$$

$$[S_{12}, \ (\boldsymbol{\nabla} S_{12})] \, \boldsymbol{\nabla} = \frac{36}{r^2} \ (\mathbf{L} \cdot \mathbf{S}) \ , \tag{A.26}$$

where $\mathbf{S} = (\boldsymbol{\sigma}_1 + \boldsymbol{\sigma}_2)/2$ and $\mathbf{L} = \mathbf{r} \times \mathbf{p} = -i (\mathbf{r} \times \boldsymbol{\nabla})$ is the orbital angular momentum operator of the relative motion.

From Equation (A.22), we can calculate

$$\left[S_{12}, \nabla^2 S_{12}\right] = 0 \ , \tag{A.27}$$

and

$$(\boldsymbol{\nabla} S_{12}) \ [S_{12}, \boldsymbol{\nabla}] = - (\boldsymbol{\nabla} S_{12})^2 \ . \tag{A.28}$$

A.5 Algebra of the six operators $O_{ij}^{n \leq 6}$

Equations (A.6), (A.18) and (A.20) show that the six operators

$$O^{1,\ldots,6} = 1, (\boldsymbol{\tau}_1 \cdot \boldsymbol{\tau}_2), (\boldsymbol{\sigma}_1 \cdot \boldsymbol{\sigma}_2), (\boldsymbol{\sigma}_1 \cdot \boldsymbol{\sigma}_2)(\boldsymbol{\tau}_1 \cdot \boldsymbol{\tau}_2), S_{12}, S_{12}(\boldsymbol{\tau}_1 \cdot \boldsymbol{\tau}_2) \ , \tag{A.29}$$

close an algebra, i.e. they satisfy

$$O^i O^j = \sum_k K_{ij}^k O^k \ . \tag{A.30}$$

The coefficients K_{ij}^k are easily obtained by calculating

$$O^1O^i = O^iO^1 = O^i \Longrightarrow K_{1i}^k = K_{i1}^k = \delta_i^k$$

$$O^2O^2 = 3O^2 - 2O^2 \Longrightarrow K_{22}^k = 3\delta_1^k - 2\delta_2^k \ ,$$
$$O^2O^3 = O^3O^2 = O^4 \Longrightarrow K_{23}^k = K_{32}^k = \delta_4^k \ ,$$
$$O^2O^4 = 3O^3 - 2O^4 \Longrightarrow K_{24}^k = K_{42}^k = \delta_3^k - 1\delta_4^k \ ,$$
$$O^2O^5 = O^5O^2 = O^6 \Longrightarrow K_{25}^k = K_{52}^k = \delta_6^k \ ,$$
$$O^2O^6 = O^6O^2 = 3O^5 - 2O^6 \Longrightarrow K_{26}^k = K_{62}^k = 3\delta_5^k - 2\delta_6^k \ ,$$
$$O^3O^3 = 3O^1 - 2O^3 \Longrightarrow K_{33}^k = 3\delta_1^k - 2\delta_3^k \ ,$$
$$O^3O^4 = O^4O^3 = 3O^2 - 2O^4 \Longrightarrow K_{34}^k = K_{43}^k = 3\delta_2^k - 2\delta_4^k \ ,$$
$$O^3O^5 = O^5O^3 = O^5 \Longrightarrow K_{35}^k = K_{53}^k = \delta_5^k \ ,$$
$$O^3O^6 = O^6O^3 = O^6 \Longrightarrow K_{36}^k = K_{63}^k = \delta_6^k \ ,$$
$$O^4O^4 = 9O^1 - 6O^2 - 6O^3 + 4O^4 \Longrightarrow K_{44}^k = 9\delta_1^k - 6\delta_2^k - 6\delta_3^k + 4\delta_4^k \ ,$$
$$O^4O^5 = O^5O^4 = O^6 \Longrightarrow K_{45}^k = K_{54}^k = \delta_6^k \ ,$$
$$O^4O^6 = O^6O^4 = 3O^5 - 2O^6 \Longrightarrow K_{46}^k = K_{64}^k = 3\delta_5^k - 2\delta_6^k \ ,$$
$$O^5O^5 = 6O^1 + 2O^3 - 2O^5 \Longrightarrow K_{55}^k = 6\delta_1^k + 2\delta_3^k - 2\delta_5^k \ ,$$
$$O^5O^6 = O^6O^5 = 6O^2 + 2O^4 - 2O^6 \Longrightarrow K_{56}^k = K_{65}^k = 6\delta_2^k + 2\delta_4^k - 2\delta_6^k \ ,$$

$$\begin{aligned} O^6O^6 \ &= \ 18O^1 - 12O^2 + 6O^3 - 4O^4 - 6O^6 + 4O^6 \\ &\Longrightarrow K_{66}^k = 18\delta_1^k - 12\delta_2^k + 6\delta_3^k - 4\delta_4^k - 6\delta_4^k + 4\delta_6^k \ . \end{aligned}$$

A.6 Matrix elements of P_{2S+1} and Π_{2T+1}

Finally, we report a number of expectation values of operators involving Pauli matrices, in two-nucleon states of definite total spin and isospion, $|S\ M_S, T\ M_T\rangle$.

$$\langle P_{2S'+1}\Pi_{2T'+1}\rangle = \delta_{SS'}\delta_{TT'} \ , \tag{A.31}$$
$$\langle P_{2S'+1}\Pi_{2T'+1}P_{\sigma\tau}\rangle = (-)^{S+T}\delta_{SS'}\delta_{TT'} \ , \tag{A.32}$$
$$\sum_{SM_S}\delta_{S'1}\langle S_{12}P_{2S'+1}\Pi_{2T'+1}\rangle = \delta_{S'1}\delta_{TT'}\sum_{M_S}\langle 1\ M_S|S_{12}|1\ M_S\rangle = 0 \ , \tag{A.33}$$
$$\sum_{SM_S}\delta_{S'1}\langle S_{12}P_{2S'+1}\Pi_{2T'+1}P_{\sigma\tau}\rangle = 0 \ . \tag{A.34}$$

A.7 Matrix elements of $O^{n\leq 6}_{ij}$

The explicit expressions for the matrices entering Eqs.(3.38) and (3.41), defined by

$$A^i_{\lambda\mu} = \langle \lambda\mu | O^i_{12} | \lambda\mu \rangle \quad , \quad B^i_{\lambda\mu} = \langle \lambda\mu | O^i_{12} | \mu\lambda \rangle \ , \tag{A.35}$$

where $|\lambda\mu\rangle$ denotes the two-nucleon spin-isospin state, can be easily obtained from the above properties of the six operators $O^{n\leq 6}$.

We find

$$A^1 = \begin{pmatrix} 1 & 1 & 1 & 1 \\ 1 & 1 & 1 & 1 \\ 1 & 1 & 1 & 1 \\ 1 & 1 & 1 & 1 \end{pmatrix} , \tag{A.36}$$

$$A^2 = \begin{pmatrix} 1 & 1 & -1 & -1 \\ 1 & 1 & -1 & -1 \\ -1 & -1 & 1 & 1 \\ -1 & -1 & 1 & 1 \end{pmatrix} , \tag{A.37}$$

$$A^3 = \begin{pmatrix} 1 & -1 & 1 & -1 \\ -1 & 1 & -1 & 1 \\ 1 & -1 & 1 & -1 \\ -1 & 1 & -1 & 1 \end{pmatrix} , \tag{A.38}$$

$$A^4 = \begin{pmatrix} 1 & -1 & -1 & 1 \\ -1 & 1 & 1 & -1 \\ -1 & 1 & 1 & -1 \\ 1 & -1 & -1 & 1 \end{pmatrix} , \tag{A.39}$$

$$A^5 = \begin{pmatrix} 1 & 1 & -1 & -1 \\ 1 & 1 & -1 & -1 \\ -1 & -1 & 1 & 1 \\ -1 & -1 & 1 & 1 \end{pmatrix} \left(3\cos^2\theta - 1\right) = A^2 \left(3\cos^2\theta - 1\right) \ , \tag{A.40}$$

$$A^6 = \begin{pmatrix} 1 & -1 & -1 & 1 \\ -1 & 1 & 1 & -1 \\ -1 & 1 & 1 & -1 \\ 1 & -1 & -1 & 1 \end{pmatrix} \left(3\cos^2\theta - 1\right) = A^4 \left(3\cos^2\theta - 1\right) \ , \tag{A.41}$$

$$B^1 = \begin{pmatrix} 1 & 0 & 0 & 0 \\ 0 & 1 & 0 & 0 \\ 0 & 0 & 1 & 0 \\ 0 & 0 & 0 & 1 \end{pmatrix} , \tag{A.42}$$

$$B^2 = \begin{pmatrix} 1 & 0 & 2 & 0 \\ 0 & 1 & 0 & 2 \\ 2 & 0 & 1 & 0 \\ 0 & 2 & 0 & 1 \end{pmatrix} , \tag{A.43}$$

$$B^3 = \begin{pmatrix} 1 & 2 & 0 & 0 \\ 2 & 1 & 0 & 0 \\ 0 & 0 & 1 & 2 \\ 0 & 0 & 2 & 1 \end{pmatrix} , \tag{A.44}$$

$$B^4 = \begin{pmatrix} 1 & 2 & 2 & 4 \\ 2 & 1 & 4 & 2 \\ 2 & 4 & 1 & 2 \\ 4 & 2 & 2 & 1 \end{pmatrix} , \tag{A.45}$$

$$B^5 = \begin{pmatrix} 1 & -1 & 0 & 0 \\ -1 & 1 & 0 & 0 \\ 0 & 0 & 1 & -1 \\ 0 & 0 & -1 & 1 \end{pmatrix} \left(3\cos^2\theta - 1\right) , \tag{A.46}$$

$$B^6 = \begin{pmatrix} 1 & -1 & 2 & -2 \\ -1 & 1 & -2 & 2 \\ 2 & -2 & 1 & -1 \\ -2 & 2 & -1 & 1 \end{pmatrix} \left(3\cos^2\theta - 1\right) , \tag{A.47}$$

where θ is the angle between $\mathbf{r}$ and the z axis.

A.8 Change of representation

In this Section we discuss the different representation for the operators of the "v_6" algebra. A generic operator x can be written as

$$x = \sum_{p=1}^{6} x_{ij}^p O^p = x_c + x_\tau(\boldsymbol{\tau}_1\cdot\boldsymbol{\tau}_2) + x_\sigma(\boldsymbol{\sigma}_1\cdot\boldsymbol{\sigma}_2) + x_{\sigma\tau}(\boldsymbol{\sigma}_1\cdot\boldsymbol{\sigma}_2)(\boldsymbol{\tau}_1\cdot\boldsymbol{\tau}_2) + x_t S_{12} + x_{t\tau} S_{12}(\boldsymbol{\tau}_1\cdot\boldsymbol{\tau}_2) , \tag{A.48}$$

in the basis of operators (A.29), or as

$$x = \sum_{TS} \left[x_{T0} + \delta_{S1} x_{tT} S_{12}\right] P_{2S+1}\Pi_{2T+1} , \tag{A.49}$$

in the "TS-representation".

The transformation matrix is given by

$$\begin{pmatrix} 1 & -3 & -3 & 9 \\ 1 & 1 & -3 & -3 \\ 1 & -3 & 1 & -3 \\ 1 & 1 & 1 & 1 \end{pmatrix} \begin{pmatrix} x_c \\ x_\tau \\ x_\sigma \\ x_{\sigma\tau} \end{pmatrix} = \begin{pmatrix} x_{00} \\ x_{10} \\ x_{01} \\ x_{11} \end{pmatrix} , \tag{A.50}$$

$$\begin{pmatrix} 1 & -3 \\ 1 & 1 \end{pmatrix} \begin{pmatrix} x_t \\ x_{t\tau} \end{pmatrix} = \begin{pmatrix} x_{t0} \\ x_{t1} \end{pmatrix} , \tag{A.51}$$

or

$$\begin{cases} x_{TS} = x_c + (4T-3)x_\tau + (4S-3)x_\sigma + (4S-3)(4T-3)x_{\sigma\tau} , \\ \\ x_{tT} = x_t + (4T-3)x_{tT} . \end{cases} \tag{A.52}$$

The inverse transformation is given by

$$\frac{1}{16} \begin{pmatrix} 1 & 3 & 3 & 9 \\ -1 & 1 & -3 & 3 \\ -1 & -3 & 1 & 3 \\ 1 & -1 & -1 & 1 \end{pmatrix} \begin{pmatrix} x_{00} \\ x_{10} \\ x_{01} \\ x_{11} \end{pmatrix} = \begin{pmatrix} x_c \\ x_\tau \\ x_\sigma \\ x_{\sigma\tau} \end{pmatrix} , \tag{A.53}$$

$$\frac{1}{4} \begin{pmatrix} 1 & 3 \\ -1 & 1 \end{pmatrix} \begin{pmatrix} x_{t0} \\ x_{t1} \end{pmatrix} = \begin{pmatrix} x_t \\ x_{t\tau} \end{pmatrix} , \tag{A.54}$$

Appendix B

Energy at two-body cluster level

The energy per particle at two-body cluster level can be written (see Eqs.(3.27) and (3.28))

$$(\Delta E)_2 = \sum_{i<j} \langle ij| \, \frac{1}{2}\Big[f_{12}, [\, t_1 + t_2, f_{12}]\Big] + f_{12} v_{12} f_{12} \, |ij - ji\rangle \ , \tag{B.1}$$

with

$$t_i = -\frac{1}{2m}\nabla_i^2 \ \ , \ \ t_1 + t_2 = -\frac{1}{m}\nabla^2 \ - \frac{1}{4m}\nabla_R^2 \ , \tag{B.2}$$

where $\boldsymbol{\nabla}$ acts on the relative coordinate $\mathbf{r}$, while $\boldsymbol{\nabla}_R$ acts on the center of mass coordinate $\mathbf{R}$, defined as

$$\mathbf{r} = \mathbf{r}_1 - \mathbf{r}_2 \ \ , \ \ \mathbf{R} = \frac{1}{2}(\mathbf{r}_1 + \mathbf{r}_2) \tag{B.3}$$

respectively.

Including only the static part of the interaction, both the correlation function f_{12} and the two-nucleon potential v_{12} are written as

$$f_{12} = \sum_{p=1}^{6} f^p(r_{12}) O_{12}^p \ \ , \ \ v_{12} = \sum_{p=1}^{6} v^p(r_{12}) O_{12}^p \ , \tag{B.4}$$

with the six operator O_{12}^n listed in Eq.(2.16), whose properties are discussed in Appendix A..

The FG two-nucleon state is given by

$$\begin{aligned} |ij\rangle &= \frac{1}{V} \, \mathrm{e}^{i(\mathbf{k}_i \cdot \mathbf{r}_1 + \mathbf{k}_j \cdot \mathbf{r}_2)} \, |S\, M_S, T\, M_T\rangle \\ &= \frac{1}{V} \, \mathrm{e}^{i(\mathbf{k} \cdot \mathbf{r} + \mathbf{K} \cdot \mathbf{R})} \, |S\, M_S, T\, M_T\rangle \ , \end{aligned} \tag{B.5}$$

with

$$\begin{aligned} |\mathbf{k}_i|, |\mathbf{k}_j| &\leq p_F \\ \mathbf{k} = \frac{1}{2}(\mathbf{k}_i - \mathbf{k}_j) \quad &, \quad \mathbf{K} = \mathbf{k}_i + \mathbf{k}_j \ . \end{aligned} \tag{B.6}$$

We will discuss the potential and kinetic energy term separately.

B.1 Potential energy

Consider the operator

$$w_{12} = f_{12} v_{12} f_{12} \ , \tag{B.7}$$

and the decomposition of f_{12} in the TS-representation (see Eq.(A.49))

$$f_{12} = \sum_{ST} \Big[f_{ST} + \delta_{S1} f_{tT} S_{12} \Big] P_{2S+1} \Pi_{2T+1} \ . \tag{B.8}$$

In the above equation, P_{2S+1} and Π_{2T+1} are spin and isospin projection operators, whose properties are given in Appendix A. By writing the corresponding decomposition for w_{12} and v_{12} and calculating

$$\begin{aligned} w_{12} &= \sum_{TS} \Bigg\{ \delta_{S0} f_{T0}^2 v_{T0} + \delta_{S1} \Big\{ v_{T1} \Big[f_{T1}^2 + 8 f_{tT}^2 + 2 \left(f_{T1} f_{tT} - f_{tT}^2 \right) S_{12} \Big] + \\ &+ v_{tT} \Big[16 \left(f_{T1} f_{tT} - f_{tT}^2 \right) + \left(f_{T1}^2 - 4 f_{T1} f_{tT} + 12 f_{t1}^2 \right) S_{12} \Big] \Big\} \Bigg\} P_{2S+1} \Pi_{2T+1} \ , \end{aligned}$$

we can identify

$$\begin{aligned} w_{T0} &= v_{T0} \ f_{T0}^2 \\ w_{T1} &= v_{T1} \Big(f_{T1}^2 + 8 f_{tT}^2 \Big) + 16 v_{tT} \Big(f_{T1} f_{tT} - f_{tT}^2 \Big) \\ w_{tT} &= 2 v_{T1} \Big(f_{T1} f_{tT} - f_{tT}^2 \Big) + v_{tT} \Big(f_{T1}^2 - 4 f_{T1} f_{tT} + 12 f_{t1}^2 \Big) \ . \end{aligned} \tag{B.9}$$

After replacing

$$\sum_{i<j} \longrightarrow \frac{1}{2} \sum_{ij} \ , \tag{B.10}$$

the potential energy contribution to $(\Delta E)_2$ reads

$$\langle w \rangle = \frac{1}{2} \frac{1}{V^2} \sum_{SM_S} \sum_{TM_T} \sum_{\mathbf{k}_i \mathbf{k}_j} \sum_{S'T'} \Bigg\{ \int d^3 r_1 d^3 r_2 \Big[w_{S'T'}(r) \langle P_{2S'+1} \Pi_{2T'+1} \rangle +$$

$$\delta_{S'1} w_{tT'}(r) \langle S_{12} P_{2S'+1} \Pi_{2T'+1} \rangle \Big] - \int d^3r_1 d^3r_2 \, \mathrm{e}^{i(\mathbf{k}_i \cdot \mathbf{r} - \mathbf{k}_j \cdot \mathbf{r})} \tag{B.11}$$

$$\Big[w_{S'T'}(r) \langle P_{2S'+1} \Pi_{2T'+1} P_{\sigma\tau} \rangle + \delta_{S'1} w_{tT'}(r) \langle S_{12} P_{2S'+1} \Pi_{2T'+1} P_{\sigma\tau} \rangle \Big] \Big\} \ ,$$

where $P_{\sigma\tau}$ is the spin-isospin exchange operator defined in Appendix A and the expectation values $\langle O \rangle$ are taken over two-nucleon states of definite total spin and isospin $|S\, M_S, T\, M_T\rangle$. Using

$$\int d^3r_1 d^3r_2 = \int d^3r \, d^3R = V \int d^3r \ , \tag{B.12}$$

the definition of the Slater function (3.7),

$$\sum_{|\mathbf{k}| \le p_F} \mathrm{e}^{i\mathbf{k}\cdot\mathbf{r}} = \frac{V}{(2\pi)^3} \int_{|\mathbf{k}| \le p_F} d^3k \, e^{i\mathbf{k}\cdot\mathbf{r}} = \frac{N}{\nu} \ell(p_F r) \ , \tag{B.13}$$

and the results of Appendix A, we finally obtain

$$\langle w \rangle = \frac{1}{2} \frac{1}{V^2} \frac{N^2}{\nu^2} V \sum_{ST} (2S+1)\,(2T+1) \int d^3r \, w_{ST}(r) \left[1 - (-1)^{S+T} \ell^2(p_F r) \right] \ , \tag{B.14}$$

i.e., in the case of symmetric nuclear matter ($\nu = 4$),

$$\begin{aligned} \frac{1}{N} \langle w \rangle \ &= \ \frac{\rho}{32} \int d^3r \Big\{ [w_{00}(r) + 9 w_{11}(r)] a_-(p_F r) + \\ &\qquad + [3 w_{01}(r) + 3 w_{10}(r)] a_+(p_F r)] \Big\} \ , \end{aligned} \tag{B.15}$$

where $\rho = N/V$ is the density and

$$a_\pm(x) = 1 \pm \ell^2(x) \ . \tag{B.16}$$

B.2 Kinetic energy

Let us now discuss the kinetic contribution to the energy, given by

$$\frac{1}{2} \Big[f_{12}, [\, t_1 + t_2, f_{12}] \Big] = -\frac{1}{2m} \Big[f_{12}, [\, \nabla^2, f_{12}] \Big] \ . \tag{B.17}$$

We consider spin-zero and spin-one channels separately.

Spin-zero channels In these channels, the relevant part of the correlation function is given by

$$f_{12} = \sum_T f_{T0}(r)\ P_1 \Pi_{2T+1}\ . \tag{B.18}$$

Making use of the results of Appendix A, as well as of

$$\Big[f_{T0}, \nabla^2 f_{T0}\Big] = 0\ \ , \ \ \Big[f_{T0}, (\boldsymbol{\nabla} f_{T0})\boldsymbol{\nabla}\Big] = -(\boldsymbol{\nabla} f_{T0})^2\ , \tag{B.19}$$

we find

$$\begin{aligned}
\Big[f_{12}, \big[\ \nabla^2, f_{12}\big]\ \Big] &= \sum_{TT'} \Big[f_{T0}\ P_1\, \Pi_{2T+1}, \big[\nabla^2,\ f_{T0}\big]\ \ P_1\, \Pi_{2T'+1}\Big] \\
&= \sum_{TT'} \Big[f_{T0}, \big[\nabla^2,\ f_{T0}\big]\ \Big]\ P_1^2 \Pi_{2T+1}\Pi_{2T'+1} \\
&= \sum_{T} \Big[f_{T0}, (\nabla^2 f_{T0}) + 2(\boldsymbol{\nabla} f_{T0})\boldsymbol{\nabla}\Big]\ P_1\, \Pi_{2T+1} \\
&= 2\sum_{T} \Big[f_{T0}, (\boldsymbol{\nabla} f_{T0})\boldsymbol{\nabla}\Big]\ P_1\, \Pi_{2T+1} \\
&= -2\sum_{T} (\boldsymbol{\nabla} f_{T0})^2\ P_1\, \Pi_{2T+1}\ .
\end{aligned} \tag{B.20}$$

Finally,

$$-\frac{1}{2m}\Big[f_{12}, \big[\ \nabla^2, f_{12}\big]\ \Big] = \frac{1}{m}\sum_T (\boldsymbol{\nabla} f_{T0})^2\ P_1\, \Pi_{2T+1}\ . \tag{B.21}$$

Spin-one channels In these channels, the correlation function is given by

$$f_{12} = \sum_T \Big[f_{T1}(r) + f_{tT}(r) S_{12}\Big] P_3\, \Pi_{2T+1}\ . \tag{B.22}$$

Relying once more on Appendix A, we calculate

$$\begin{aligned}
&\sum_{T'} \Big[\nabla^2, (f_{T'1} + f_{tT'} S_{12}) P_3\, \Pi_{2T'+1}\Big] = \sum_{T'} \Big\{[\nabla^2, f_{T'1}] + [\nabla^2, f_{tT'} S_{12}]\Big\} P_3\, \Pi_{2T'+1} \\
&= \sum_{T'} \Big\{(\nabla^2 f_{T'1}) + 2(\boldsymbol{\nabla} f_{tT'})\boldsymbol{\nabla} + (\nabla^2 f_{tT'} S_{12}) + 2(\boldsymbol{\nabla} f_{tT'} S_{12})\boldsymbol{\nabla}\Big\} P_3\, \Pi_{2T'+1} \\
&= \sum_{T'} \Big\{(\nabla^2 f_{T'1}) + 2(\boldsymbol{\nabla} f_{tT'})\boldsymbol{\nabla} + (\nabla^2 f_{tT'}) S_{12} + (\nabla^2 S_{12}) f_{tT'} \\
&+ 2(\boldsymbol{\nabla} f_{tT'})(\boldsymbol{\nabla} S_{12}) + 2 S_{12}(\boldsymbol{\nabla} f_{tT'})\boldsymbol{\nabla} + 2 f_{tT'}(\boldsymbol{\nabla} S_{12})\boldsymbol{\nabla}\Big\} P_3\, \Pi_{2T'+1}\ .
\end{aligned} \tag{B.23}$$

Hence, the commutator in Eq.(B.17) can be rewritten as

$$\begin{aligned}\Big[f_{12},\big[\,\nabla^2,f_{12}\big]\,\Big] &= \sum_{TT'}\Big[(f_{T1}+f_{tT}S_{12})P_3\,\Pi_{2T+1},\{\ldots\}\,P_3\,\Pi_{2T'+1}\Big]\\ &= \sum_{T}\Big[f_{T1}+f_{tT}S_{12},\{\ldots\}\Big]P_3\,\Pi_{2T+1}\\ &= \sum_{T}\Big(F_T^{(1)}+F_T^{(2)}\Big)P_3\,\Pi_{2T+1}\ , \end{aligned} \tag{B.24}$$

with

$$F_T^{(1)}=\Big[f_{T1},\{\ldots\}\Big]\ \ ,\ \ F_T^{(2)}=\Big[f_{tT}S_{12},\{\ldots\}\Big]\ , \tag{B.25}$$

and

$$\begin{aligned}\Big\{\ldots\Big\} &= \Big\{(\nabla^2 f_{T'1})+2(\boldsymbol{\nabla}f_{tT'})\boldsymbol{\nabla}+(\nabla^2 f_{tT'})S_{12}+(\nabla^2 S_{12})f_{tT'}\\ &+\ 2(\boldsymbol{\nabla}f_{tT'})(\boldsymbol{\nabla}S_{12})+2S_{12}(\boldsymbol{\nabla}f_{tT'})\boldsymbol{\nabla}+2f_{tT'}(\boldsymbol{\nabla}S_{12})\boldsymbol{\nabla}\Big\}\ . \end{aligned} \tag{B.26}$$

We find

$$F_T^{(1)}=-2(\boldsymbol{\nabla}f_{T1})^2-2(\boldsymbol{\nabla}f_{T1})(\boldsymbol{\nabla}f_{tT})S_{12}\ , \tag{B.27}$$

and

$$\begin{aligned}F_T^{(2)} &= \Big[f_{tT}S_{12},2(\boldsymbol{\nabla}f_{T1})\boldsymbol{\nabla}\Big]+\Big[f_{tT}S_{12},2S_{12}(\boldsymbol{\nabla}f_{T1})\boldsymbol{\nabla}\Big]+\\ &\quad+\Big[f_{tT}S_{12},2f_{T1}(\boldsymbol{\nabla}S_{12})\boldsymbol{\nabla}\Big]=\\ &= -2(\boldsymbol{\nabla}f_{T1})(\boldsymbol{\nabla}f_{tT})S_{12}-2(\boldsymbol{\nabla}f_{tT})^2S_{12}^2+\\ &\quad+2f_{tT}^2\Big[S_{12},(\boldsymbol{\nabla}S_{12})\boldsymbol{\nabla}\Big]\\ &= -2\ (\boldsymbol{\nabla}f_{T1})(\boldsymbol{\nabla}f_{tT})S_{12}-2(\boldsymbol{\nabla}f_{tT})^2(8-2S_{12})\ \ +\\ &-\ 2f_{tT}^2\left[\frac{36}{r^2}\,(\mathbf{L}\cdot\mathbf{S})+\frac{6}{r^2}\,(8-S_{12})\right]. \end{aligned} \tag{B.28}$$

Collecting all pieces togheter, we find for the spin-one channels

$$\begin{aligned}-\frac{1}{2m}\Big[f_{12},\big[\,\nabla^2,f_{12}\big]\,\Big] &= \frac{1}{m}\sum_{T}\Big\{(\boldsymbol{\nabla}f_{T1})^2+(\boldsymbol{\nabla}f_{T1})(\boldsymbol{\nabla}f_{tT}S_{12})+\\ &\quad+\ (\boldsymbol{\nabla}f_{tT})^2(8-2S_{12})\ \ +f_{tT}^2\left[\frac{36}{r^2}\,(\mathbf{L}\cdot\mathbf{S})+\frac{6}{r^2}\,(8-S_{12})\right]\Big\}P_3\,\Pi_{2T+1}\\ &= \frac{1}{m}\sum_{TS}\Big\{(\boldsymbol{\nabla}f_{TS})^2+\delta_{S1}\Big[2(\boldsymbol{\nabla}f_{TS})(\boldsymbol{\nabla}f_{tT})S_{12}+\end{aligned}$$

$$+(\boldsymbol{\nabla} f_{tT})^2 S_{12}^2 + f_{tT}\frac{36}{r^2}\,(\mathbf{L}\cdot\mathbf{S}) + \frac{6}{r^2}\,(8 - S_{12})\Big]\Big\} P_{2S+1}\Pi_{2T+1}$$
$$= \sum_{TS}\Big\{t_{TS}(r) + \delta_{S1}\Big[t_{tT}(r)S_{12} + t_{bT}(r)(\mathbf{L}\cdot\mathbf{S})\Big]\Big\} P_{2S+1}\Pi_{2T+1}\ , \quad \text{(B.29)}$$

with

$$\begin{aligned}
t_{T0} &= \frac{1}{m}(\boldsymbol{\nabla} f_{T0})^2 \\
t_{T1} &= \frac{1}{m}\Big[(\boldsymbol{\nabla} f_{T1})^2 + 8(\boldsymbol{\nabla} f_{tT})^2 + \frac{48}{r^2}\,f_{tT}^2\Big] \\
t_{tT} &= \frac{1}{m}\Big[2(\boldsymbol{\nabla} f_{T1})(\boldsymbol{\nabla} f_{tT}) - 2(\boldsymbol{\nabla} f_{tT})^2 - \frac{6}{r^2}\,f_{tT}^2\Big] \\
t_{bT} &= \frac{1}{m}\frac{36}{r^2}\,f_{tT}^2\ .
\end{aligned}$$

B.3 Final expression for $(\Delta E)_2$

We can rewrite

$$(\Delta E)_2 = \sum_{i<j}\langle ij|W_{12}|ij - ji\rangle\ , \quad \text{(B.30)}$$

with

$$W_{12} = -\frac{1}{m}\Big[f_{12},\,[\,\nabla^2,\,f_{12}]\,\Big] + f_{12}v_{12}f_{12}$$

$$= \sum_{TS}\Big\{W_{TS}(r) + \delta_{S1}\Big[W_{tT}(r)S_{12} + W_{bT}(r)(\mathbf{L}\cdot\mathbf{S})\Big]\Big\} P_{2S+1}\Pi_{2T+1}\ ,$$

where

$$\begin{aligned}
W_{T0} &= \frac{1}{m}(\boldsymbol{\nabla} f_{T0})^2 + v_{T0}f_{T0}^2 \\
W_{T1} &= \frac{1}{m}\Big[(\boldsymbol{\nabla} f_{T1})^2 + 8(\boldsymbol{\nabla} f_{tT})^2 + \frac{48}{r^2}\,f_{tT}^2\Big] + \\
&\quad + v_{T1}\Big(f_{T1}^2 + 8f_{tT}^2\Big) + 16v_{tT}\Big(f_{T1}f_{tT} - f_{tT}^2\Big) \\
W_{tT} &= \frac{1}{m}\Big[2(\boldsymbol{\nabla} f_{T1})(\boldsymbol{\nabla} f_{tT}) - 2(\boldsymbol{\nabla} f_{tT})^2 - \frac{6}{r^2}\,f_{tT}^2\Big] + \\
&\quad + 2v_{T1}\Big(f_{T1}f_{tT} - f_{tT}^2\Big) + v_{tT}\Big(f_{T1}^2 - 4f_{T1}f_{tT} + 12f_{t1}^2\Big) \\
W_{bT} &= \frac{1}{m}\,\frac{36}{r^2}\,f_{tT}^2\ .
\end{aligned}$$

Making use of the expression for the expectation values given in Appendix A, we finally obtain (compare to Eq.(B.15))

$$\begin{aligned}\frac{(\Delta E)_2}{N} &= \frac{\rho}{32}\int d^3r\Big\{\Big[W_{00}(r)+9W_{11}(r)\Big]a_-(p_Fr)+\\ &\quad+\Big[3W_{01}(r)+3W_{10}(r)\Big]a_+(p_Fr)\Big\}\,. \end{aligned} \tag{B.31}$$

Appendix C

Euler-Lagrange equations for the correlation functions

C.1 Spin singlet channels: uncoupled equations

In the spin-zero channels, the energy per partcicle of SNM, evaluated at two-body cluster level, reads (compare to Eqs.(B.15) and (B.21))

$$\begin{aligned}\frac{(\Delta E)_2}{N} &= \frac{\rho}{32}\ (2T+1)\int\ d^3r\left[\frac{1}{m}(\boldsymbol{\nabla} f_{T0})^2+v_{T0}f_{T0}^2\right]a_{T0}(p_F r)\\ &= \frac{\rho}{32}\ (2T+1)\ 4\pi\int\ r^2dr\left[\frac{1}{m}(f'_{T0})^2+v_{T0}f_{T0}^2\right]a_{T0}(p_F r)\\ &= \text{const}\int_0^\infty dr\ F\left[f_{T0},\, f'_{T0}\right]\ ,\end{aligned} \tag{C.1}$$

where $a_{TS}(x)=1-(-)^{T+S}\ell^2(x)$ and

$$F\left[f_{T0},\, f'_{T0}\right]=\left[(f'_{T0})^2+m\ v_{T0}f_{T0}^2\right]\phi_{T0}^2\ , \tag{C.2}$$

with

$$\phi_{T0}=r\sqrt{a_{T0}}\ . \tag{C.3}$$

The corresponding Euler-Lagrange (EL) equations for the unknown functions f_{T0} are given by

$$\frac{d}{dr}\frac{\partial F}{\partial f'_{T0}}-\frac{\partial F}{\partial f_{T0}}=0\ . \tag{C.4}$$

From

$$\frac{\partial F}{\partial f_{T0}}\ =\ 2\ m\ v_{T0}\ f_{T0}^2\ \phi_{T0}^2\ ,$$

$$\begin{aligned} \frac{\partial F}{\partial f'_{T0}} &= 2\, f'_{T0}\, \phi^2_{T0}\ , \\ \frac{d}{dr}\frac{\partial F}{\partial f'_{T0}} &= 2\, f''_{T0}\, \phi^2_{T0} + 4\, f'_{T0}\, \phi'_{T0}\, \phi_{T0}\ , \end{aligned} \tag{C.5}$$

we obtain

$$f''_{T0}\, \phi^2_{T0} + 2\, f'_{T0}\, \phi'_{T0} - m\, v_{T0}\, f^2_{T0}\, \phi^2_{T0} = 0\ . \tag{C.6}$$

Introducing

$$g_{T0} \equiv f_{T0}\, \phi_{T0}\ , \tag{C.7}$$

we can put Eq.(C.6) in the form

$$g''_{T0} - \left(\frac{\phi''_{T0}}{\phi_{T0}} + m\, v_{T0} \right) g_{T0} = 0\ . \tag{C.8}$$

Now we introduce a Lagrange multiplier, in order to fulfill the requirement (see Eqs.(3.34)-(3.36))

$$g'_{T0}|_{r=d} = \phi'_{T0}|_{r=d}\ . \tag{C.9}$$

The resulting equation is Eq.(4) of Ref.[57]

$$g''_{T0} - \left(\frac{\phi''_{T0}}{\phi_{T0}} + m\ (v_{T0} + \lambda) \right) g_{T0} = 0\ , \tag{C.10}$$

to be integrated with the boundary conditions

$$g_{T0}|_{r=0} = 0\ , \tag{C.11}$$

$$g_{T0}|_{r=d} = \phi_{T0}|_{r=d}\ . \tag{C.12}$$

C.2 Spin triplet channels: coupled equations

In the spin-one channels, the contribution to the energy is given by (see Eqs.(B.15) and (B.31))

$$\begin{aligned} \frac{(\Delta E)_2}{N} &= \frac{\rho}{32}\ (2T+1) \int d^3r \Bigg\{ \frac{1}{m} \left[(\boldsymbol{\nabla} f_{T1})^2 + 8 (\boldsymbol{\nabla} f_{tT})^2 + \frac{48}{r^2}\, f^2_{tT} \right] + \\ &\quad + v_{T1} \Big(f^2_{T1} + 8 f^2_{tT} \Big) + 16 v_{tT} \Big(f_{T1} f_{tT} - f^2_{tT} \Big) \Bigg\}\, a_{T1}(p_F r) \\ &= \text{const} \int_0^\infty dr\ F \left[f_{T1},\, f_{tT};\ f'_{T1},\, f'_{tT} \right]\ , \end{aligned} \tag{C.13}$$

where

$$F\left[f_{T1},\, f_{tT};\; f'_{T1},\, f'_{tT}\right] = \left(f'_{T1}\right)^2 \phi_{T1}^2 + 8\left(f'_{tT}\right)^2 \phi_{T1}^2 + \frac{48}{r^2}\, f_{tT}^2 \phi_{T1}^2 + \\ + m\Big[v_{T1}\left(f_{T1}^2 + 8 f_{tT}^2\right) + 16 v_{tT}\left(f_{T1} f_{tT} - f_{tT}^2\right)\Big] \,. \quad \text{(C.14)}$$

In this case we have two coupled EL equations

$$\begin{cases} \frac{d}{dr}\frac{\partial F}{\partial f'_{T1}} - \frac{\partial F}{\partial f_{T1}} = 0 \\ \\ \frac{d}{dr}\frac{\partial F}{\partial f'_{tT}} - \frac{\partial F}{\partial f_{tT}} = 0 \,. \end{cases} \quad \text{(C.15)}$$

Carrying out the derivativees as in the spin-zero channels and defining

$$g_{T1} \equiv f_{T1}\phi_{T1} \;\;,\;\; g_{tT} \equiv \sqrt{8} f_{tT}\phi_{T1} \,, \quad \text{(C.16)}$$

we find

$$\begin{cases} g''_{T1} - \left(\frac{\phi''_{T1}}{\phi_{T1}} + m\, v_{T1}\right)\, g_{T1} - m\sqrt{8} v_{tT} g_{tT} = 0 \\ \\ g''_{tT} - \left[\frac{\phi''_{T1}}{\phi_{T1}} + m\, \left(v_{T1} - 2v_{tT}\right) + \frac{6}{r^2}\right]\, g_{tT} - m\sqrt{8} v_{tT} g_{T1} = 0 \,. \end{cases} \quad \text{(C.17)}$$

Finally, inclusion of the Lagrange multipliers needed to guarantee

$$g'_{T1}|_{r=d_1} = \phi'_{T1}|_{r=d_1} \,, \quad \text{(C.18)}$$
$$g'_{tT}|_{r=d_2} = \phi'_{T1}|_{r=d_2} \,, \quad \text{(C.19)}$$

with, in general, $d_1 \neq d_2$, leads to (compare to Eq.(5) of Ref.[57])

$$\begin{cases} g''_{T1} - \left[\frac{\phi''_{T1}}{\phi_{T1}} + m\, \left(v_{T1} + \lambda_1\right)\right]\, g_{T1} - m\left(\sqrt{8} v_{tT} + \lambda_2\right) g_{tT} = 0 \\ \\ g''_{tT} - \left[\frac{\phi''_{T1}}{\phi_{T1}} + m\, \left(v_{T1} - 2v_{tT} + \lambda_1\right) + \frac{6}{r^2}\right]\, g_{tT} - m\left(\sqrt{8} v_{tT} + \lambda_2\right) g_{T1} = 0 \,, \end{cases} \quad \text{(C.20)}$$

with the boundary conditions

$$g_{T1}|_{r=0} = 0 \,, \quad \text{(C.21)}$$
$$g_{T1}|_{r=d_1} = \phi_{T1}|_{r=d_1} \,, \quad \text{(C.22)}$$

and

$$g_{tT}|_{r=0} = 0 \,, \quad \text{(C.23)}$$
$$g_{tT}|_{r=d_2} = 0 \,. \quad \text{(C.24)}$$

Appendix D

Nucleon-nucleon scattering

In this Appendix, we describe the formalism employed to obtain the NN scattering from section in free space from the *bare* potential.

D.1 Partial wave expansion

The total angular momentum J of two interacting nucleons in their center of mass frame is given by the sum of the relative orbital angular momentum $\mathbf{L}$ and the total spin $\mathbf{S}$ of the nucleons. As nuclear forces are invariant under spatial rotations, the angular momentum J and its projection M_J are good quantum numbers. However, the orbital angular momentum L and its projection m are not good quantum numbers, since the tensor component of the potential couples states with $L = J \pm 1$. The fact that the tensor operator commutes with the total spin S, implies that S is a good quantum number, while the projection M_S is not. The parity, $\pi = +\ (-)$ for even (odd) values of L, is also a good quantum number since the strong as well as electromagnetic forces are invariant under space reflection. The main part of the strong interaction is isoscalar, and thus the total isospin T is an approximately good quantum number, while its projection M_T is exactly conserved due to charge conservation. As a consequence, the two-nucleon eigenstates can be labeled with the quantum numbers J^π,M_J,S,T and M_T.

In the notation of atomic spectroscopy, waves with quantum numbers J,L,S are denoted by ${}^{2S+1}L_J$ using letters $L = S$,P,D,F,G... for $L = 0$,1,2,3,4..., respectively. For example, ${}^3P_2$ denotes a state with $J = 2$, $L = 1$ and $S = 1$. The parity of the wave is given by $(-1)^L$. The $J = L$ states have "natural parity" $\pi = (-1)^J$. Hence, the ${}^1S_0$ and ${}^3D_2$ are natural parity waves. All natural parity waves are uncoupled to other waves by nuclear forces. The tensor force has no effect on the $S = 0$, $L = J$ waves, while the triplet waves having $S = 1$ and $L = J$ are uncoupled because there are no other waves with the same J^π and S. For example, the ${}^3D_2$ wave can not

mix with any other wave because it is the only positive parity wave with $J = 2$ and $S = 1$. On the other hand, triplet waves with $L = J \pm 1$ have "unnatural parity", $-$ $(+)$ for even (odd) J. The tensor force mixes unnatural parity waves having the same values of J, such as ${}^3S_1$ and ${}^3D_1$ for example. The only exception to this rule is the ${}^3P_0$ wave which, being the only negative parity $J = 0$ wave, is an eigenstate of the two-nucleon hamiltonian.

It is convenient to use the spin-angle functions $\mathcal{Y}^M_{JSL}$ to express two-nucleon partial waves. These eigenfunctions of total $\mathbf{J}$,$\mathbf{L}$,$\mathbf{S}$ and M_J, are obtained by coupling $\mathbf{L} + \mathbf{S}$ to the appropriate value of $\mathbf{J}$ and M_J. They are given by:

$$\mathcal{Y}^{M_J}_{JSL} = \sum_{M_S} \langle L,m = M_J - M_S;\ S,M_S|JM_J\rangle\ Y^m_L(\theta,\phi)\ |S,M_S\rangle\ , \tag{D.1}$$

where θ and ϕ are the polar angles of the relative position vector $\mathbf{r} = \mathbf{r}_1 - \mathbf{r}_2$, and $Y^m_L(\theta,\phi)$ are spherical harmonics. The Clebsch-Gordon coefficients for the case $S = 1$ are tabulated in Table D.1. Obviously, for $S = 0$ $M_S = 0$, and the Clebsch-Gordon coefficient is $\delta_{JL}\delta_{M_J m}$.

	$M_S = 1$	$M_S = 0$	$M_S = -1$
$L = J - 1$	$\sqrt{\frac{(L+M_J)(L+M_J+1)}{(2L+1)(2L+2)}}$	$\sqrt{\frac{(L-M_J+1)(L+M_J+1)}{(2L+1)(L+1)}}$	$\sqrt{\frac{(L-M_J)(L+M_J+1)}{(2L+1)(2L+2)}}$
$L = J$	$-\sqrt{\frac{(L+M_J)(L-M_J+1)}{2L(L+1)}}$	$\frac{M_J}{\sqrt{L(L+1)}}$	$\sqrt{\frac{(L-M_J)(L+M_J+1)}{2L(L+1)}}$
$L = J + 1$	$\sqrt{\frac{(L-M_J)(L-M_J+1)}{2L(2L+1)}}$	$-\sqrt{\frac{(L-M_J)(L+M_J)}{L(2L+1)}}$	$\sqrt{\frac{(L+M_J+1)(L+M_J)}{2L(2L+1)}}$

Table D.1. Clebsch-Gordan coefficients entering the definition of the spin-angle functions, Eq.(D.1).

The two-nucleon wave function in a JM_JSL partial wave is given by

$$\psi^M_{JSL} = R_{JSL}(r)\ \mathcal{Y}^M_{JSL}, \tag{D.2}$$

where $R_{JSL}(r)$ is the radial wave function, independent of M_J. The total isospin T of the wave is determined by the requirement of antisymmety under the exchange of the two nucleons. On exchanging the spatial positions of the nucleons, $\mathbf{r}_1 \rightleftharpoons \mathbf{r}_2$, implying

$\mathbf{r} \to -\mathbf{r}$. The radial wave function $R_{JSL}(r)$ does not change, while $Y_L^m \to (-1)^L Y_L^m$. Under spin exchange, $M_{s_1} \rightleftharpoons M_{s_2}$ the total spin state $|S,M_S\rangle \to -(-1)^S|S,M_S\rangle$. Hence

$$P_{12}^{\text{space}} P_{12}^{\text{spin}} \psi_{JSL}^{M_J} = -(-1)^{S+L} \psi_{JSL}^{M_J}, \tag{D.3}$$

where P_{12}^{space} and P_{12}^{spin} are the operators exchanging space and spin coordinates, respectively. Like the spin state, the isospin state $|T,M_T\rangle \to -(-1)^T|T,M_T\rangle$ under isospin exchange. Therefore the complete two-nucleon wave function $\psi_{JSL}^M|T,M_T\rangle$ satisfies

$$\begin{aligned} P_{12}^{\text{tot}} \psi_{JSL}^{M_J}|T,M_T\rangle &= P_{12}^{\text{space}} P_{12}^{\text{spin}} P_{12}^{\text{isospin}} \psi_{JSL}^{M_J}|T,M_T\rangle \\ &= (-1)^{T+S+L} \psi_{JSL}^{M_J}|T,M_T\rangle \ , \end{aligned} \tag{D.4}$$

where P_{12}^{tot} is the total two-nucleon exchange operator. This wave function is antisymmetric only when $T+S+L$ is odd. Its isospin factor is often omitted, and the partial waves are denoted by quantum numbers JSL. The isospin of the partial wave is implicit via the antisymmetry constraint, requiring $T=0$ if $S+L$ is odd, and $T=1$ if $S+L$ is even.

The partial waves are not eigenstates of the tensor operator S_{12}. We will now consider the operation of S_{12} on the partial waves. Since it contains the unit vector $\hat{\mathbf{r}} = \mathbf{r}/|\mathbf{r}|$ and the spins, it operates on the spin-angle functions $\mathcal{Y}_{JSL}^{M_J}$ according to

$$S_{12} \mathcal{Y}_{J0J}^{M_J} = 0 \ . \tag{D.5}$$

As the $\mathcal{Y}_{JSL}^{M_J}$ form a complete orthonormal set and the tensor operator commutes with J, M_J and S, we can write

$$S_{12} \mathcal{Y}_{J1L}^{M_J} = \sum_{L'} c_{L'L}^J \mathcal{Y}_{J1L'}^{M_J}, \tag{D.6}$$

$$c_{L'L}^J = \langle \mathcal{Y}_{J1L'}^{M_J} | S_{12} | \mathcal{Y}_{J1L}^{M_J} \rangle \ . \tag{D.7}$$

The values of the coefficients $c_{L'L}^J$ are given in Table D.2.

D.2 The Two-Nucleon Schrödinger Equation

The natural parity waves are not coupled by nuclear forces. Therefore in these states the two-nucleon eigenfunctions have a simpler form

$$\Psi_{JSJ}^{M_J} = R_{JSJ}(r) \mathcal{Y}_{JSJ}^{M_J} = \frac{1}{r} u(r) \mathcal{Y}_{JSJ}^{M_J} \ . \tag{D.8}$$

	$L'=J-1$	$L'=J$	$L'=J+1$
$L=J-1$	$-2\frac{J-1}{2J+1}$	0	$6\frac{\sqrt{J(J+1)}}{2J+1}$
$L=J$	0	2	0
$L=J+1$	$6\frac{\sqrt{J(J+1)}}{2J+1}$	0	$-2\frac{J+2}{2J+1}$

Table D.2. Matrix elements of the tensor operator S_{12}, $c^J_{L'L}$, between spin-angle states (see Eq.(D.7)).

On the other hand, the unnatural parity eigenstates have two coupled waves with $L = J \pm 1$. Their wave function is represented by

$$\begin{aligned}\Psi^{M_J}_{JST} &= R_{JS(J-1)}(r)\mathcal{Y}^{M_J}_{JS(J-1)} + R_{JS(J+1)}(r)\mathcal{Y}^{M_J}_{JS(J+1)} \\ &= \frac{1}{r}u(r)\mathcal{Y}^{M_J}_{JS(J-1)} + \frac{1}{r}w(r)\mathcal{Y}^{M_J}_{JS(J+1)} \ . \end{aligned} \tag{D.9}$$

The radial functions $u(r)$ and $w(r)$ are more convenient to use than the $R_{JSL}(r)$, and the requirement that $R_{JSL}(r)$ be finite at the origin implies that $u(r=0)=0$ and $w(r=0)=0$. The JSL subscripts of u and w are suppressed for brevity.

The two-nucleon Schrödinger equation describing scattering state is given by

$$\left[-\frac{1}{m}\nabla^2 + v(12)\right]\Psi^{M_J}_{JST} = E\Psi^{M_J}_{JST} \equiv \frac{1}{m}k^2\Psi^{M_J}_{JST}, \tag{D.10}$$

where $v(12)$ is the two-nucleon interaction operator and $E \equiv k^2/m$ the center of mass energy. For uncoupled waves this Schrödinger equation can be simplified to the form

$$-\frac{1}{m}\frac{1}{r}\mathcal{Y}^{M_J}_{JSJ}\left(\frac{d^2}{dr^2} - \frac{J(J+1)}{r^2}\right)u(r) + v(12)\frac{1}{r}u(r)\mathcal{Y}^{M_J}_{JSJ} = E\frac{1}{r}u(r)\mathcal{Y}^{M_J}_{JSJ}, \tag{D.11}$$

by using the identity

$$\nabla^2\frac{1}{r}u(r)\mathcal{Y}^{M_J}_{JSL} = \frac{1}{r}\mathcal{Y}^{M_J}_{JSL}\left(\frac{d^2}{dr^2} - \frac{L(L+1)}{r^2}\right)u(r) \ . \tag{D.12}$$

For coupled waves we find

$$-\frac{1}{m}\frac{1}{r}\left[\mathcal{Y}^{M_J}_{JS(J-1)}\left(\frac{d^2}{dr^2}-\frac{J(J-1)}{r^2}\right)u(r)+\mathcal{Y}^{M_J}_{JS(J+1)}\left(\frac{d^2}{dr^2}-\frac{(J+1)(J+2)}{r^2}\right)w(r)\right]$$
$$+v_{12}\frac{1}{r}\left(u(r)\mathcal{Y}^{M_J}_{JS(J-1)}+w(r)\mathcal{Y}^{M_J}_{JS(J+1)}\right) \tag{D.13}$$
$$=E\frac{1}{r}\left(u(r)\mathcal{Y}^{M_J}_{JS(J-1)}+w(r)\mathcal{Y}^{M_J}_{JS(J+1)}\right).$$

As the operators in $v(12)$ operate only on the $\mathcal{Y}^{M_J}_{JSL}$, we can define potentials $v_{JSL}(r)$ in the partial wave with quantum numbers JSL, and channel coupling tensor potentials v^t_J which couple the $L=J\pm1$ partial waves as follows

$$\begin{aligned}
v(12)\ \mathcal{Y}^{M_J}_{JSJ} &= \mathcal{Y}^{M_J}_{JSJ}\ v_{JSJ}(r),\\
v(12)\ \mathcal{Y}^{M_J}_{JS(J-1)} &= \mathcal{Y}^{M_J}_{JS(J-1)}\ v_{JS(J-1)}(r)+\mathcal{Y}^{M_J}_{JS(J+1)}\ v^t_J(r)\ c^J_{(J-1)(J+1)},\\
v(12)\ \mathcal{Y}^{M_J}_{JS(J+1)} &= \mathcal{Y}^{M_J}_{JS(J+1)}\ v_{JS(J+1)}(r)+\mathcal{Y}^{M_J}_{JS(J-1)}\ v^t_J(r)\ c^J_{(J-1)(J+1)},
\end{aligned} \tag{D.14}$$

In the case of uncoupled waves, we can multiply the Schrödinger Eq. D.11 by ${\mathcal{Y}^{M}_{JSJ}}^{\dagger}$ from the left, integrate over angles using the orthonormality of the spin-angle functions and obtain the simple radial equation:

$$-\frac{1}{m}\left(\frac{d^2}{dr^2}-\frac{J(J+1)}{r^2}\right)u(r)+v_{JSJ}(r)u(r)=Eu(r)\ . \tag{D.15}$$

In the case of coupled waves we obtain two, coupled radial equations by multiplying eq.(D.13) with ${\mathcal{Y}^{M_J}_{JS(J\pm1)}}^{\dagger}$ and integrating over angles. The final result is

$$\begin{aligned}
-\frac{1}{m}\left(\frac{d^2}{dr^2}-\frac{J(J-1)}{r^2}\right)u(r) &+ v_{JS(J-1)}(r)u(r) \qquad\qquad (D.16)\\
&+ v^t_J(r)c^J_{(J-1)(J+1)}w(r)=Eu(r)
\end{aligned}$$

$$-\frac{1}{m}\left(\frac{d^2}{dr^2}-\frac{(J+1)(J+2)}{r^2}\right)w(r) + v_{JS(J+1)}(r)w(r) \tag{D.17}$$
$$+ v^t_J(r)c^J_{(J-1)(J+1)}u(r)=Ew(r). \tag{D.18}$$

The above equations have been used to obtain the scattering wave function, solution of the Lipmann-Shcwinger equation, needed to calculate the NN cross section. It is worth mentioning that, to carry out numerical calculations, it is more convenient to use interaction operators v_{JSL} and v^t_J in the T,S representation, discussed in Appendix A.

Appendix E

Transition probability in Born approximation

This appendix decribes the calculation of the transition probability $|\hat{v}_{\rm eff}(\mathbf{q})|^2$, appearing in Eq.(4.7).

We need to calculate the matrix elements of $v_{\rm eff}$ between antisymmetric plane-wave two-nucleon states

$$\langle \mathbf{r}|\mathbf{k},SM,T\rangle_a = \frac{1}{\sqrt{2}}\left(\mathrm{e}^{i\mathbf{k}\cdot\mathbf{r}} - \mathrm{e}^{-i\mathbf{k}\cdot\mathbf{r}}P_{\sigma\tau}\right)|SM,T\rangle \ , \tag{E.1}$$

where $P_{\sigma\tau}$ is the spin-isospin exchange operator, defined in Appendix A. Note that, due to charge conservation, the matrix elements do not depend on the projection of the total isospin. Hence, we can set $M_T = 0$.

Using the expansion ($r = |\mathbf{r}|$, $k = |\mathbf{k}|$, $\hat{\mathbf{r}} = \mathbf{r}/|\mathbf{r}|$, $\hat{\mathbf{k}} = \mathbf{k}/|\mathbf{k}|$)

$$\mathrm{e}^{i\mathbf{k}\cdot\mathbf{r}} = \sum_L \sqrt{4\pi(2L+1)}\ i^L j_L(kr) Y_L^0(\hat{\mathbf{k}}\cdot\hat{\mathbf{r}}) \tag{E.2}$$

and

$$Y_L^0(\hat{\mathbf{k}}\cdot\hat{\mathbf{r}}) = \sqrt{\frac{4\pi}{2L+1}}\ \sum_m Y_L^{m\star}(\hat{\mathbf{k}}) Y_L^m(\hat{\mathbf{r}}) \tag{E.3}$$

we obtain

$$\mathrm{e}^{i\mathbf{k}\cdot\mathbf{r}}|SM\rangle = \sum_{Lm} 4\pi\ i^L j_L(kr) Y_L^{m\star}(\hat{\mathbf{k}}) Y_L^m(\hat{\mathbf{r}})|SM\rangle \ . \tag{E.4}$$

Using the the spin-angle functions, defined through (see Appendix D)

$$Y_L^m(\hat{\mathbf{r}})|SM\rangle = \sum_J \langle LmSM|JM_J\rangle \mathcal{Y}_{LSJ}^{M_J} = |LSJM_J\rangle \ , \tag{E.5}$$

we can rewrite Eq.(E.4) in the form ($M_J = m + M$)

$$\mathrm{e}^{i\mathbf{k}\cdot\mathbf{r}}|SM\rangle = 4\pi \sum_{LJM_J} i^L j_L(kr) Y_L^{M_J-M\star}(\hat{\mathbf{k}}) \langle L(M_J-M)SM|JM_J\rangle |LSJM_J\rangle \ . \quad \text{(E.6)}$$

The matrix elements of v_{eff} reads

$$\begin{aligned} \mathcal{M}_{if} = \frac{(4\pi)^2}{2} \sum_{JM_J} \sum_{LL'} \qquad & i^{L-L'} \left[1-(-)^{L+S+T}\right] \left[1-(-)^{L'+S+T}\right] \\ & \times \ \langle JM_J|L'(M_J-M')SM'\rangle Y_{L'}^{M_J-M'\star}(\hat{\mathbf{k}}') \\ & \times \ \langle L(M_J-M)SM|JM_J\rangle Y_L^{M_J-M}(\hat{\mathbf{k}}) \\ & \times \ \int_0^\infty dr r^2 j_{L'}(k'r) \langle L'SJM_JT|v_{\text{eff}}|LSJM_JT\rangle j_L(kr) \ . \end{aligned} \quad \text{(E.7)}$$

Writing the effective interaction in the TS-representation (see Appendix A) and using the properties of the spin-isospin projection operators we obtain the following expressions:

• **Spin zero channels.** $L' = L$:

$$\mathcal{M}_{if} = \frac{(4\pi)^2}{2} \sum_{Lm} \left[1-(-)^{L+S+T}\right]^2 Y_L^{m\star}(\hat{\mathbf{k}}') Y_L^m(\hat{\mathbf{k}}) \int_0^\infty dr r^2 j_L(k'r) v_{\text{eff}}^{TS} j_L(kr) \ . \quad \text{(E.8)}$$

• **Spin one channels.** The calculation of $\mathcal{M}_{if}$ requires the matrix elements

$$c_{LL'}^J = \langle \ell' 1 JM_J|S_{12}|L1JM_J\rangle = c_{L'L}^J \quad \text{(E.9)}$$

whose values are given in Table D.2.

The matrix elements involving the tensor component v_{eff}^{tT} are

$$\begin{aligned} \mathcal{M}_{if}^t = \frac{(4\pi)^2}{2} \sum_{JM_J} \sum_{LL'} \qquad & i^{L-L'} \left[1-(-)^{L+S+T}\right] \left[1-(-)^{L'+S+T}\right] \\ & \times \ \langle JM_J|L'(M_J-M')SM'\rangle Y_{L'}^{M_J-M'\star}(\hat{\mathbf{k}}') \\ & \times \ \langle L(M_J-M)SM|JM_J\rangle Y_L^{M_J-M}(\hat{\mathbf{k}}) \\ & \times \ c_{LL'}^J \int_0^\infty dr r^2 j_{L'}(k'r) v_{\text{eff}}^{tT} j_L(kr) \ , \end{aligned} \quad \text{(E.10)}$$

and can be readily evaluated using the Clebsch-Gordan coefficients of Table D.1.

Finally, the matrix elements involving the central components $v_{\rm eff}^{T1}$ are given by

$$\begin{aligned}\mathcal{M}_{if}^{c} = \frac{(4\pi)^2}{2}\sum_{JM_J}\sum_{L} \quad & \left[1-(-)^{L+S+T}\right]^2 \\ \times \quad & \langle JM_J|L(M_J-M')1M'\rangle Y_L^{M_J-M'\star}(\hat{\mathbf{k}}') \\ \times \quad & \langle L(M_J-M)1M|JM_J\rangle Y_L^{M_J-M}(\hat{\mathbf{k}}) \\ \times \quad & c_{LL}^{J}\int_0^\infty drr^2 j_L(k'r)v_{\rm eff}^{T1}j_L(kr)\ . \end{aligned} \tag{E.11}$$

Bibliography

[1] S. Chandrasekhar, Phys. Rev. Lett. **24** (1970) 611.

[2] J.L. Friedman and B.F. Schutz, Ap. J. **221** (1978) 937; *ibidem* **222** (1978) 281.

[3] L. Lindblom, in *Gravitational Waves: a Challenge to Theoretical Astrophysics*, edited by V. Ferrari, J.C. Miller and L. Rezzolla, ICTP Lecture Notes Series Vol. 3 (ICTP, Trieste, 2001).

[4] C. Cutler and L. Lindblom, Ap. J. **314** (1987) 234.

[5] E. Flowers and N. Itoh, Astrophys. J. **206** (1976) 218.

[6] E. Flowers and N. Itoh, Astrophys. J. **230** (1979) 847.

[7] A. Akmal and V.R. Pandharipande, Phys. Rev. C **56** (1997) 2261.

[8] A. Akmal, V.R. Pandharipande and D.G. Ravenhall, Phys. Rev. C **58** (1998) 1804.

[9] N.K. Glendenning, *Compact Stars* (Springer, Berlin, 2000)

[10] L.D. Landau, Soviet Phys. JETP **3** (1957) 920; *ibid.* **8** (1959) 70.

[11] D.A. Baiko and P. Haensel, Acta Phys. Pol. **30** (1999) 1097.

[12] A.A. Abrikosov and I.M. Khalatnikov, Soviet Phys. JETP **5** (1957) 887; Rep. Prog. Phys. **22** (1959) 329.

[13] R.P. Feynman, *The Feynman Lectures on Physics, Vol. I* (Addison Wesley, New York, NY, 1977).

[14] L.D. Landau and E.M. Lifshitz, *Fluid Mechanics*, (Elsevier, Amsterdam, 1987).

[15] G. Baym and C. Pethick, *Landau Fermi-Liquid Theory* (John Wiley & Sons, New York, NY, 1991).

[16] L.D. Landau, E.M. Lifshitz and L.P. Pitaevskii, *Statistical Physics, Part 2* (Pergamon, Oxford, 1980).

[17] G.A. Brooker and J. Sykes, Phys. Rev. Lett. **21** (1968) 279.

[18] J. Sykes and G.A. Brooker, Ann. of Phys. (N.Y.) **56** (1970) 1.

[19] A.A. Abrikosov, L.P. Gorkov and I.E. Dzyaloshinski, *Methods of Quantum Field Theory in Statistical Physics* (Dover, New York, 1975).

[20] E.M. Lifshitz and L.P. Pitaevskii, *Physical Kinetics*, (Elsevier, Amsterdam, 1981).

[21] D. Pines and P. Nozières, *The theory of quantum fluids* (Perseus Books, Cambridge, MA, 1999).

[22] S. Shlomo and D.H. Youngblood, *Phys. Rev.* C **47** (1993) 529.
[23] S.L. Shapiro and S.A. Teukolski, *Black holes, white dwarfs and neutron stars* (Wiley-Interscience, New York, NY, 1983)
[24] S.E. Thorsett, Z. Arzoumanian and J.H. Taylor, Ap. J. **405** (1993) L29.
[25] L. Lindblom and S. Detweiler, Ap. J. Suppl. **53** (1983) 73.
[26] N. Andersson and K.D. Kokkotas, MNRAS **299** (1998) 1059.
[27] O. Benhar, V. Ferrari and L. Gualtieri, Phys. Rev. D **70** (2004) 124015.
[28] V.G.J. Stoks, R.A.M. Klomp, M.C.M. Rentmeester and J.J. de Swart, Phys. Rev. C **48** (1993) 792.
[29] R.B. Wiringa, V.G.J. Stoks and R. Schiavilla, Phys. Rev. C **51** (1995) 38.
[30] B.S. Pudliner, V.R. Pandharipande, J. Carlson, S.C. Pieper and R.B. Wiringa, Phys. Rev. C **56** (1997) 1720.
[31] B.S. Pudliner, V.R. Pandharipande, J. Carlson and R.B. Wiringa, Phys. Rev. Lett. **74** (1995) 4396.
[32] S.C. Pieper and R.B. Wiringa, Ann. Rev. Nucl. Part. Sci. **51** (2001) 53.
[33] *Nuclear Methods and Nuclear Equation of State*, Ed. M. Baldo (World Scientific, Singapore, 1999).
[34] J. Carlson, J. Morales, Jr, V.R. Pandharipande and D.G. Ravenhall, Phys. Rev. C **68** (2003) 025802.
[35] A. Sarsa, S. Fantoni, K.E. Schmidt and F. Pederiva, Phys. Rev. C **68** (2003) 024308.
[36] S. Gandolfi, F. Pederiva, S. Fantoni and K.E. Schmidt, Phys. Rev. Lett. **98** (2007) 102503
[37] E. Feenberg, *Theory of quantum fluids* (Academic Press, New York, NY, 1969).
[38] J.W. Clark, Prog. Part. Nucl. Phys. **2** (1979) 89.
[39] S. Fantoni and V.R. Pandharipande, Phys. Rev. C **37** 1697 (1988) 1697.
[40] A.L. Fetter and J.D. Walecka, *Quantum theory of many-particle systems* (McGraw-Hill, New York, NY, 1971).
[41] O. Benhar, A. Fabrocini and S. Fantoni, Nucl. Phys. A **505** (1989) 267.
[42] O. Benhar, A. Fabrocini and S. Fantoni, Nucl. Phys. A **550** (1992) 201.
[43] S. Fantoni and S. Rosati, Nuovo Cimento A **25** (1975) 593.
[44] V.R. Pandharipande and R.B. Wiringa, Rev. Mod. Phys. **51** (1979) 821.
[45] S. Cowell, Ph.D. Thesis, University of Illinois at Urbana-Champaign (2004).
[46] S. Cowell and V.R. Pandharipande, Phys. Rev. C **70** (2004) 035801.
[47] I. Lagaris and V.R. Pandharipande, Nucl. Phys. A **359** (1981) 349.
[48] A. Akmal, Ph.D. Thesis, University of Illinois at Urbana-Champaign (1998).
[49] S. Fantoni, B.L. Friman and V.R. Pandharipande, Nucl. Phys. **A399** (1983) 51.
[50] S. Fantoni, A. Sarsa and K.E. Schmidt, Phys. Rev. Lett. **87** (2001) 181101.
[51] O. Benhar and M. Valli, arXiv:0707.2681, submitted to Physical Review Letters.
[52] V.R. Pandharipande and S.C. Pieper, Phys. Rev. C **45** (1992) 791.

[53] R.A. Arndt, L.D. Roper, R.A. Bryan, R.B. Clark, B.J. VerWest and P. Signell, Phys. Rev. D **28** (1983) 97.
[54] Center for Nuclear Studies, Data Analysis Center, http://gwdac.phys.gwu.edu/
[55] J. Wambach, T.L. Ainsworth and D. Pines, Nucl. Phys. A **555** (1993) 128.
[56] A. Fabrocini, S. Fantoni, A.Yu. Illarionov and K.E. Schmidt, Phys. Rev. Lett. **95** (2005) 192501.
[57] O. Benhar, C. Ciofi degli Atti, S. Fantoni and S. Rosati, Phys. Lett. B **70** (1977) 1.